Exploring the Self-Assembly and Energy Transfer of Dynamic Supramolecular Iridium-Porphyrin Systems

*Diego Rota Martir,[a] Gordon J. Hedley,[b] David B. Cordes,[a] Alexandra M. Z. Slawin,[a] Daniel Escudero,[c] Denis Jacquemin,[c,d] Tamara Kosikova,[a] Douglas Philp,[a] Daniel M. Dawson,[e] Sharon E. Ashbrook,[e] Ifor D.W. Samuel,[b] and Eli Zysman-Colman[a]**

[a] Organic Semiconductor Centre, EaStCHEM School of Chemistry, University of St Andrews, St Andrews, Fife, KY16 9ST, UK, Fax: +44-1334 463808; Tel: +44-1334 463826; E-mail: eli.zysman-colman@st-andrews.ac.uk;
URL: http://www.zysman-colman.com
[b] Organic Semiconductor Centre, SUPA, School of Physics and Astronomy, University of St Andrews, St Andrews, Fife, KY16 9SS, UK
[c] CEISAM UMR CNRS 6230, Université de Nantes, 2 rue de la Houssinière, BP 92208, 44322 Nantes Cedex 3, France
[d] Institut Universitaire de France, 1, rue Descartes, 75231 Paris Cedex 5, France
[e] EaStCHEM School of Chemistry and the Centre for Magnetic Resonance, University of St Andrews, North Haugh, St Andrews, Fife, KY16 9ST, UK

SUPPORTING INFORMATION

Table of contents:

Experimental section.

General Synthetic Procedures. Commercial chemicals were used as supplied. All reactions were performed using standard Schlenk techniques under inert (N_2) atmosphere with reagent-grade solvents. Flash column chromatography was performed using silica gel (Silia-P from Silicycle, 60 Å, 40-63 μm). Analytical thin layer chromatography (TLC) was performed with silica plates with aluminum backings (250 μm with indicator F-254). Compounds were visualized under UV light. ^{1}H,^{13}C and^{19}F solution-phase NMR spectra were recorded on a Bruker Avance spectrometer operating at 11.7 T (Larmor frequencies of 500, 126 and 471 MHz, respectively). The following abbreviations have been used for multiplicity assignments: “s” for singlet, “d” for doublet, “t” for triplet, “m” for multiplet and “br” for broad. The solvent was CD_2Cl_2. Melting points (Mps) were recorded using open-ended capillaries on an Electrothermal melting point apparatus and are uncorrected. High-resolution mass spectra were recorded at the EPSRC UK National Mass Spectrometry Facility at Swansea University on a quadrupole time-of-flight (ESI-Q-TOF), model ABSciex 5600 Triple TOF in positive electrospray ionization mode and spectra were recorded using sodium formate solution as the calibrant. High-resolution MALDI mass spectra were recorded for assemblies **1a**, **1b**, **2a** and **2b** at the Mass Spectrometry Facility at University of St Andrews.

Ligand Syntheses.

2-Chloro-4-(2,4,6-trimethylphenyl)pyridine. The synthesis of this ligand is by a previously reported method.[1] 2-Chloro-4-iodopyridine (4.0 g, 16.74 mmol), 2,4,6-trimethylphenyl boronic acid (4.0 g, 25.11 mmol) and potassium carbonate (50 mmol) were added to a round-bottomed flask containing 50 mL of a mixture of 1,4-dioxane and distilled water (4:1 v/v). The reaction mixture was degassed by multiple vacuum and N_2 purging cycles, and $Pd(PPh_3)_4$ (0.693 g, 0.60 mmol) was added to the flask under positive nitrogen pressure. The mixture was refluxed under nitrogen atmosphere for 48 h and then cooled to room temperature. The mixture was poured onto distilled water and extracted multiple times with DCM. The organic fractions were combined, washed with a portion of brine and dried over magnesium sulfate. Filtration and evaporation under reduced pressure gave the crude product (3.80 g). The crude product was purified by flash column chromatography (5% ethyl acetate/hexane on silica) to give 3.30 g of pure compound as a colourless oil. **Yield:** 85%. **R_f:** 0.40 (20% EtOAc/hexanes on silica). **^{1}H NMR (500 MHz,$CDCl_3$) δ (ppm):** 8.46 (d, *J* = 5.1 Hz, 1H), 7.18 (s, 1H), 7.06 (dd, *J* = 5.1, 1.4 Hz, 1H), 6.99 (s, 2H), 2.36 (s, 3H), 2.04 (s, 6H). The characterization matches that reported.[1]

2-phenyl-4-(2,4,6-trimethylphenyl)pyridine (mesppy). The synthesis of this ligand is by a previously reported method.[1]2-Chloro-4-(2,4,6-trimethylphenyl)pyridine (**A**) (3.3 g, 14.24 mmol), phenyl boronic acid (2.78 g, 22.78 mmol), potassium carbonate (40 mmol) were added to a round bottomed flask containing 50 mL of a mixture of 1,2-dimethoxyethane and distilled water (4:1 v/v). The reaction mixture was degassed by multiple vacuum and N_2 purging cycles, and $Pd(PPh_3)_4$ (0.548 g, 0.48 mmol) was added to the flask under positive nitrogen pressure. The mixture was refluxed under nitrogen atmosphere for 19 h and then cooled to room temperature. The mixture was poured onto distilled water and extracted multiple times with DCM. The organic fractions were combined, washed with a portion of brine and dried over magnesium sulfate. Filtration and evaporation under reduced pressure gave the crude product (3.90 g). The crude product was purified by flash column chromatography (silica, hexane/ethyl acetate gradient 100:0 to 80:20) to give 3.50 g of pure compound as a colourless oil. **Yield:** 87%. **R_f:** 0.38 (10% EtOAc/hexanes on silica). **^{1}H NMR (500 MHz,$CDCl_3$) δ (ppm):** 8.77 (dd, *J* = 5.0, 0.8 Hz, 1H), 8.05 (m, 2H), 7.60 (q, *J* = 0.8 Hz, 1H), 7.54 - 7.42 (m, 3H), 7.09 (dd, *J* = 5.3, 1.3 Hz, 1H), 7.01 (s, 2H), 2.4 (s, 3H), 2.08 (s, 3H). **^{13}C NMR (126 MHz, CD_2Cl_2) δ(ppm):**157.7, 150.3, 149.9, 139.4, 137.6, 136.5, 135.2, 129.1, 128.8, 128.6, 128.4, 127.0, 123.2, 121.5, 21.1, 20.7. **FT-MS:** Calculated: ($C_{20}H_{19}N$) 273.1585, found: 274.1585. The characterization matches that reported.[1]

2-(2,4-Difluorophenyl)-4-(2,4,6-trimethylphenyl)pyridine (dFmesppy). The synthesis of this ligand is by a previously reported method.[1] 2-Chloro-4-(2,4,6-trimethylphenyl)pyridine (**A**) (2.28 g, 9.88 mmol), 2,4-difluorphenylphenyl boronic acid (2.18 g, 13.82 mmol), potassium carbonate (3.41 g, 24.51 mmol) were added to a Schlenk tube containing a mixture of 1,2-dimethoxyethane and distilled water (4:1 v/v). The reaction mixture was degassed by multiple vacuum and N_2 purging cycles, and $Pd(PPh_3)_4$ (0.571 g, 0.494 mmol) was added to the tube under positive nitrogen pressure. The mixture was refluxed under nitrogen atmosphere for 19 h and then cooled to room temperature. The mixture was poured onto distilled water and extracted multiple times with DCM. The organic fractions were combined, washed with a portion of brine and dried over magnesium sulfate. Filtration and evaporation under reduced pressure gave the crude product (3.59 g). The crude product was purified by flash column chromatography (silica, hexane/ethyl acetate 9:1) to give 2.88 g of pure compound as a colourless oil. **Yield**: 94%. **R_f:** 0.43 (hexane/ethyl acetate, 6:1 on silica). **^{1}H NMR (500 MHz,CDCl$_3$) δ (ppm):** 8.75 (dd, J = 7.5 Hz, 1.5 Hz, 1H), 8.08 (dt, J = 8.5, 10 Hz, 1H), 7.59 (m, 1H), 7.09 (dd, J = 5.0 Hz, 1.5 Hz, 1H), 7.02 (tdd, J = 10.0, 3.3, 1.0 Hz, 1H) 6.97 (d, J = 1.0 Hz, 2H), 6.90 (dt, J = 3.0, 12.5 Hz, 1H), 2.34 (s, 3H), 2.05 (s, 6H). **^{13}C NMR (126 MHz, CDCl$_3$) δ (ppm):** 164.67, 161.97, 159.45, 152.85, 122.83, 150.16, 150.05, 137.78, 136.39, 135.37, 132.40, 132.36, 132.30, 132.26, 128.53, 125.48, 125.38, 123.67, 112.15, 112.12, 111.94, 111.91, 104.80, 104.54, 104.28, 21.20, 20.76. **^{19}F {^{1}H} NMR (471 MHz, CDCl$_3$) δ (ppm):**–109.3 (d, J = 9.4 Hz, 1F), –112.7 (d, J = 9.4 Hz, 1F). **HR-MS (**APCI$^+$**): [M+H]$^+$ Calculated:** ($C_{20}H_{17}F_2NH$) 310.1402;**Found:** 310.1402. The characterization matches that reported.[1]

Synthesis of 4,4':2',2'':4'',4'''-quaterpyridine (qpy). The synthesis of this ligand was adapted from a previously reported protocol.[2]4,4'-Bipyridine (5.0 g, 0.032 mol), Pd/C (0.70 g, 10% weight Pd) and DMF (50 mL) were added to a dry round bottomed flask, and the reaction mixture was sonicated and oxygenated by bubbling air through the solution. The mixture was refluxed for 48 h, cooled to room temperature and the solvent was removed using a high-vacuum rotary evaporator. The crude product was dissolved in $CHCl_3$ (50 mL) and the catalyst was filtered. A bright yellow solution was obtained and $CHCl_3$ was removed under vacuum to obtain a brown solid. The crude product was purified by flash chromatography (5% methanol / DCM) to give 0.9 g of pure compound as a white solid. **Yield:** 15%. **R_f:** 0.40 (5% MeOH/DCM on silica). **^{1}H NMR (500 MHz, $CDCl_3$) δ (ppm):** 8.86 (d, J = 5.4 Hz, 2H),8.82 – 8.79 (m, 6H), 7.71 (d, J = 5.1 Hz, 4H), 7.64 (d, J = 5.5, 2H). **^{13}C NMR (126 MHz, $CDCl_3$) δ (ppm):** 156.6, 150.7, 150.1, 146.7, 145.6, 121.7, 121.5, 119.1. The characterization matches that reported.[2]

General procedure for the synthesis of $[Ir(C^\wedge N)_2]_2Cl_2$ dimers. The iridium (III) dimers, $[Ir(mesppy)_2(\mu\text{-}Cl)]_2$ and $[Ir(dFmesppy)_2(\mu\text{-}Cl)]_2$ were prepared according to the procedure described by Nonoyama.[3] Briefly, to $IrCl_3{\cdot}3H_2O$ (1.0 equiv.) and C^N ligand (2.2 equiv.) was added 2-ethoxyethanol to give a concentration of 0.02 M. The reaction mixture was degassed by multiple vacuum and N_2 purging cycles and the mixture was heated to reflux for 19 h. The solution was cooled to room temperature and the yellow precipitate was filtered, washed with water, hexane and ether and finally dried under vacuum to afford the desired material, which was used without further purification.

Tetrakis[2-(phenyl)-4-(2,4,6-trimethylphenyl)pyridinato-*N*,*C*$^{2'}$]-bis(μ-chloro)diiridium(III)$[Ir(mesppy)_2(\mu\text{-}Cl)]_2$(**D2**). **Yield:** 70%. **^{1}H NMR (500 MHz, CD_2Cl_2) δ(ppm):** 9.69 (d, J = 6.4 Hz, 2H), 7.77 (s, 4H), 7.55 (d, J = 9.0 Hz, 4H), 7.05 (d, J = 10.9 Hz, 8H), 6.86 (m, 7H), 6.72 (dt, J = 8.1 Hz, 4H), 5.95 (d, J = 8.1 Hz, 4H), 2.42 (s, 12H), 2.16 (s, 12H), 2.15 (s, 12H).

Tetrakis[2-(4',6'-difluorophenyl)-4-(2,4,6-trimethylphenyl)pyridinato-*N*,*C*$^{2'}$]-bis(μ-chloro)diiridium(III), [Ir(dFmesppy)$_2$(μ-Cl)]$_2$ (D4). Yield: 81%. **^{1}H {^{19}F} NMR (400 MHz,CD$_2$Cl$_2$) δ (ppm):** 9.57 (d, *J* = 6.0 Hz, 4H), 8.13 (s, 4H), 7.02 (d, *J* = 10.4 Hz, 8H), 6.89 (dd, *J* = 6.0, 2.0 Hz, 4H), 5.29 (m, 4H) 2.38 (s, 12H), 2,12 (s, 24H). **^{19}F {^{1}H} NMR (471 MHz, CD$_2$Cl$_2$) δ (ppm):** –108.1 (d, *J* = 11.1 Hz, 4F), –110.2 (d, *J* = 10.8 Hz, 4F).

General procedure for the synthesis of [Ir(C^N)$_2$(N^N)]PF$_6$ complexes. To a Schlenk tube containing,[Ir(mesppy)$_2$Cl]$_2$ (**D1**) or [Ir(dFmesppy)$_2$Cl]$_2$, (**D2**) (1.0 equiv.) and N^N ligand (2.5 equiv.) were added DCE (DCM with 4,4'-di*tert*butyl-2,2'-bipyridine) and MeOH (1:1 v/v) to give a concentration of 0.03 M. The reaction mixture was degassed by multiple vacuum and N_2 purging cycles and the mixture and the mixture was heated to 55 °C for 19 h under nitrogen atmosphere. The solution was cooled to room temperature and solid NH_4PF_6 (10.0 equiv.) was added and the reaction mixture was left to stir for a further 1 h. The resulting suspension was evaporated to dryness, with the residue then copiously washed with Et_2O and distilled water. This crude product was purified by flash column chromatography (silica, DCM/MeOH gradient 100:0 to 60:40). Fractions containing the desired complex were combined and solid NH_4PF_6 (10 equiv.) was added. The suspension was stirred at room temperature for 0.5 h. This mixture was then evaporated to dryness, washed vigorously with distilled water and dried to afford the pure material.

Iridium(III)bis[2-phenyl-4-(2,4,6-trimethylphenyl)pyridinato]-4,4':2',2'':4'',4'''-quaterpyridine hexafluorophosphate, [Ir(mesppy)$_2$(qpy)](PF$_6$) (1): **Yield**: 55%. **R*$_f$***: 0.20 (DCM + 3% MeOH + 2% NEt_3). **Mp**: 351 - 354 °C (decomposed). **^{1}H NMR(500 MHz, CDCl$_3$) δ(ppm)**: 9.51 (s, 2H), 8.88 (d, *J* = 5.7 Hz, 4H), 8.25 (dd, *J* = 6.1, 2.1 Hz, 2H), 8.17 (s, 2H), 8.12 (d, *J* = 5.6 Hz, 2H), 8.08 (d, *J* = 6.7 Hz, 3H), 8.03 (d, *J* = 7.8 Hz, 2H), 7.78 (d, *J* = 5.6 Hz, 2H), 7.05 - 6.98 (m, 10H), 6.30 (d, *J* = 6.3 Hz, 2H), 2.29 (s, 6H), 2.10 (s, 6H), 1.90 (s, 6H). **^{13}C NMR (126 MHz, CDCl$_3$) δ(ppm)**: 167.8, 165.5, 152.4, 151.5, 150.9, 149.8, 149.0, 148.6, 143.9, 143.0, 138.3, 134.9, 133.2, 131.5, 130.8, 128.5, 126.2, 125.1, 124.9, 122.9, 122.3, 121.3, 29.7, 20.8, 20.3.**HR NSI$^+$ MS**: [M-PF$_6$]$^+$ Calculated: (C$_{60}$H$_{50}$IrN$_6$): 1047.3726 Found: 1047.3719.

Iridium(III)bis[2-(2,4-difluoro)-phenyl-4-(2,4,6-trimethylphenyl)pyridinato]-4,4':2',2'':4'',4'''-quaterpyridine hexafluorophosphate, [Ir(dFmesppy)$_2$(qpy)](PF$_6$) (2). Yield: 39%. **R$_f$:** 0.20 (DCM + 3% MeOH + 2% NEt$_3$). **Mp:** 340 - 344 °C (decomposed) **^{1}H NMR (500 MHz, CD$_2$Cl$_2$) δ(ppm):** 8.83 (m, 5H), 8.31 (d, J = 5.4 Hz, 1H), 8.22 (bs, 2H), 7.85 (d, *J* = 5.9 Hz, 1H), 7.80 (d, *J* = 5.3 Hz, 2H), 7.69 (d, *J* = 5.8 Hz, 2H), 7.04 (m, 6H), 6.68 (m, 3H), 5.81 (m, 3H), 2.35 (s, 6H), 2.16 (s, 6H), 1.99 (s, 6H).**^{19}F NMR(417 MHz, CD$_2$Cl$_2$) δ (ppm):** –72.5 (d,*J* = 707.5 Hz,6F), –106.0(d, *J* = 10.3 Hz, 2F), –108.3(d, *J* = 10.3 Hz, 2F). **HR NSI$^+$ MS: [M-PF$_6$]$^+$ Calculated:** (C$_{60}$H$_{46}$F$_4$IrN$_6$): 1119.3349 **Found:** 1119.3326.

Iridium(III)bis[2-phenyl-4-(2,4,6-trimethylphenyl)pyridinato]-4,4'-di-tert-butyl-2,2'-bipyridine hexafluorophosphate, [Ir(mesppy)$_2$(dtbubpy)](PF$_6$) (3). Yield: 89%. **R$_f$:** 0.55 (DCM + 5% MeOH). **Mp:** 264 - 268 °C. **^{1}H NMR (500 MHz, CD$_2$Cl$_2$) δ(ppm)** 8.36 (d, *J* = 1.7 Hz, 2H), 8.03 (d, *J* = 6.5 Hz, 2H), 7.82 (d, *J* = 2.3 Hz, 2H), 7.73 (dd, *J* = 8.2, 1.3 Hz, 2H), 7.93 (d, *J* = 6.0 Hz, 2H), 7.54 (dd, *J* = 6.0, 2.1 Hz, 2H), 7.10 (dt, *J* = 8.1, 1.5 Hz, 2H), 7.05 (bm, 2H), 7.02 (d, *J* = 5.6, 1.4 Hz, 1H), 7.01 (bs, 2H), 6.87 (dd, *J* = 6.0, 1.9 Hz, 2H), 6.43 (d, *J* = 10. 0 Hz, 2H), 2.36 (s, 6H), 2.16 (s, 6H), 1.97 (s, 6H).**^{13}C NMR(126 MHz, CDCl$_3$) δ(ppm)**167.7, 164.2, 156.0, 151.8, 151.0, 149.7, 143.8, 138.2, 135.1, 134.9, 131.7, 130.7, 128.6, 128.5, 125.2, 124.8, 124.6, 122.4, 122.2, 120.5, 30.3, 21.1, 20.5. **HR NSI$^+$ MS: [M-PF$_6$]$^+$ Calculated:** (C$_{58}$H$_{60}$IrN$_4$): 1005.4447**Found:** 1005.4427.

Procedure for the synthesis of zinc tetraphenylphorphyrin(ZnTPP). The synthesis of ZnTPP followed a modified method to that previously reported.[4] Tetraphenylporphyrin TPP (0.1 g, 0.162

mmol) was dissolved in 25 mL of chloroform. The solution was purged with nitrogen for 10 min. Zinc acetate (0.073 g, 0.33 mmol) was dissolved in ~ 5 mL methanol and then added to the porphyrin solution. The mixture was stirred under nitrogen overnight at room temperature. All solvents were removed under reduced pressure leaving, a purple solid. The solid was dissolved in DCM and washed with 3 × 20 mL portions of 5 % w/v aqueous sodium bicarbonate, followed by 3 × 20 mL portions of water. The organic layer dried over $MgSO_4$ and the solvent was removed under reduced pressure. The zinc porphyrin was purified by flash column chromatography on a silica gel using 100% chloroform as the eluent. **Yield:** 90%. **R_f:** 0.65 ($CHCl_3$). **^{1}H NMR (500 MHz, CD_2Cl_2) δ(ppm)**:8.88 (s, 8H), 8.15 (dd, *J* = 7.4, 1.6 Hz, 8H), 7.69 (m, 12H). **^{13}C NMR (126 MHz, $CDCl_3$) δ(ppm)**: 150.2, 142.8, 134.4, 131.9, 127.5, 126.6, 121.1.The characterization matches that reported.[4]

*General procedure for the synthesis of **1a, 1b, 2a, 2b**.*In a dry 2 mL vial, complexes **1** and **2** and ZnTPP (1 or 2 equiv.) were dissolved in CD_2Cl_2 (1 mL) to give a concentration of the iridium complex of approximately 0.05 M. The solution was sonicated for few seconds and subsequently transferred to an NMR tube for characterization.

Iridium(III)bis[2-phenyl-4-(2,4,6-trimethylphenyl)pyridinato]-4,4':2',2'':4'',4'''-quaterpyridine hexafluorophosphate, $[Ir(mesppy)_2(qpy)](PF_6)$ – zinc tetraphenylporphyrin (ZnTPP) (1a).^{1}H NMR(500 MHz, CD_2Cl_2) δ(ppm): 8.94 (s, 12H), 8.25 (d, *J* = 7.8 Hz, 12H), 7.90 (m, 4H), 7.80 (m, 14H), 7.64 (s, 2H), 7.93 (d, J = 8.60 Hz, 2H), 7.26 (d, *J* = 6.0 Hz, 2H), 7.05 (d, *J* = 6.5 Hz, 2H), 6.99 (m, 4H), 6.89 (m, 4H), 6.66 (dd, *J* = 6.5, 1.5 Hz, 2H), 6.52 (bs, 3H), 6.20 (d, J = 7.4 Hz, 2H), 5.36 (s, 4H), 2.31 (s, 6H), 2.02 (s, 6H), 1.71 (s, 6H). **^{13}C NMR (126 MHz, $CDCl_3$) δ(ppm)**: 167.28, 152.21, 151.08, 149.31, 148.31, 147.42, 143.62, 143.24, 142.82, 138.30, 134.69, 131.70, 131.92, 131.24, 130.67, 128.41, 127.30, 126.42, 125.63, 124.78, 122.75, 122.09, 120.73, 20.72, 20.01.**MALDI-MS**: $[M-PF_6]^+$ Calculated: ($C_{105}H_{81}F_6IrN_{10}PZn$): 1870.4 Found: 1863.6.

Iridium(III)bis[2-phenyl-4-(2,4,6-trimethylphenyl)pyridinato]-4,4':2',2'':4'',4'''-quaterpyridine hexafluorophosphate, [Ir(mesppy)$_2$(qpy)](PF$_6$) – zinc tetraphenylporphyrin (ZnTPP) (1b).^{1}H NMR(500 MHz, CDCl$_3$) δ(ppm): 8.94 (s, 36H), 8.38 (d, *J* = 7.8 Hz, 36H), 7.80 (m, 56H), 7.72 (d, *J* = 4.9 Hz, 2H), 7.95 (bs, 2H), 7.49 (d, *J* = 8.05 Hz, 2H), 7.44 (bs, 2H), 7.42 (s, 1H), 7.09 (d, *J* = 5.7 Hz, 2H), 6.92 (t, *J* = 7.09 Hz, 4H), 6.86 (bs, 2H), 6.81 (t, *J* = 7.40 Hz, 3H), 6.71 (d, J = 7.2 Hz, 2H), 6.53 (dd, *J* = 7.2, 2.1 Hz, 4H), 6.09 (d, J = 9.4 Hz, 2H), 5.95 (d, J = 5.8 Hz, 2H), 2.29 (s, 6H), 1.95 (s, 6H), 1.67 (s, 6H). **^{13}C NMR (126 MHz, CDCl$_3$) δ(ppm)**: 167.23, 162.08, 157.40, 155.55, 155.20, 152.12, 150.62, 150.14, 149.10, 143.20, 146.65, 144.48, 143.01, 141.59, 138.24, 135.66, 134.48, 131.80, 131.13, 130.59, 128.37, 127.40, 126.50, 125.32, 124.68, 122.68, 121.40, 120.95, 120.35, 20.63, 19.90.

Iridium(III)bis[2-(2,4-difluoro)-phenyl-4-(2,4,6-trimethylphenyl)pyridinato]-4,4':2',2'':4'',4'''-quaterpyridine hexafluorophosphate, [Ir(dFmesppy)$_2$(qpy)](PF$_6$) – zinc tetraphenylporphyrin (ZnTPP) (2a).^{1}H NMR (500 MHz, CD$_2$Cl$_2$) δ(ppm): 8.98 (s, 18H), 8.26 (bs, 18H), 7.98 (s, 2H), 7.82 (m, 21H), 7.23 (d, *J* = 5.3 Hz, 2H), 7.94 (m, 12H), 6.69 (d, *J* = 5.9 Hz, 4H), 6.53 (m, 4H), 6.35 (bs, 4H), 6.10 (d, J = 6.2 Hz, 3H), 5.95 (m, 4H), 5.13 (s, 1H) 2.30 (s, 6H), 2.06 (s, 6H), 1.99 (s, 6H).**^{19}F NMR(471 MHz, CD$_2$Cl$_2$) δ (ppm):** –72.8 (d, *J* = 707.5 Hz,6F), –106.3(d, *J* = 14.6 Hz, 2F), –108.6(d, *J* = 14.6 Hz, 2F)(d, *J* = 14.6 Hz, 2F). **HR NSI$^+$ MS: [M-PF$_6$]$^+$ Calculated:** ($C_{105}H_{77}F_{10}IrN_{10}PZn$): 1942.33 **Found:** 1943.56

Iridium(III)bis[2-(2,4-difluoro)-phenyl-4-(2,4,6-trimethylphenyl)pyridinato]-4,4':2',2'':4'',4'''-quaterpyridine hexafluorophosphate, [Ir(dFmesppy)$_2$(qpy)](PF$_6$) – zinc tetraphenylporphyrin (ZnTPP) (2b). ^{1}H NMR (500 MHz, CD$_2$Cl$_2$) δ(ppm): 8.97 (s, 38H), 8.27 (bs, 40H), 7.95 (s, 4H), 7.80 (m, 50H), 7.60 (m, 6H), 7.15 (d, J = 5.8 Hz, 3H), 6.91 (m, 8H), 6.64 (d, *J* = 4.2 Hz, 4H), 6.48 (bt, *J* = 9.14 Hz, 4H), 6.12 (bs, 4H), 5.95 (m, 3H), 5.54 (m, 4H), 5.18 (s, 3H), 2.29 (s, 6H), 1.97 (s, 6H), 1.71 (s, 6H).**^{19}F NMR(471 MHz, CD_2Cl_2) δ (ppm):** –72.3 (d, J = 707.6 Hz,6F), –73.3 (s, 6F), –106.3(d, *J* = 14.8 Hz, 2F), –108.6(d, *J* = 14.8 Hz, 2F).

Photophysical measurements. All samples were prepared in HPLC grade dichloromethane with varying concentrations in the order of 10^{-4} – 10^{-6} M. Absorption spectra were recorded at room temperature using a Shimadzu UV-1800 double beam spectrophotometer. Molar absorptivity determination was verified by linear least-squares fit of values obtained from at least four independent solutions at varying concentrations with absorbance ranging from 6.05×10^{-5} to 2.07×10^{-5}M.

The sample solutions for the emission spectra were prepared in HPLC-grade DCM and degassed *via* three freeze-pump-thaw cycles using a quartz cuvette designed in-house. Steady-state emission and excitation spectra and time-resolved emission spectra were recorded at 298 K using an Edinburgh Instruments F980. All samples for steady-state measurements were excited at 360, 420 and 550 nm, while samples for time-resolved measurements were excited at 378 nm. Emission quantum yields were determined using the optically dilute method.[5] A stock solution with absorbance of *ca.* 0.5 was prepared and then four dilutions were prepared with dilution factors between 2 and 20 to obtain solutions with absorbances of *ca.* 0.095 0.065, 0.05 and 0.018, respectively. The Beer-Lambert law was found to be linear at the concentrations of these solutions. The emission spectra were then measured after the solutions were rigorously degassed *via* three freeze-pump-thaw cycles prior to spectrum acquisition. For each sample, linearity between absorption and emission intensity was verified through linear regression analysis and additional measurements were acquired until the Pearson regression factor (R^2) for the linear fit of the data set surpassed 0.9. Individual relative quantum yield values were calculated for each solution and the values reported represent the slope value. The equation $\Phi_s = \Phi_r(A_r/A_s)(I_s/I_r)(n_s/n_r)^2$ was used to calculate the relative quantum yield of each of the sample, where Φ_r is the absolute quantum yield of the reference, *n* is the refractive index of the solvent, *A* is the absorbance at the excitation wavelength, and *I* is the integrated area under the corrected emission curve. The subscripts s and r refer to the sample and reference, respectively. A solution of quinine sulfate in 0.5 M H_2SO_4 (Φ_r = 54.6%)[6] and $[Ru(bpy)_3]Cl_2$ in aerated H_2O at 298 K (Φ_r = 4%)[7] were used as external references.[8]

Streak camera measurements

Picosecond temporal dynamics were measured with a Hamamatsu synchroscan universal streak camera. The solution cuvette was mounted in either transmission or reflection geometry with respect to the camera spectrograph. Excitation (310 nm, 360 nm) was provided by the tuneable output of an Orpheus optical parametric amplifier, pumped by a Pharos regenerative amplifier, both from Light Conversion. Laser excitation was at 100 kHz, with 300 fs full-width half-maximum pulses.

Electrochemistry measurements. Cyclic voltammetry measurements were performed on an Electrochemical Analyzer potentiostat model 600D from CH Instruments. Solutions for cyclic voltammetry were prepared in DCM and degassed with DCM-saturated nitrogen by bubbling for about 10 min prior to scanning. Tetra(*n*-butyl)ammoniumhexafluorophosphate ($TBAPF_6$; *ca.* 0.1 M in ACN) was used as the supporting electrolyte. A Ag/Ag^+ electrode (silver wire in a solution of 0.1 M KCl in H_2O) was used as the pseudoreference electrode; a Pt electrode was used for the working electrode and a Pt electrode was used as the counter electrode. The redox potentials are reported relative to a saturated calomel electrode (SCE) electrode with a ferrocene/ferrocenium (Fc/Fc^+) redox couple as an internal reference (0.46 V *vs.* SCE).[9]

Solid-state NMR spectroscopy. Solid-state NMR spectra were recorded on a Bruker Avance III spectrometer equipped with a wide-bore 9.4 T superconducting magnet, at Larmor frequencies of

400.13 and 100.61 MHz for ^{1}H and ^{13}C, respectively. Samples were packed into ZrO_2 rotors with an outer diameter of 1.9 mm and rotated at the magic angle at 35 kHz (^{1}H spectra) or 14 kHz (^{13}C spectra). ^{1}H spectra were recorded using a rotor-synchronised DEPTH sequence to remove the probe background. Signal averaging was carried out over 16 transients with a recycle interval of 10 (ZnTPP), 5 (**1**) or 3 (**1a**) s. ^{13}C spectra were recorded with cross polarisation (CP) from ^{1}H. A contact pulse between 1.5-2.5 ms (ramped for ^{1}H) was used and ^{1}H decoupling (TPPM-15, ν_1 ~100 kHz) was applied during acquisition. Signal averaging was carried out over 2048 (ZnTPP), 5120 (**1**) or 10240 (**1a**) transients with recycle intervals of 10 (ZnTPP), 5 (**1**) or 3 (**1a**) s. Chemical shifts are reported in ppm relative to $(CH_3)_4Si$, using the N**H**$_3$ (δ = 8.5 ppm) and **C**H$_3$ (δ = 20.5 ppm) resonances of solid L-alanine as a secondary reference.

Characterization of Precursors and Ligand.

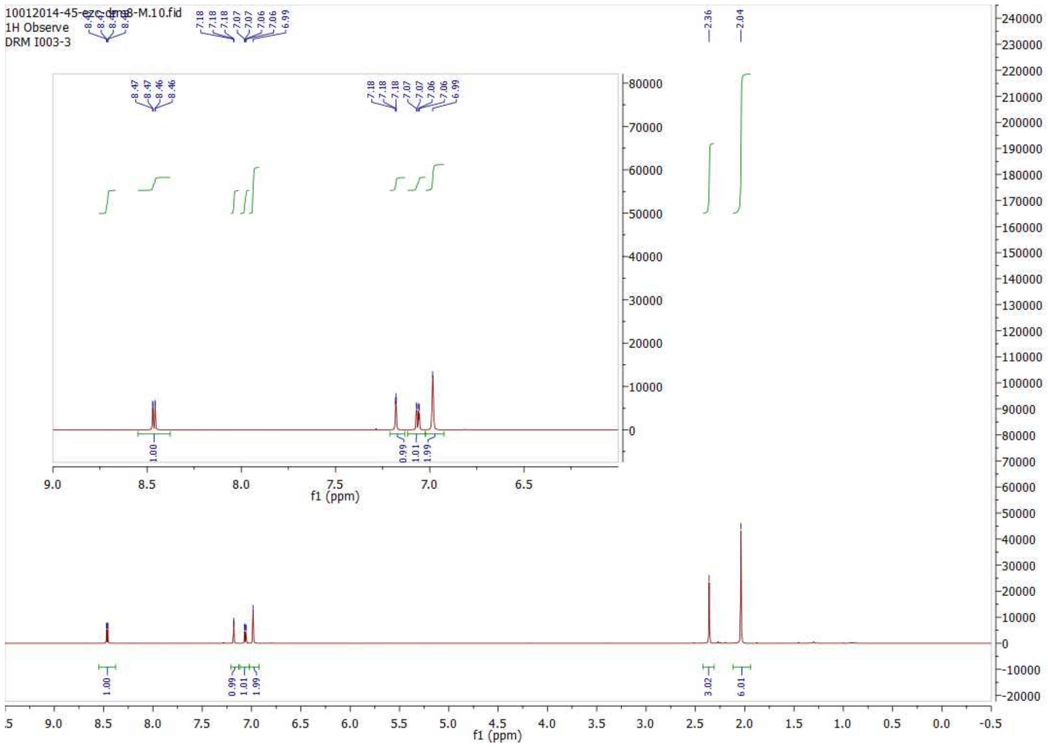

Figure **S1**. ^{1}H NMR spectra of 2-Chloro-4-(2,4,6-trimethylphenyl)pyridine in $CDCl_3$

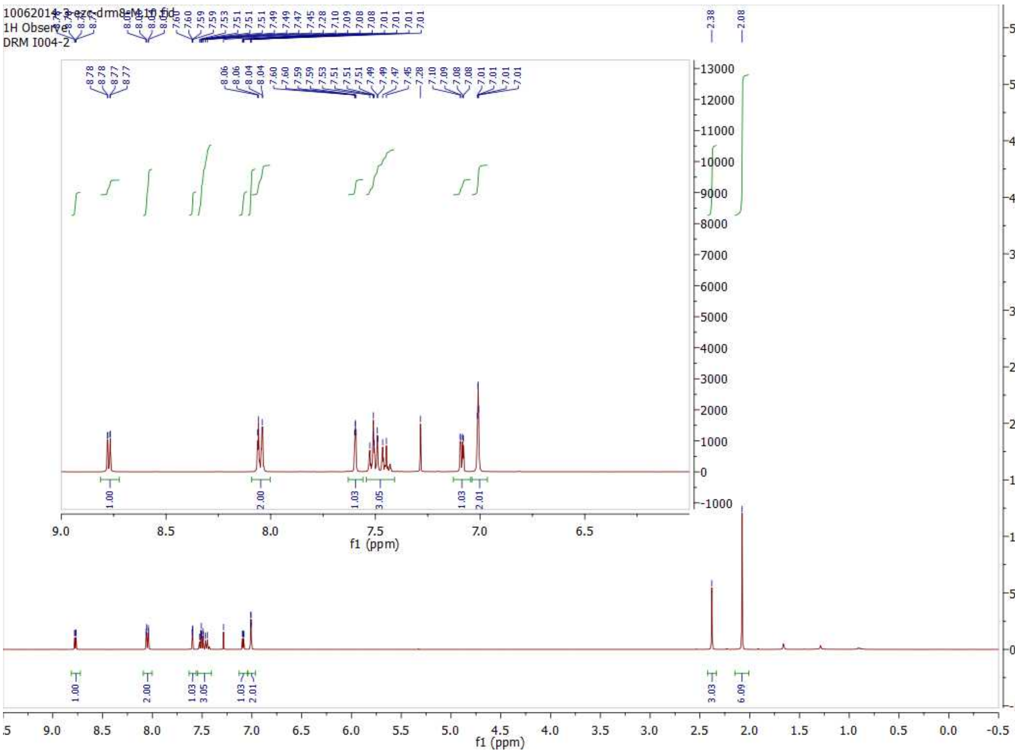

Figure **S2**. ^{1}H NMR spectra of **2-phenyl-4-(2,4,6-trimethylphenyl)pyridine(mesppy)** in CDCl$_3$.

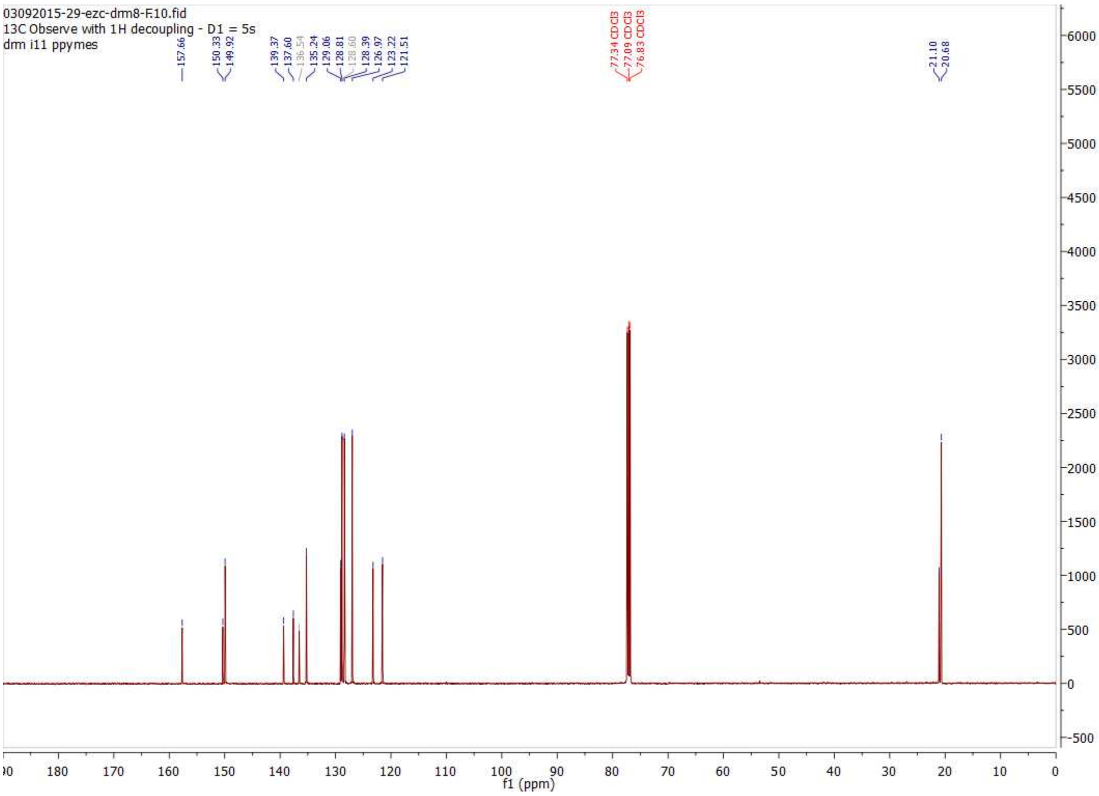

Figure **S3**. ^{13}C NMR spectra of **2-phenyl-4-(2,4,6-trimethylphenyl)pyridine(mesppy)** in CDCl$_3$.

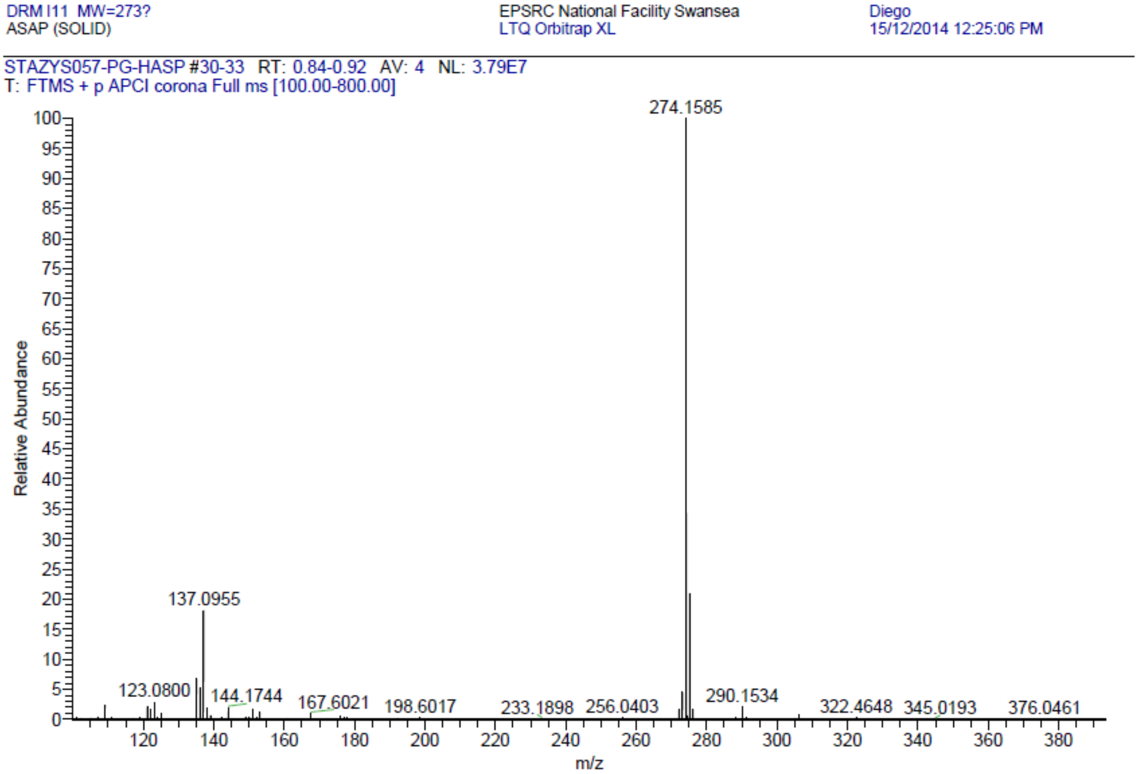

Figure **S4.** FTMS spectra of **2-phenyl-4-(2,4,6-trimethylphenyl)pyridine (mesppy)**.

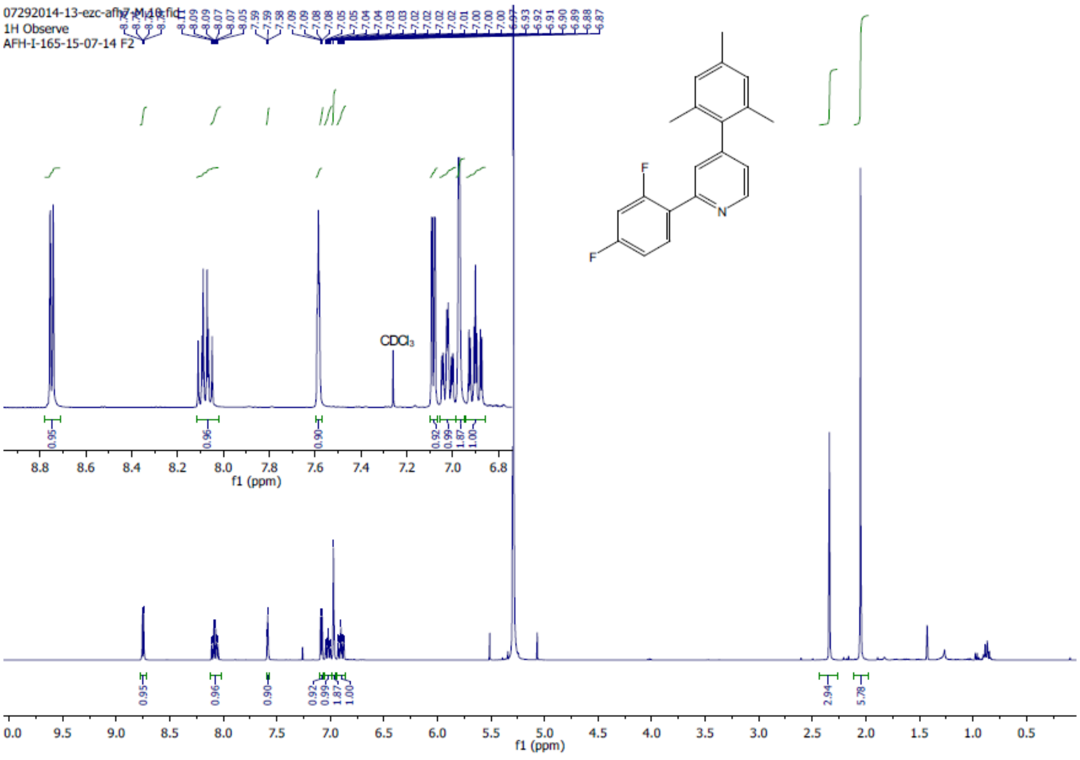

Figure **S5**. ^{1}H NMR spectrum of **2-(2,4-difluorophenyl)-4-(2,4,6-trimethylphenyl)pyridine (dFmesppy)** in CDCl$_3$.

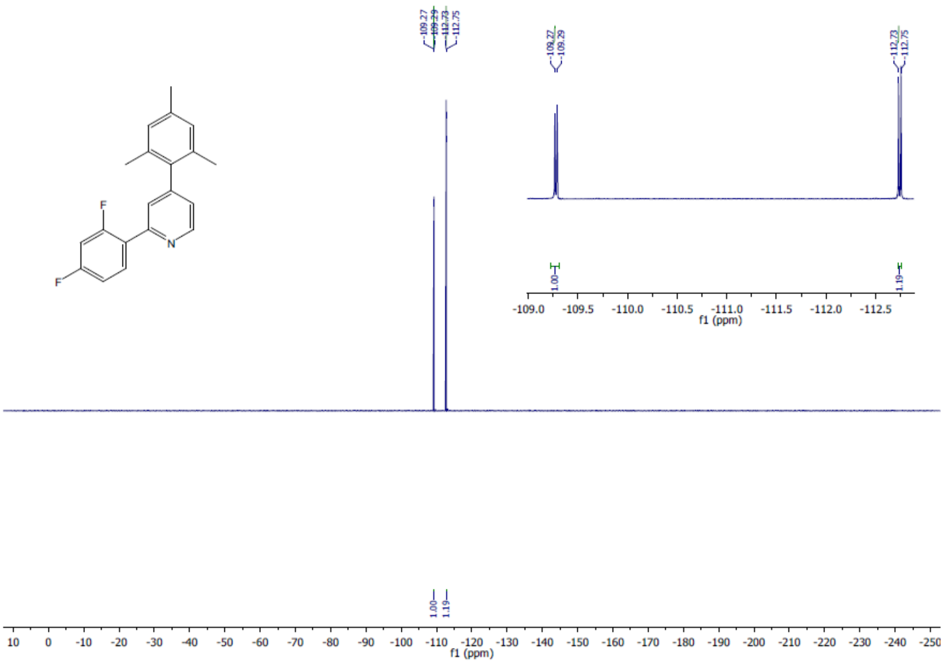

Figure **S6**. ^{19}F NMR spectrum of **2-(2,4-difluorophenyl)-4-(2,4,6-trimethylphenyl)pyridine (dFmesppy)** in $CDCl_3$.

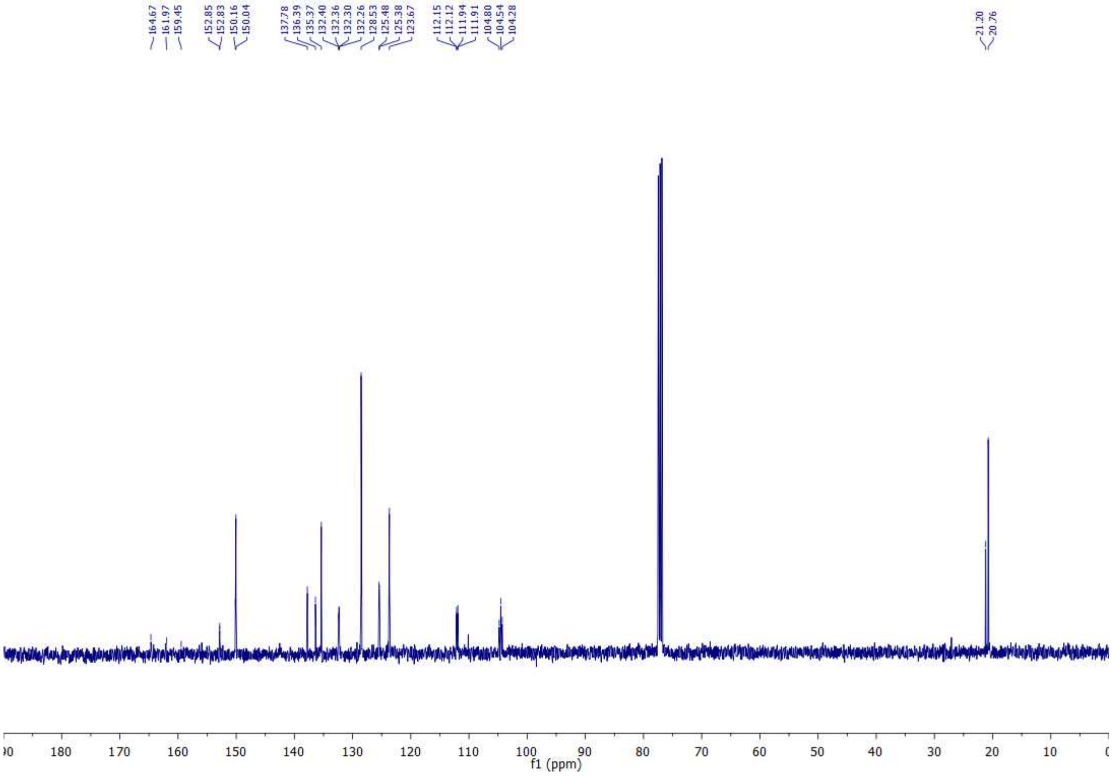

Figure **S7.** ^{13}C NMR spectrum of **2-(2,4-difluorophenyl)-4-(2,4,6-trimethylphenyl)pyridine (dFmesppy)** in $CDCl_3$.

Characterization of Iridium dimers.

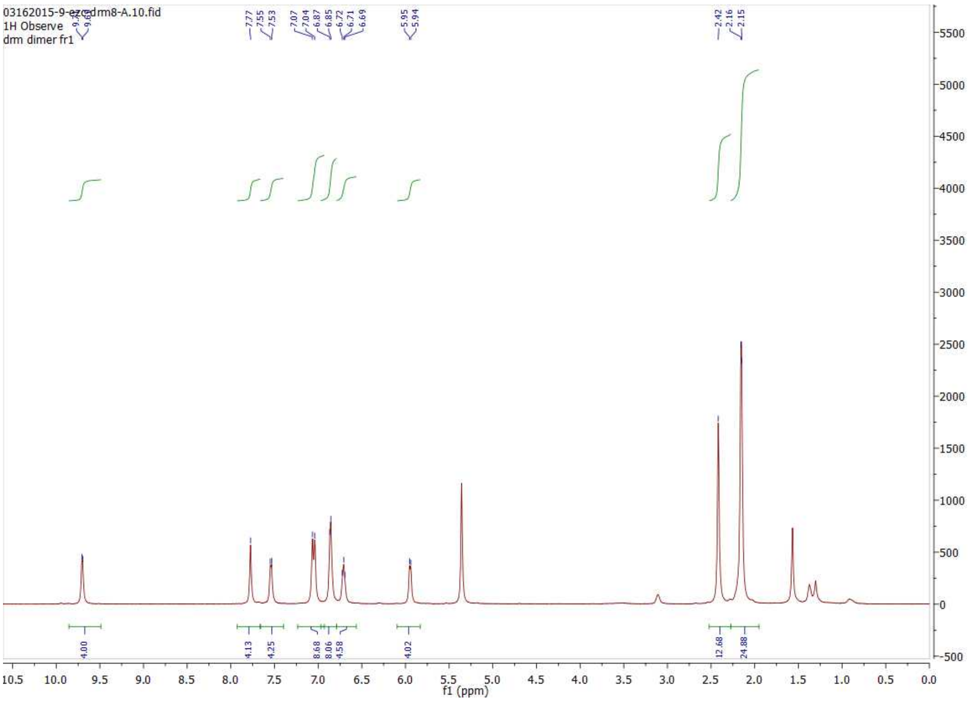

Figure **S8**. ^{1}H NMR spectrum of **tetrakis[2-(phenyl)-4-(2,4,6-trimethylphenyl)pyridinato-*N*,*C*$^{2'}$]-bis(*μ*-chloro)diiridium(III), [Ir(mesppy)$_2$(*μ*-Cl)]$_2$(D1)** in CD_2Cl_2.

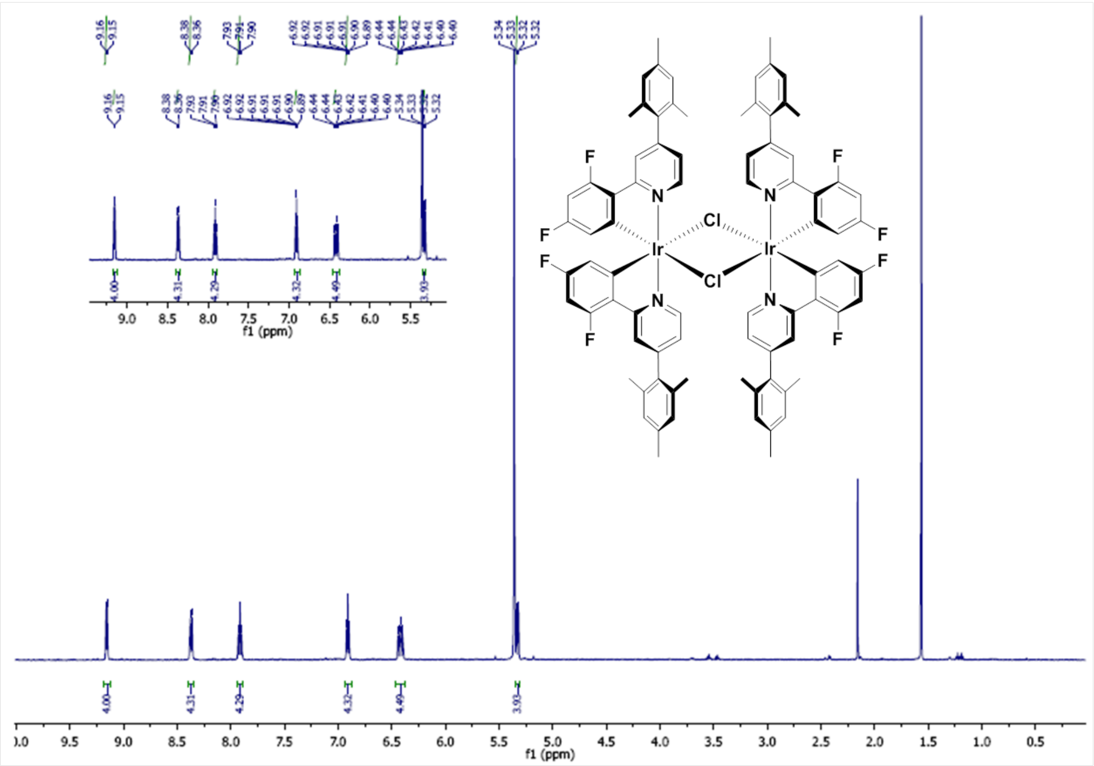

Figure **S9**. ^{1}H NMR spectrum of **tetrakis[2-(4’,6’-difluorophenyl)-4-(2,4,6-trimethylphenyl)pyridinato-*N*,*C*$^{2'}$]-bis(*μ*-chloro)diiridium(III)**, **[Ir(dFmesppy)$_2$(*μ*-Cl)]$_2$ (D2)** in CD_2Cl_2.

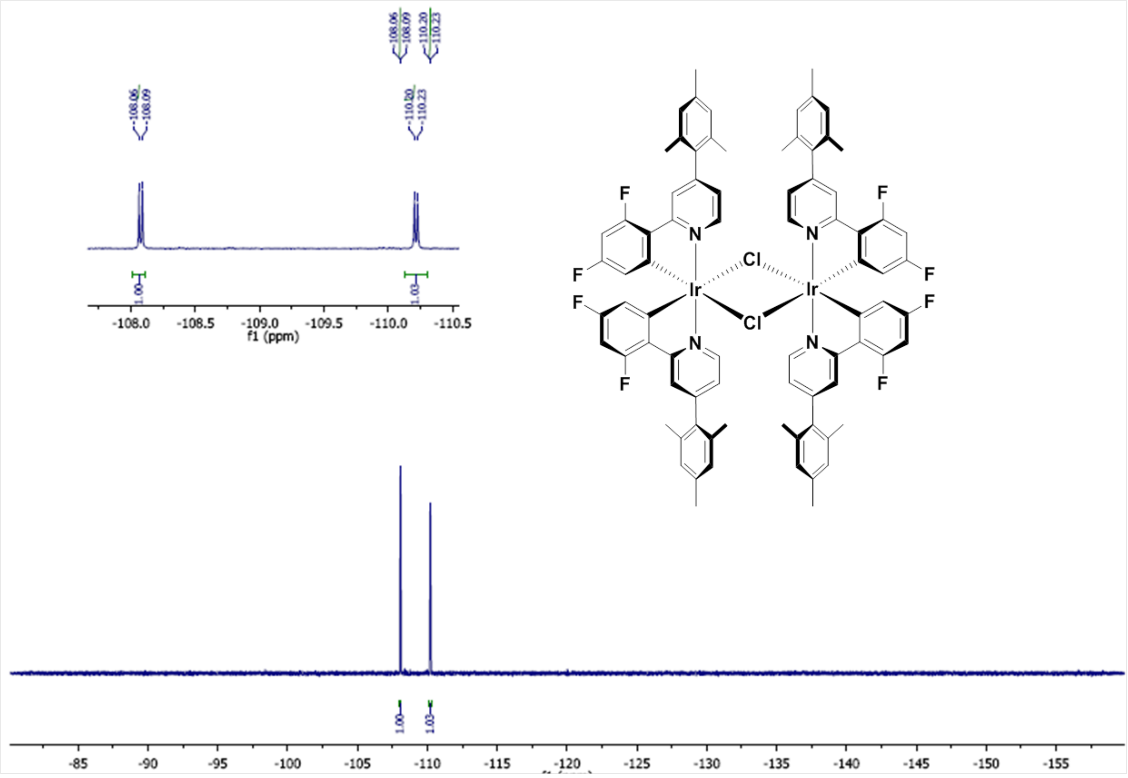

Figure **S10**. ^{19}F NMR spectrum of **tetrakis[2-(4',6'-difluorophenyl)-4-(2,4,6-trimethylphenyl)pyridinato-*N*,*C*$^{2'}$]-bis(*μ*-chloro)diiridium(III), [Ir(dFmesppy)$_2$(*μ*-Cl)]$_2$ (D2)** in CD$_2$Cl$_2$.

Characterization of [Ir(C^N)$_2$(N^N)]PF$_6$and ZnTPP complexes.

Iridium (III) bis[2-phenyl-4-(2,4,6-trimethylphenyl)pyridinato]-4,4':2',2'':4'',4'''-quaterpyridine hexafluorophosphate, [Ir(mesppy)$_2$(qpy)](PF$_6$) (1)

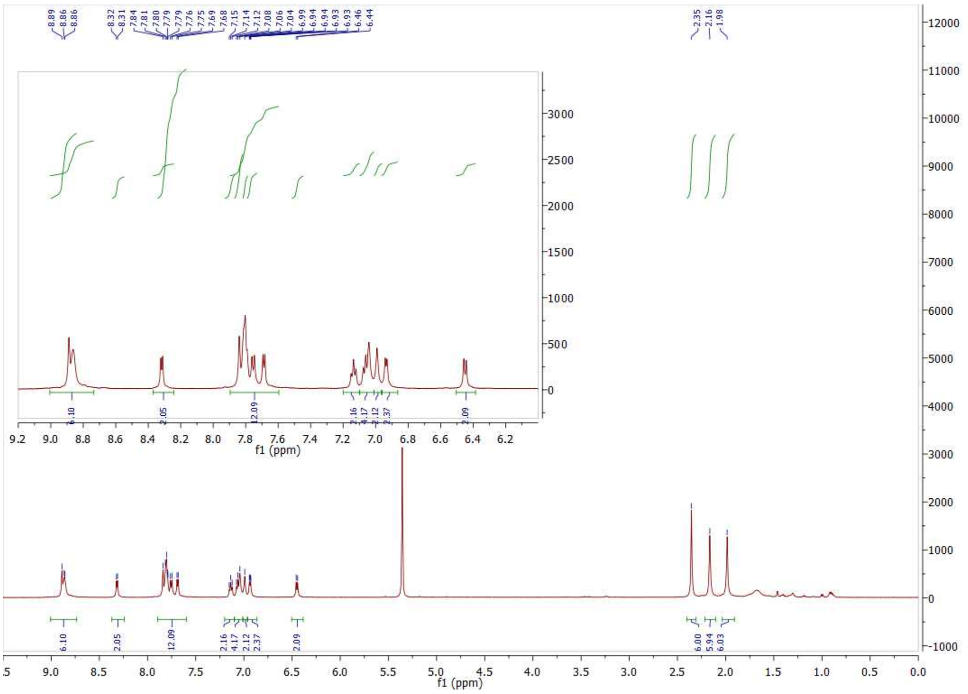

Figure **S11.** ^{1}H NMR spectrum of **[Ir(mesppy)$_2$(qpy)]PF$_6$ (1)** in CD$_2$Cl$_2$.

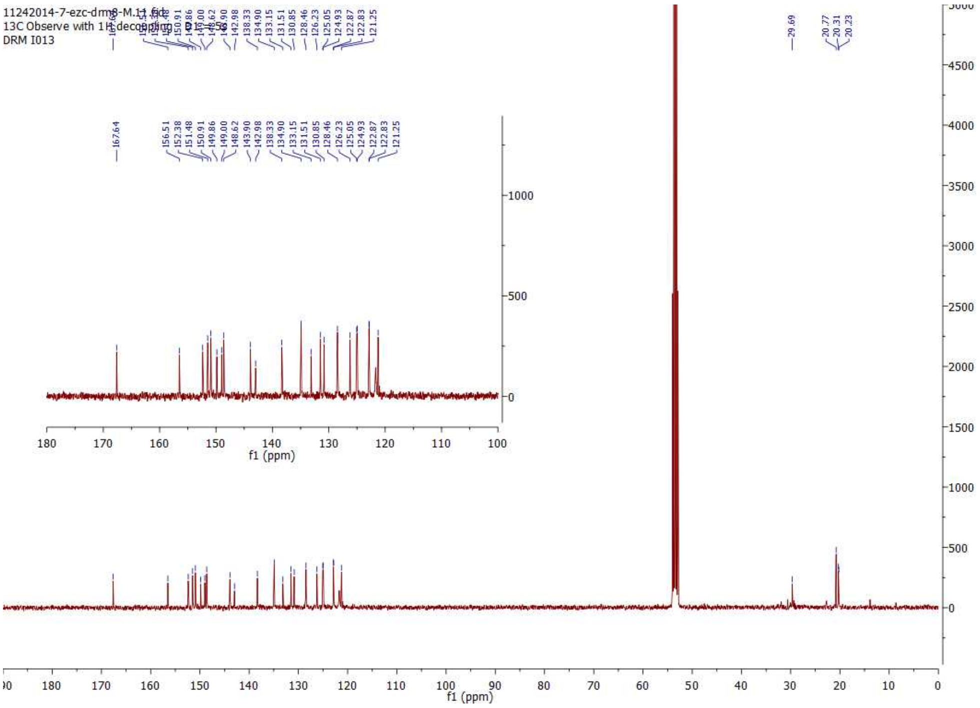

Figure **S12**. ^{13}C NMR spectrum of **[Ir(mesppy)$_2$(qpy)]PF$_6$ (1)** in CD$_2$Cl$_2$.

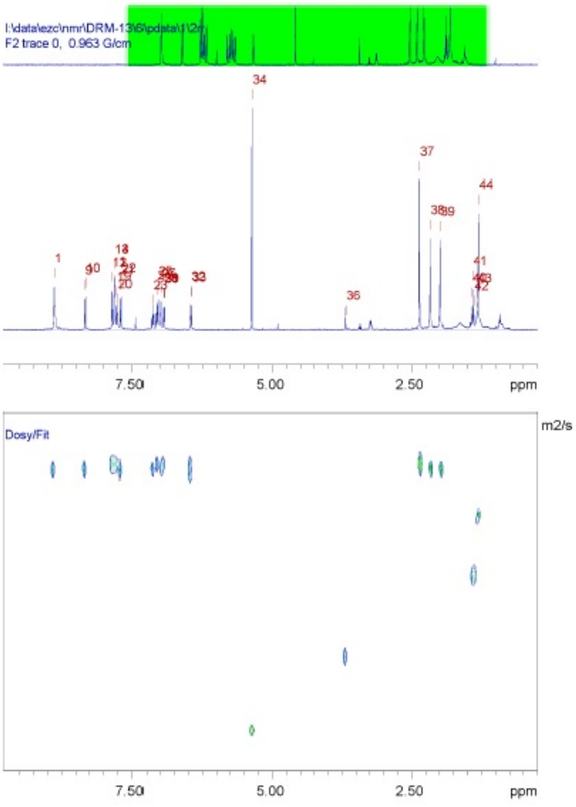

D = 1.32 x 10^{-9} m^2/s

Figure **S13.** DOSY NMRspectrum of **[Ir(mesppy)$_2$(qpy)]PF$_6$ (1)**.

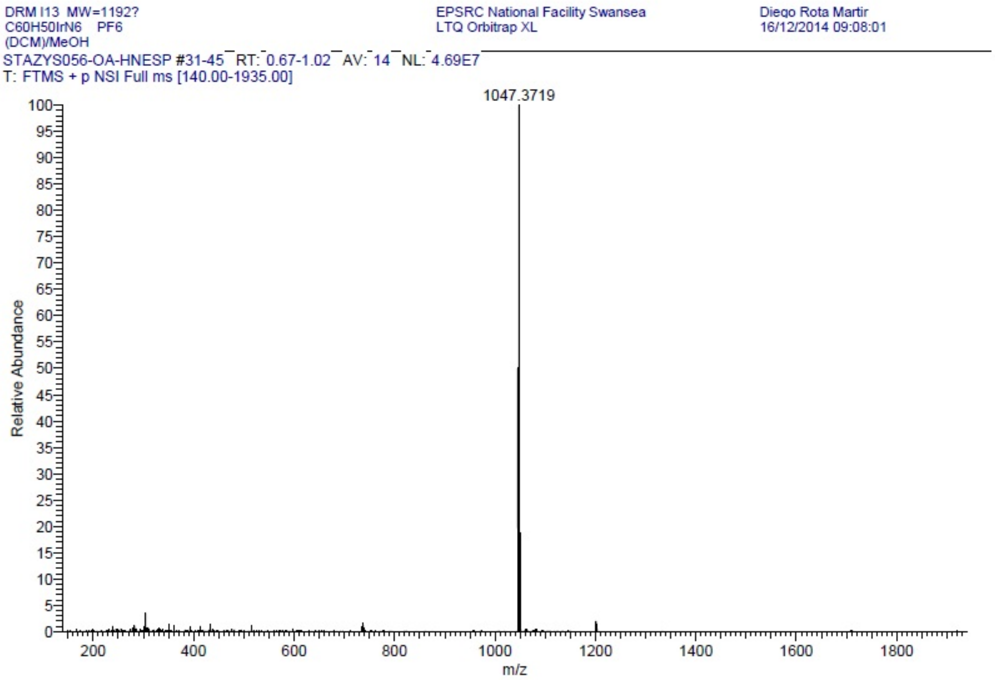

Figure **S14.** HR-MSspectrum of **[Ir(mesppy)$_2$(qpy)]PF$_6$ (1)**.

Iridium(III)bis[2-(2,4-difluoro)-phenyl-4-(2,4,6-trimethylphenyl)pyridinato]-4,4':2',2'':4'',4'''-quaterpyridine hexafluorophosphate, [Ir(dFmesppy)$_2$(qpy)](PF$_6$) (2)

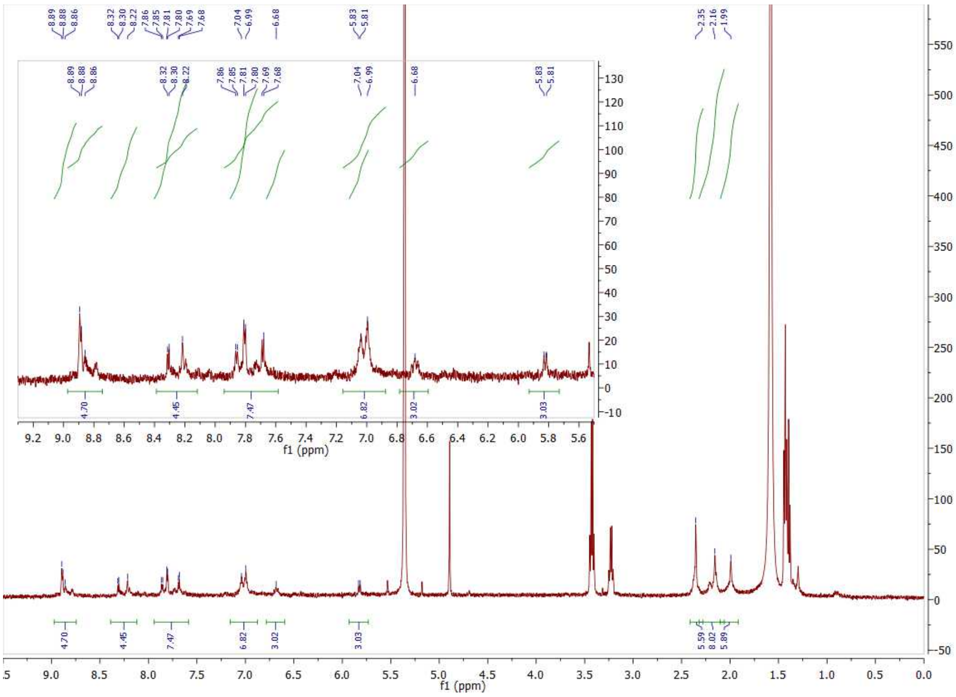

Figure **S15**. ^{1}H NMR spectrum of **[Ir(dFmesppy)$_2$(qpy)]PF$_6$ (2)** in CD$_2$Cl$_2$.

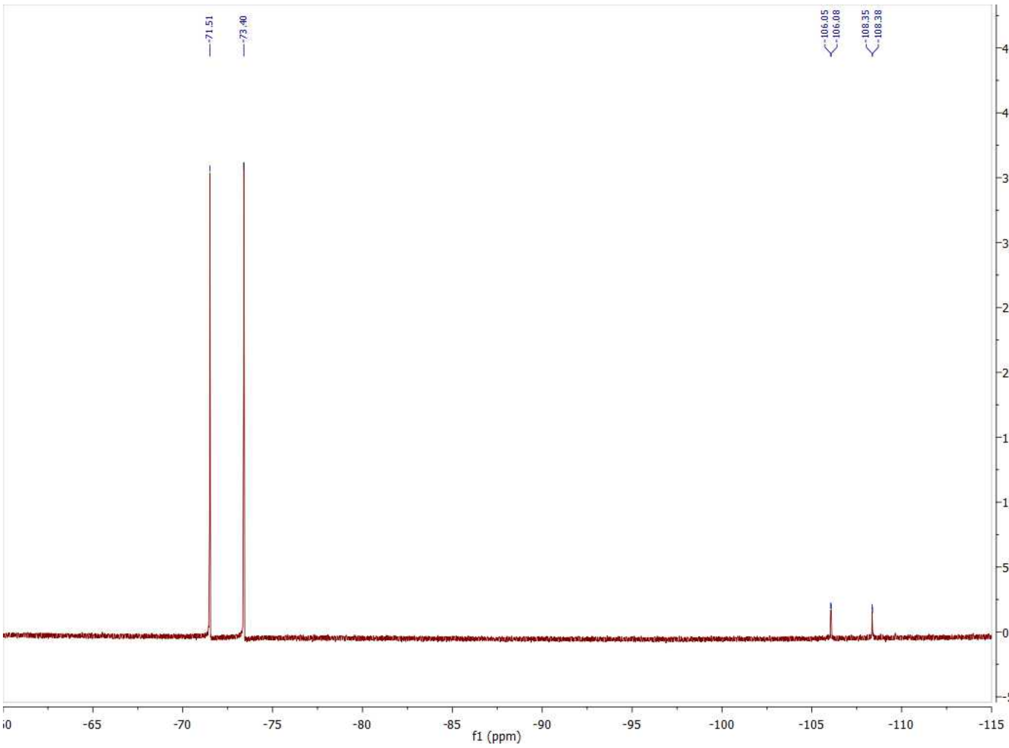

Figure **S16.** ^{19}FNMR spectrum of **[Ir(dFmesppy)$_2$(qpy)]PF$_6$ (2)** in CD$_2$Cl$_2$.

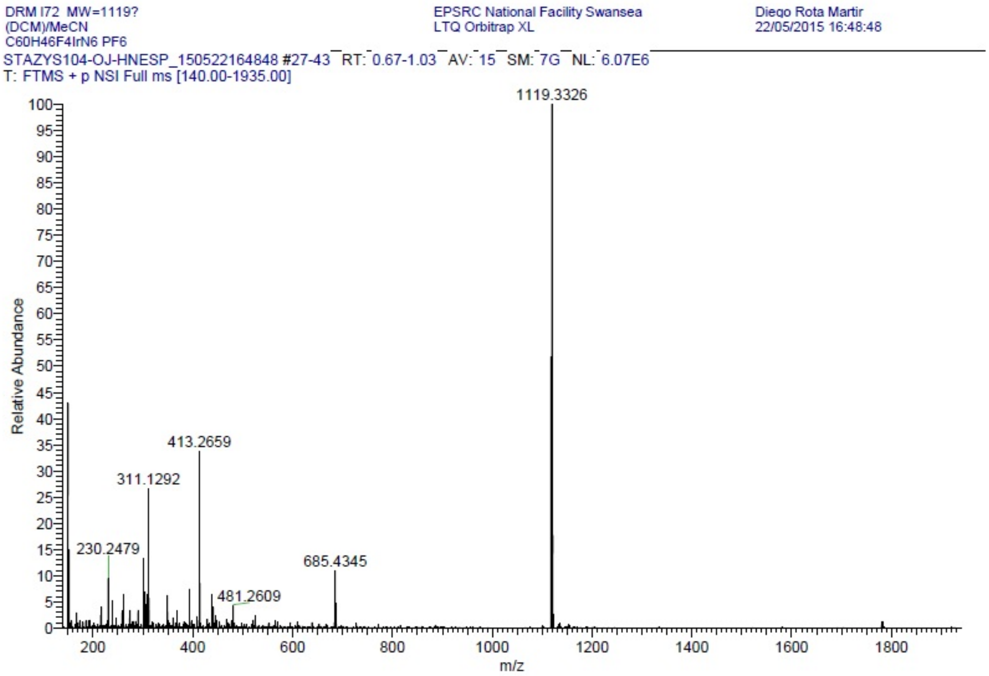

Figure **S17**. HRMS spectrum of **[Ir(dFmesppy)$_2$(qpy)]PF$_6$ (2)**.

Iridium(III)bis[2-phenyl-4-(2,4,6-trimethylphenyl)pyridinato]-4,4'-di-*tert*-butyl-2,2'-bipyridinehexafluorophosphate, [Ir(ppymes)$_2$(dtbubpy)](PF$_6$) (3)

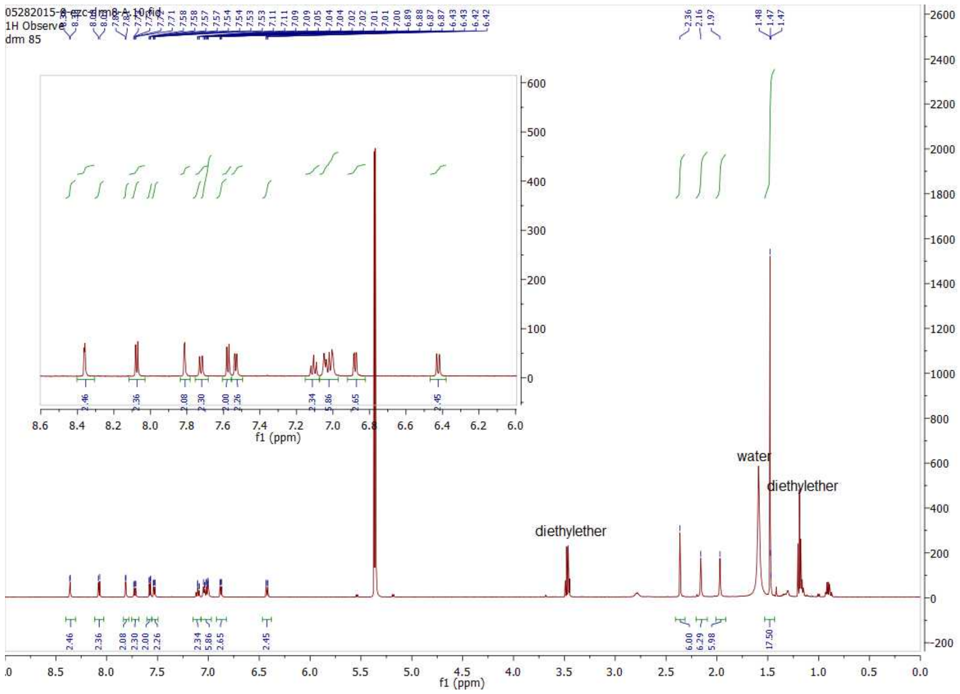

Figure **S18**. ^{1}H NMR spectrum of **[Ir(mesppy)$_2$(dtbubpy)]PF$_6$ (3)** in CD$_2$Cl$_2$.

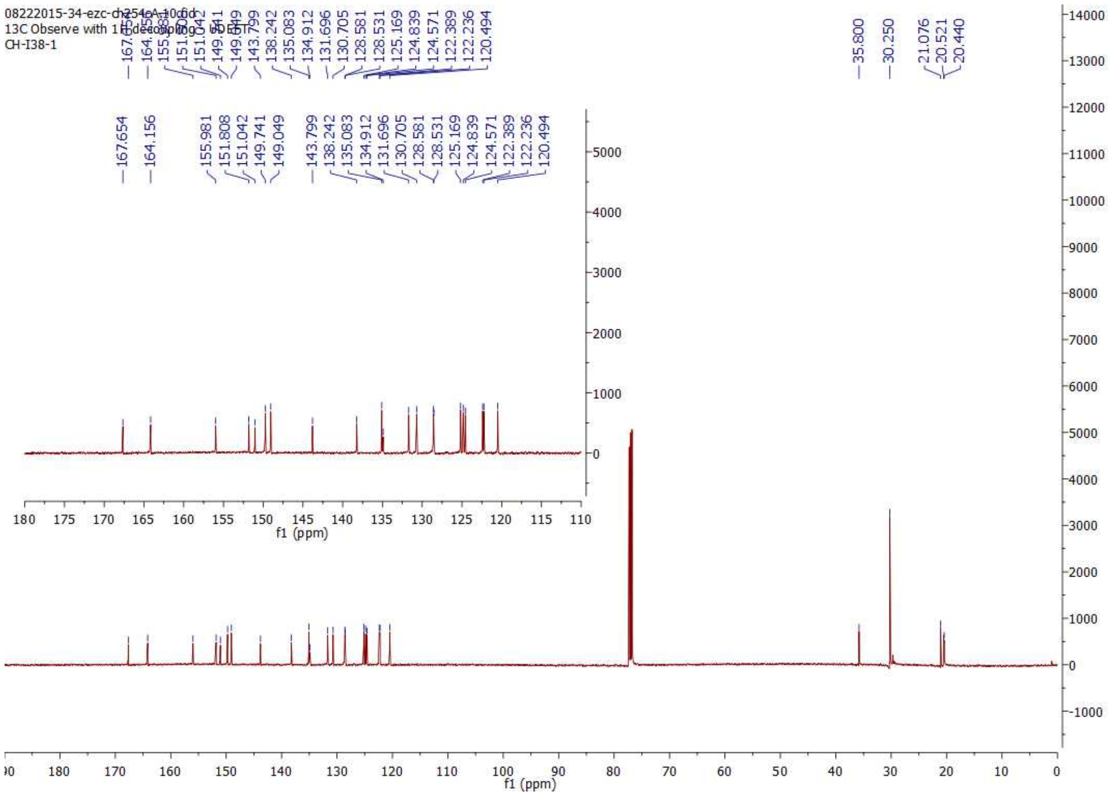

Figure **S19**. ^{13}C NMR spectrum of **[Ir(mesppy)$_2$(dtbubpy)](PF$_6$) (3)** in CD$_2$Cl$_2$.

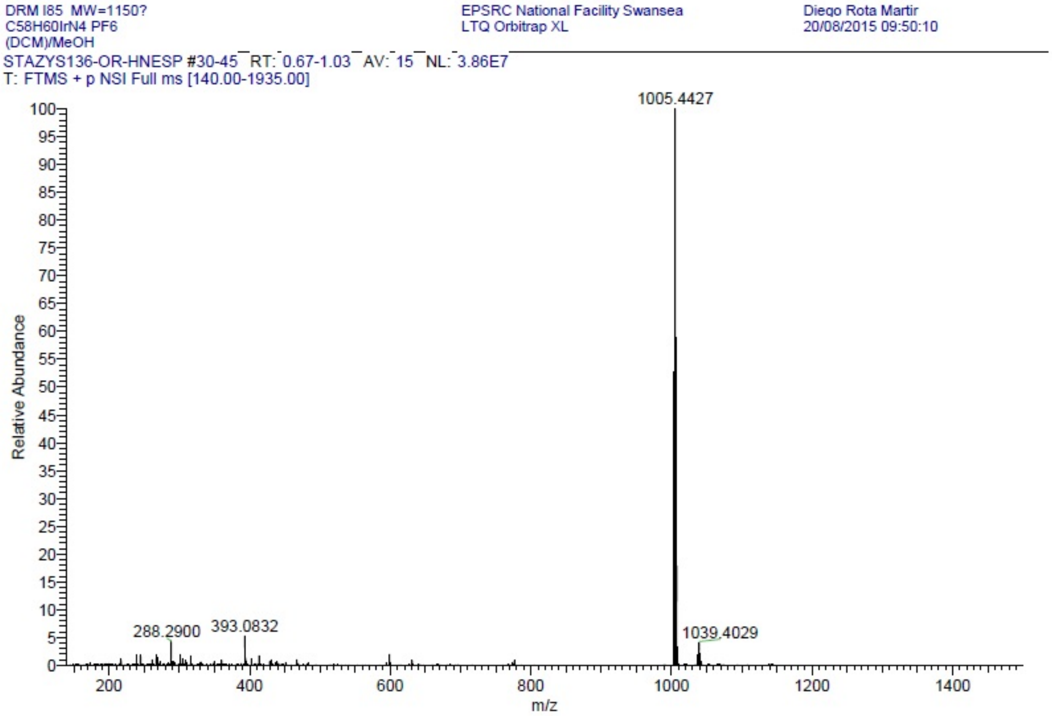

Figure **S20**. HRMS spectrum of **[Ir(mesppy)$_2$(dtbubpy)]PF$_6$ (3)**.

zinc tetraphenylphorphyrin(ZnTPP)

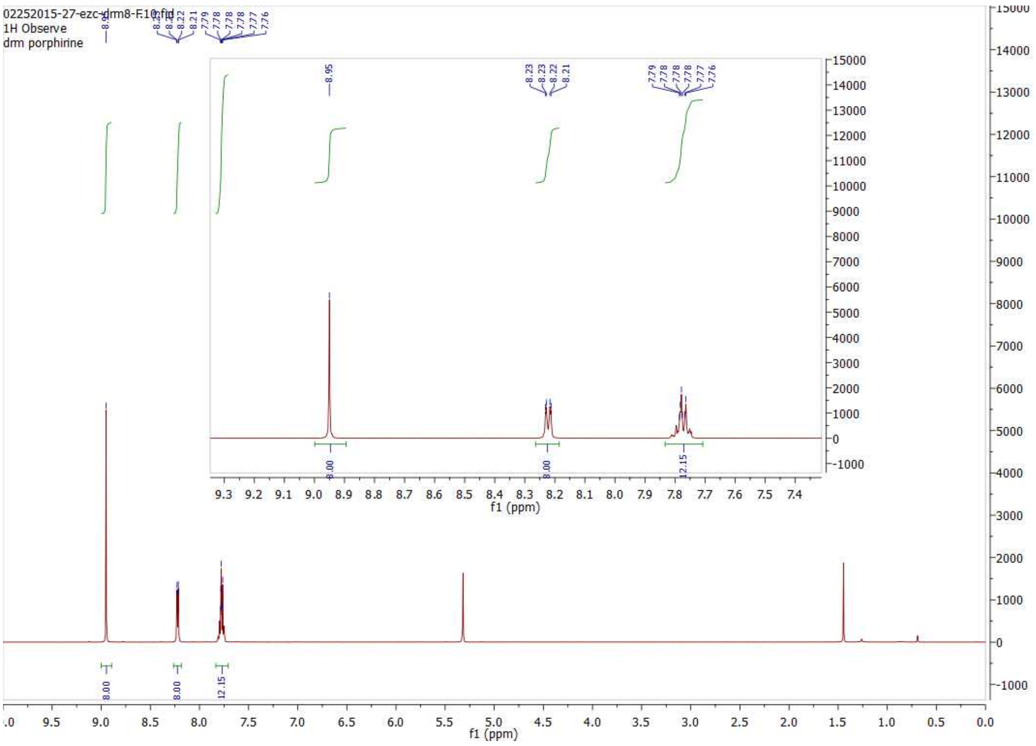

Figure **S21**. ^{1}H NMR spectrum of **ZnTPP** in CD_2Cl_2.

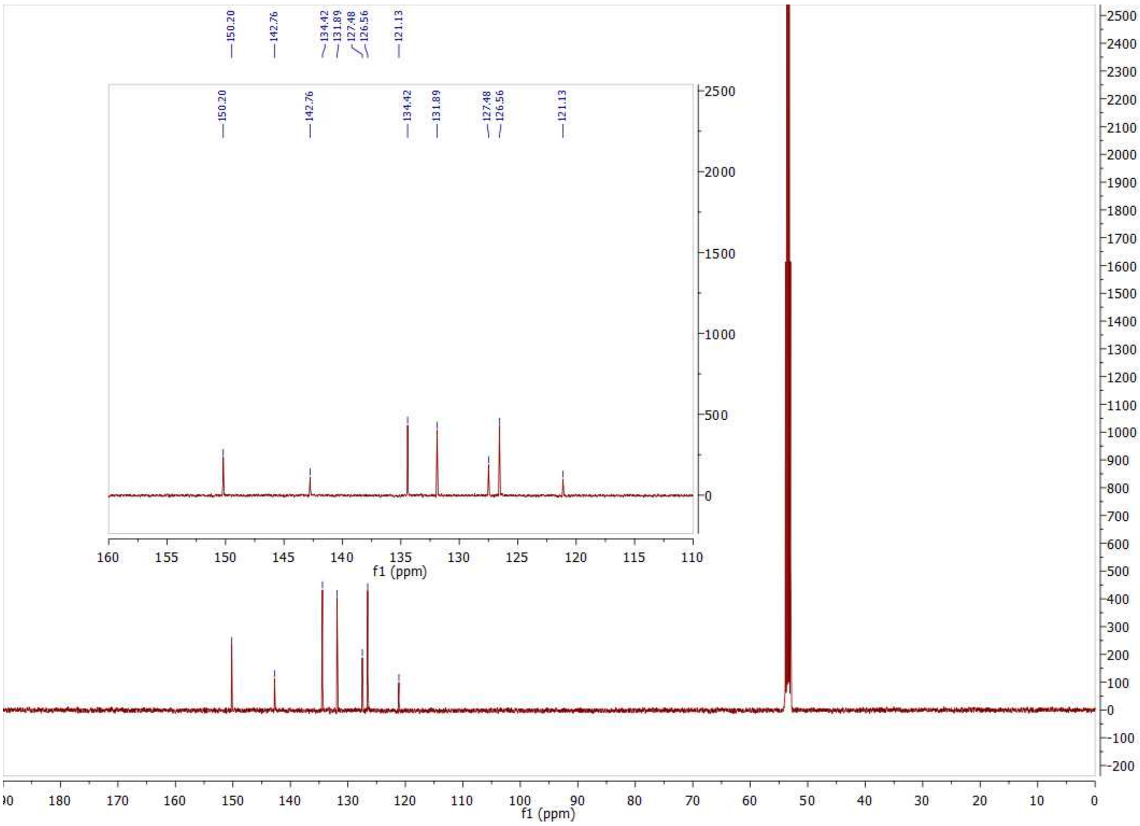

Figure **S22**. ^{13}C NMR spectrum of **ZnTPP** in CD_2Cl_2.

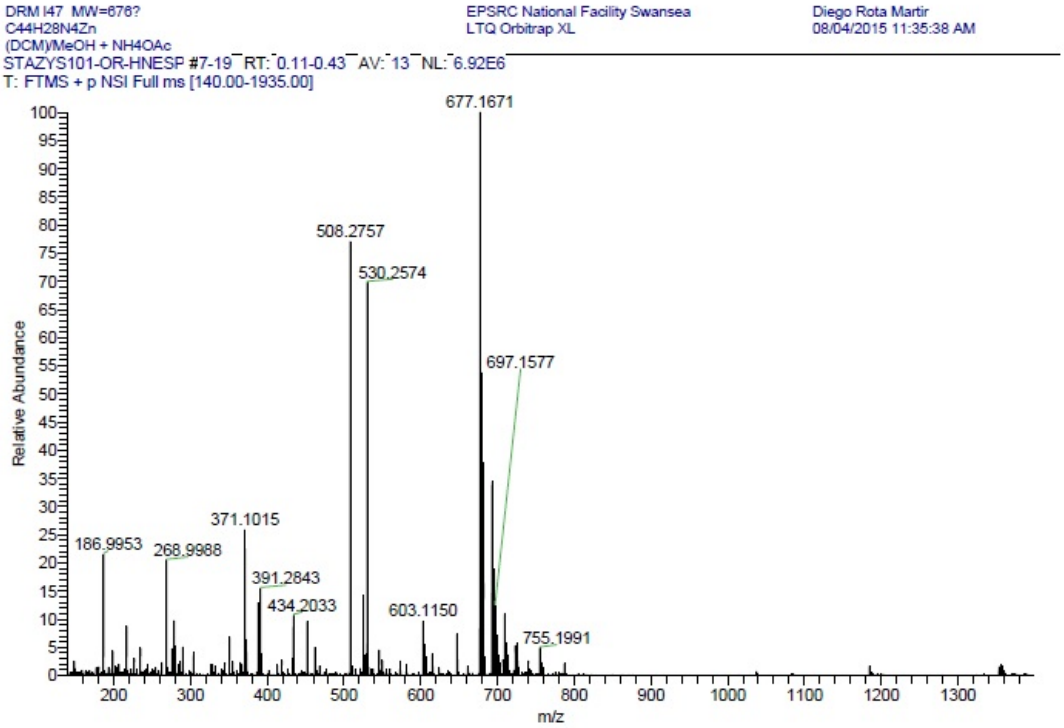

Figure **S23**. HRMS spectrum of **ZnTPP**

Characterization of [Ir(C^N)$_2$(N^N)]PF$_6$– ZnTPP assemblies.

Iridium (III) bis[2-phenyl-4-(2,4,6-trimethylphenyl)pyridinato]-4,4':2',2'':4'',4'''-quaterpyridine hexafluorophosphate, [Ir(mesppy)$_2$(qpy)](PF$_6$) : zinc tetraphenylphorphyrin(ZnTPP) 1:1 (1a)

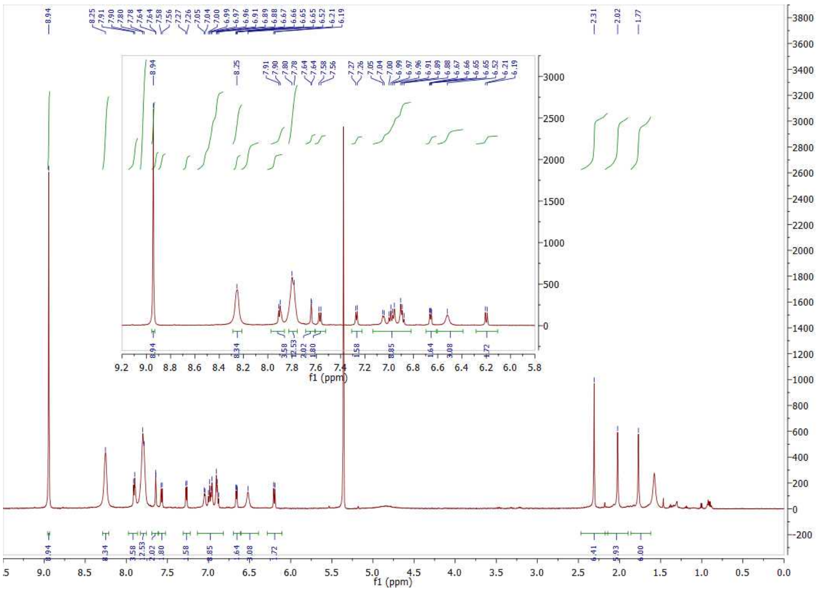

Figure **S24**. ^{1}H NMR spectrum of **1a** [Ir(mesppy)$_2$(qpy)]PF$_6$: ZnTPP 1:1 ratio in CD$_2$Cl$_2$.

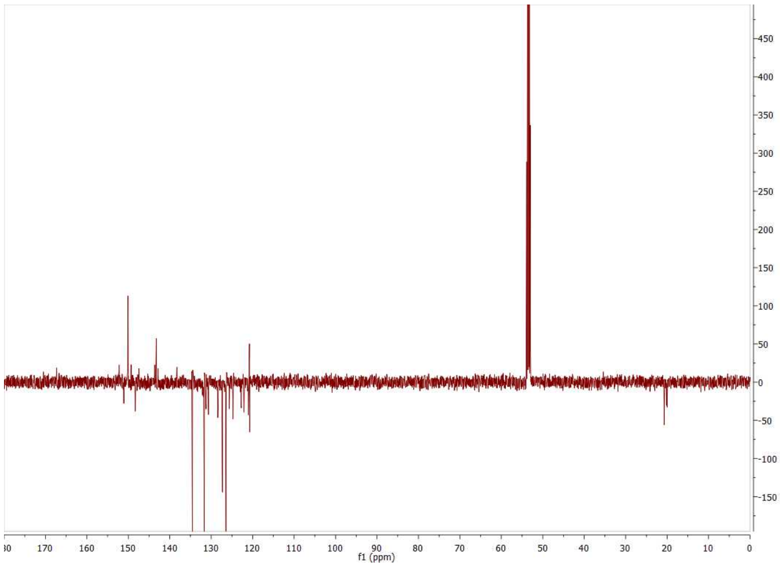

Figure **S25**. ^{13}C NMR spectrum of **1a** [Ir(mesppy)$_2$(qpy)]PF$_6$: ZnTPP 1:1 ratio in CD$_2$Cl$_2$.

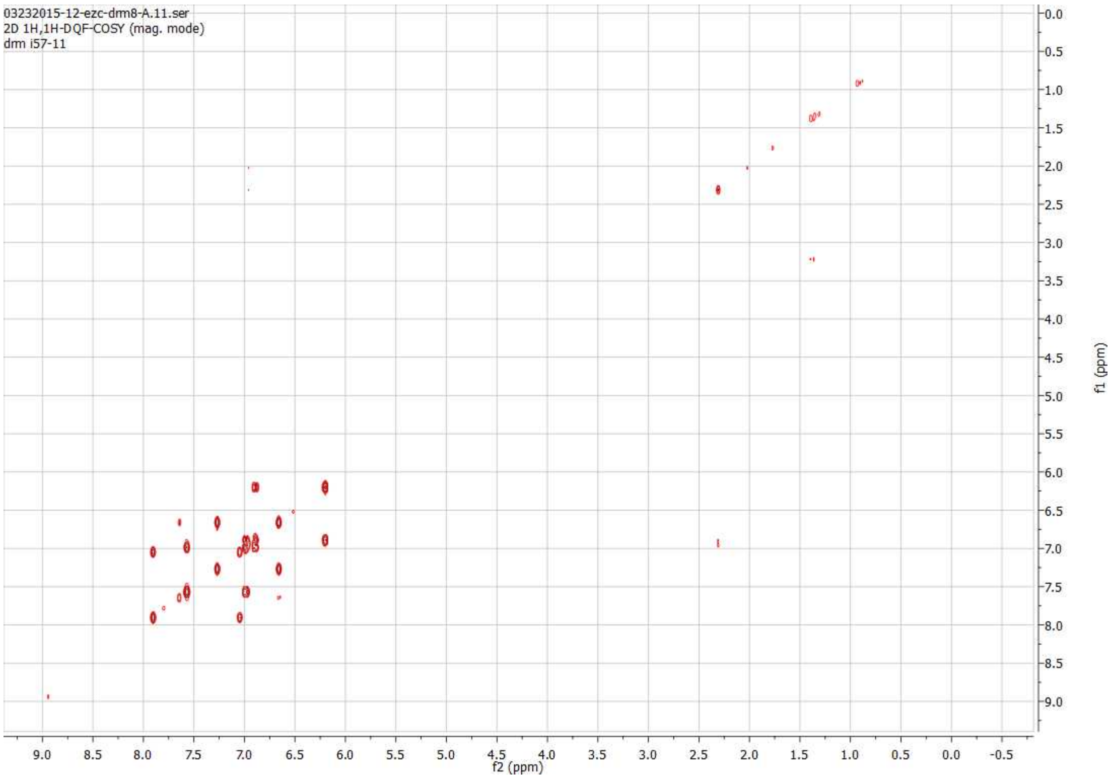

Figure **S26.** 2D COSY NMR spectrum of **1a** [Ir(mesppy)$_2$(qpy)]PF$_6$: ZnTPP 1:1 ratio in CD$_2$Cl$_2$.

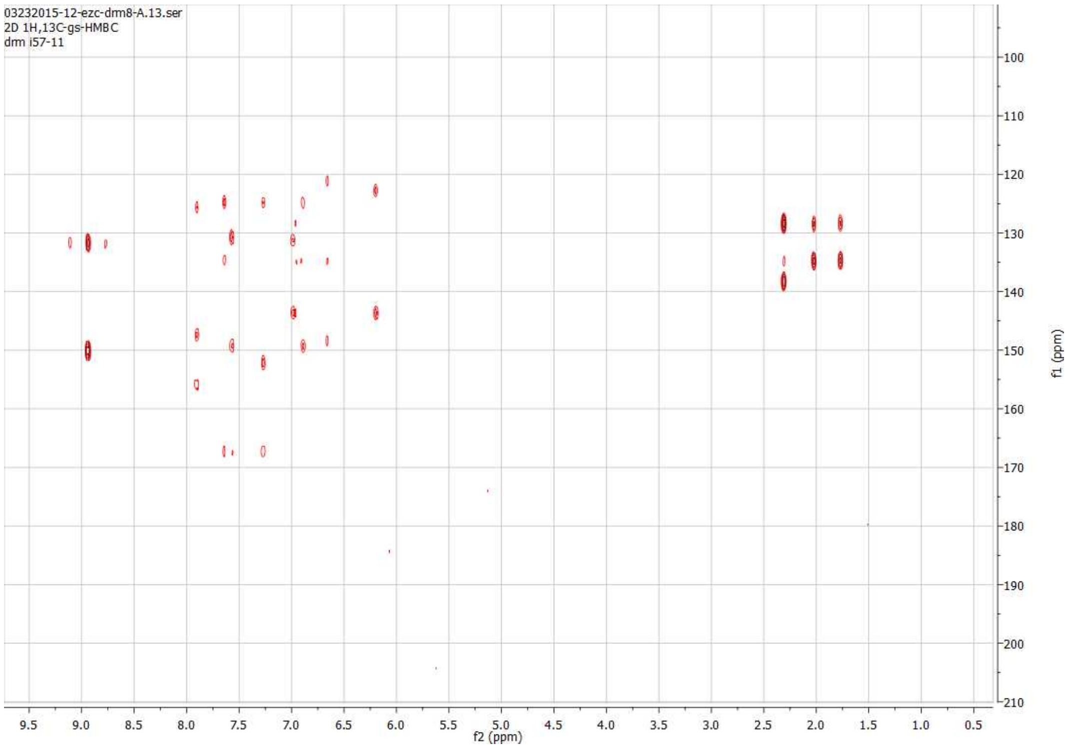

Figure **S27**. 2D HMBC NMR spectrum of **1a** [Ir(mesppy)$_2$(qpy)]PF$_6$: ZnTPP 1:1 ratio in CD$_2$Cl$_2$.

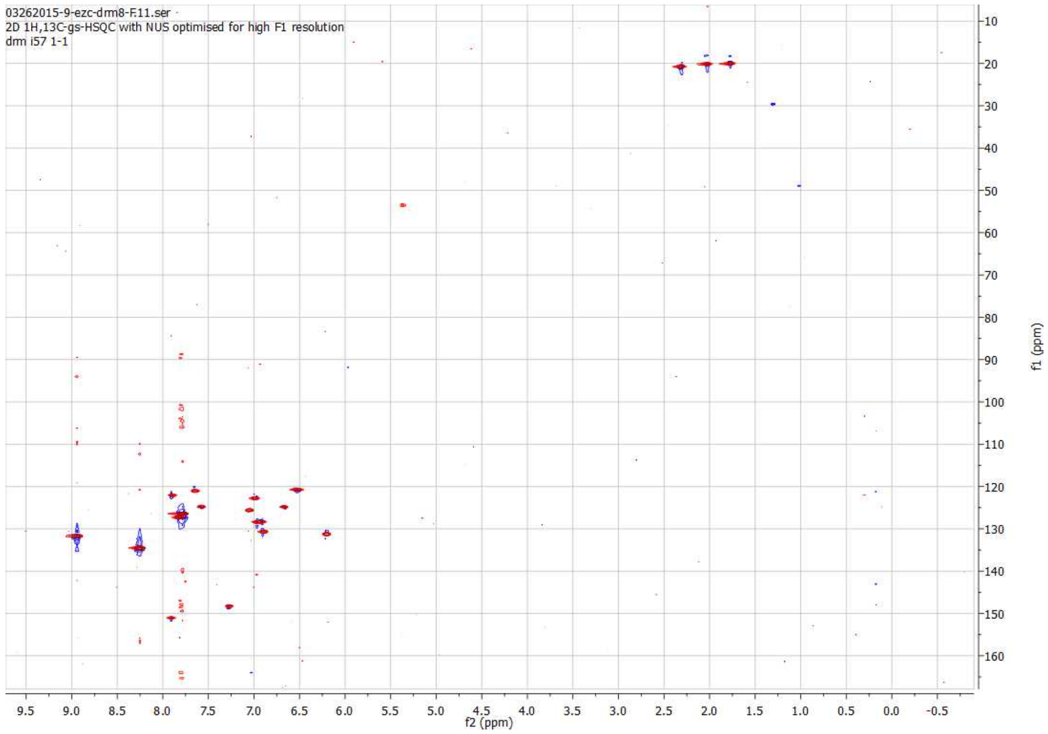

Figure **S28**. 2D HSQC NMR spectrum of **1a** [Ir(mesppy)$_2$(qpy)]PF$_6$: ZnTPP 1:1 ratio in CD$_2$Cl$_2$.

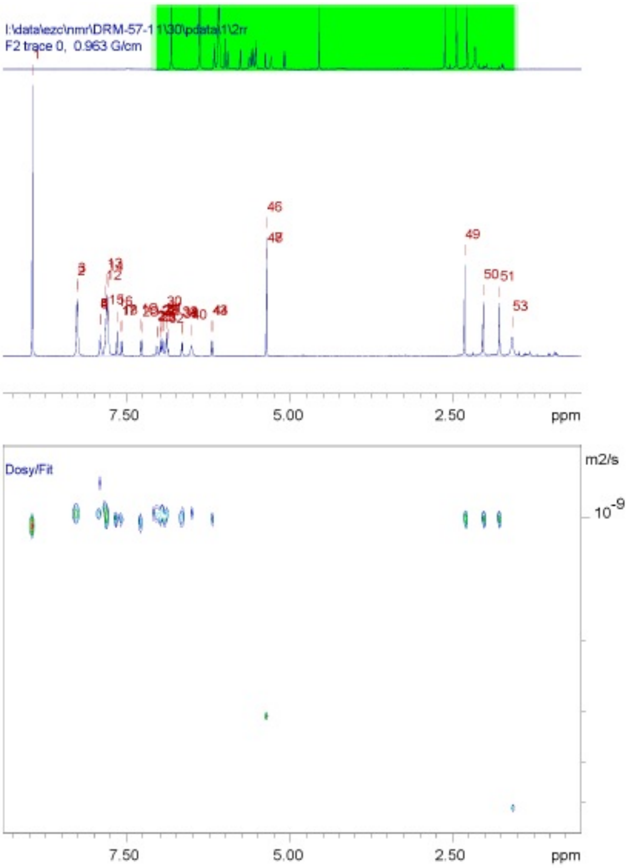

D = 1.37 x 10^{-9} m^2/s

Figure **S29**. DOSY NMR spectrum of **1a** [Ir(mesppy)$_2$(qpy)]PF$_6$: ZnTPP 1:1 ratio in CD$_2$Cl$_2$.

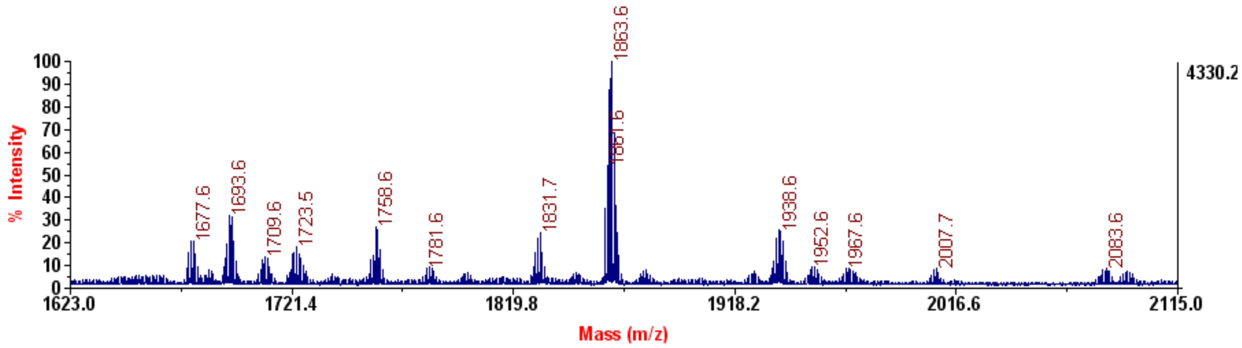

Figure **S30**. MALDI MS spectrum of **1a** [Ir(mesppy)$_2$(qpy)]PF$_6$: ZnTPP 1:1 ratio.

Iridium (III) bis[2-phenyl-4-(2,4,6-trimethylphenyl)pyridinato]-4,4':2',2'':4'',4'''-quaterpyridine hexafluorophosphate, [Ir(mesppy)$_2$(qpy)](PF$_6$) : zinc tetraphenylphorphyrin(ZnTPP) 1:2 (1b)

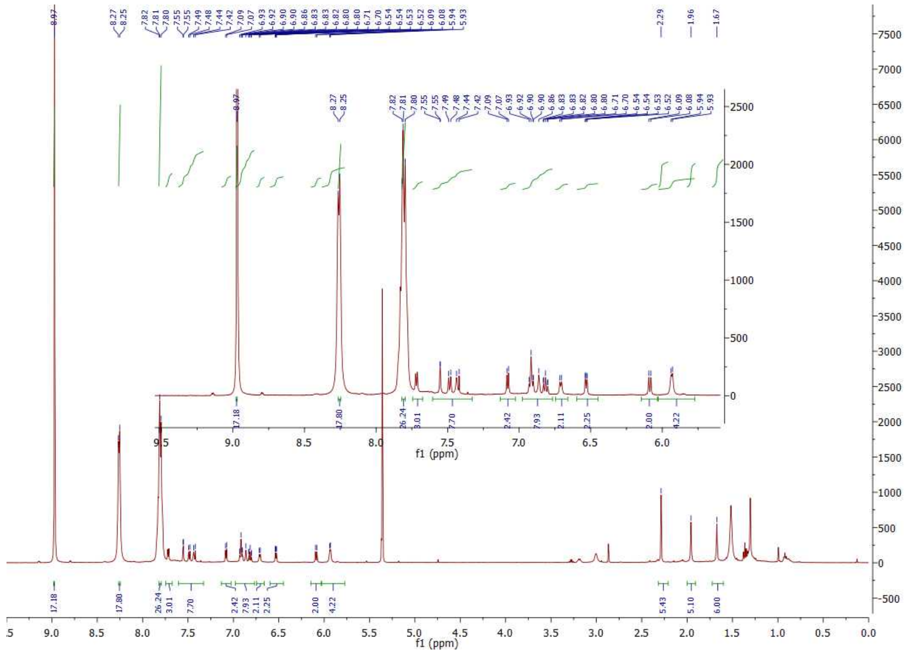

Figure **S31**. ^{1}H NMR spectrum of **1b** [Ir(mesppy)$_2$(qpy)]PF$_6$ + excess of ZnTPP in CD_2Cl_2.

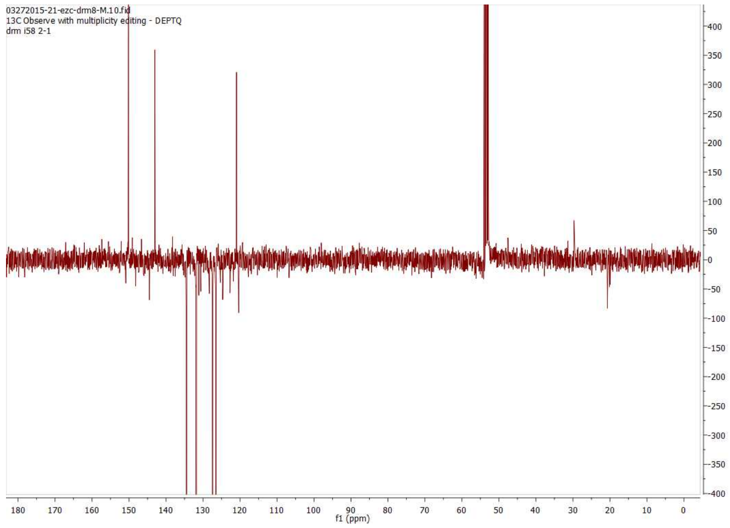

Figure **S32**. ^{13}C NMR spectrum of **1b** [Ir(mesppy)$_2$(qpy)]PF$_6$: ZnTPP 1:2 ratio in CD_2Cl_2.

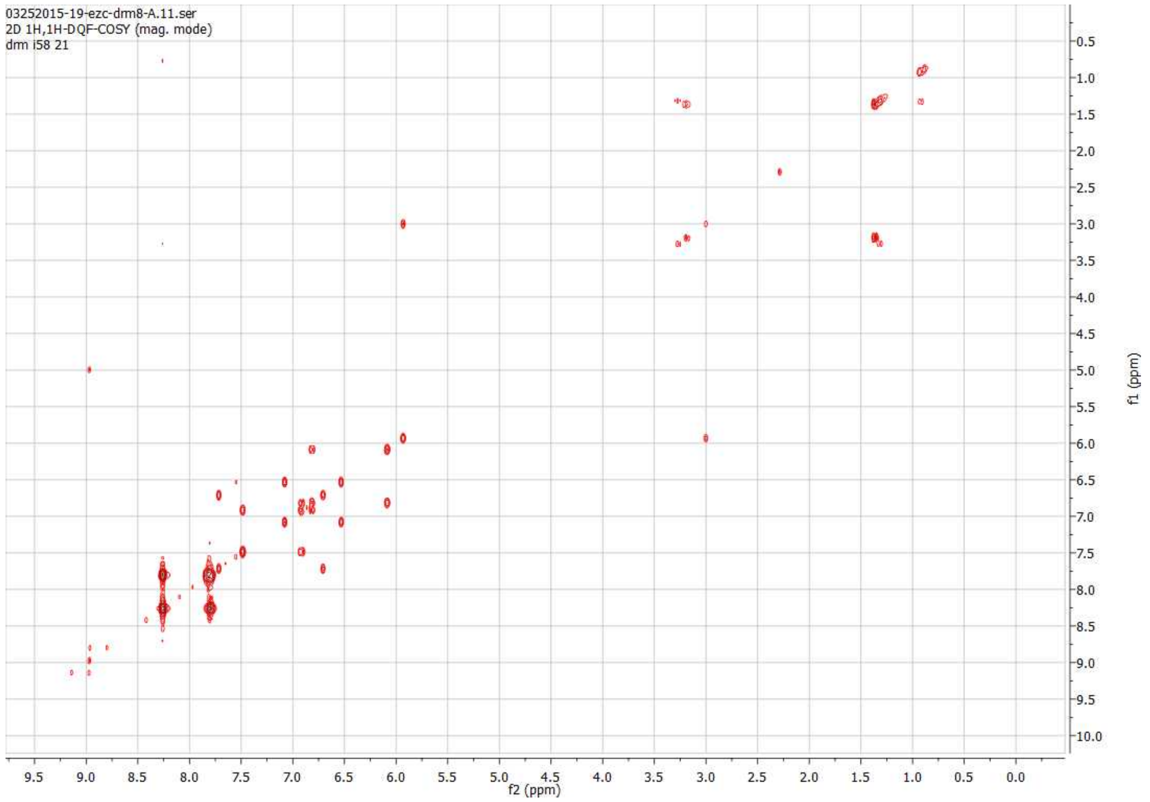

Figure **S33**. 2D COSY NMR spectrum of **1b** [Ir(mesppy)$_2$(qpy)]PF$_6$: ZnTPP 1:2 ratio in CD_2Cl_2.

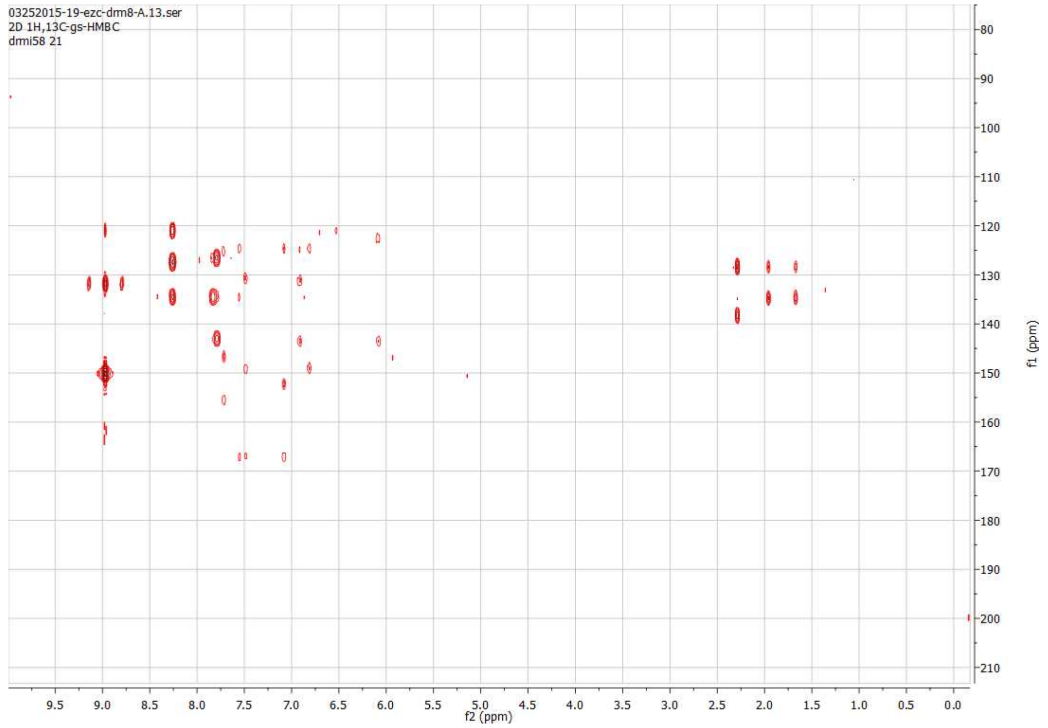

Figure **S34**. 2D HMBC NMR spectrum of **1b** [Ir(mesppy)$_2$(qpy)]PF$_6$: ZnTPP 1:2 ratio in CD$_2$Cl$_2$.

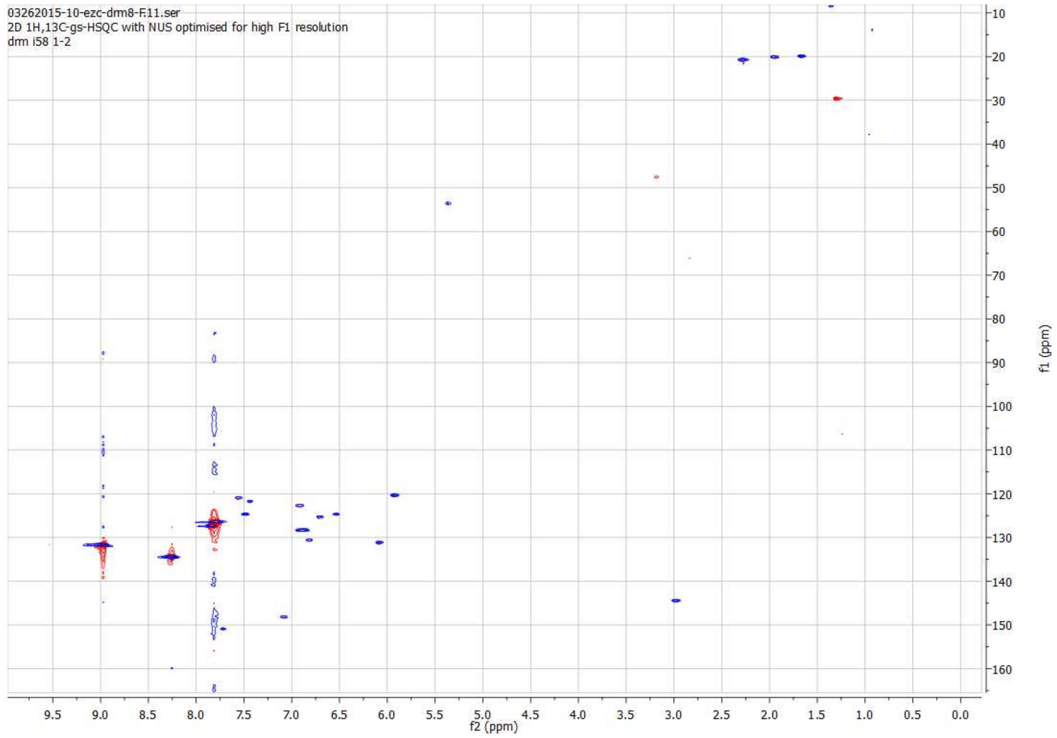

Figure **S35**. 2D HSQC NMR spectrum of **1b** [Ir(mesppy)$_2$(qpy)]PF$_6$: ZnTPP 1:2 ratio in CD$_2$Cl$_2$.

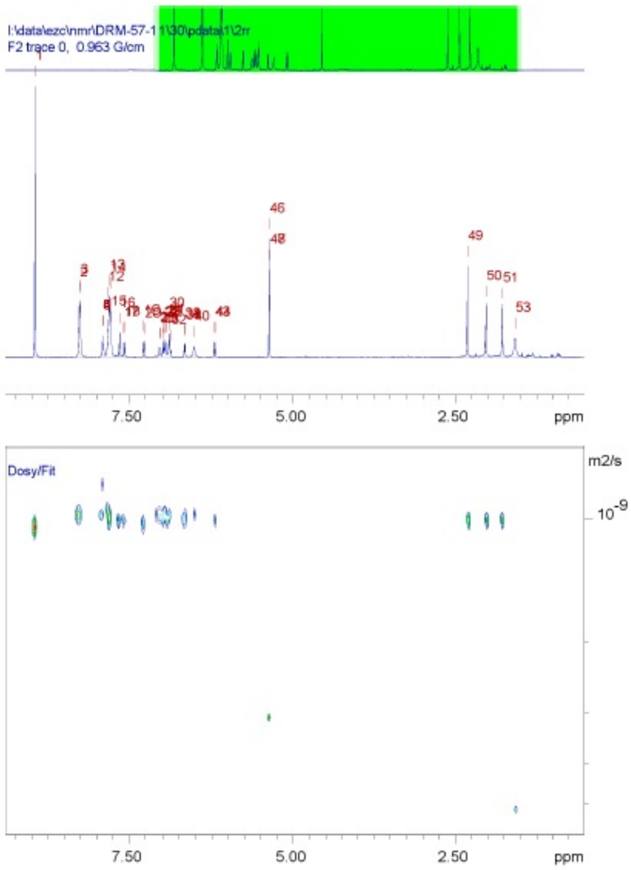

D = 1.39 x 10^{-9} m^2/s

Figure **S36**. DOSY NMR spectrum of **1b** [Ir(mesppy)$_2$(qpy)]PF$_6$: ZnTPP 1:2 ratio in CD_2Cl_2.

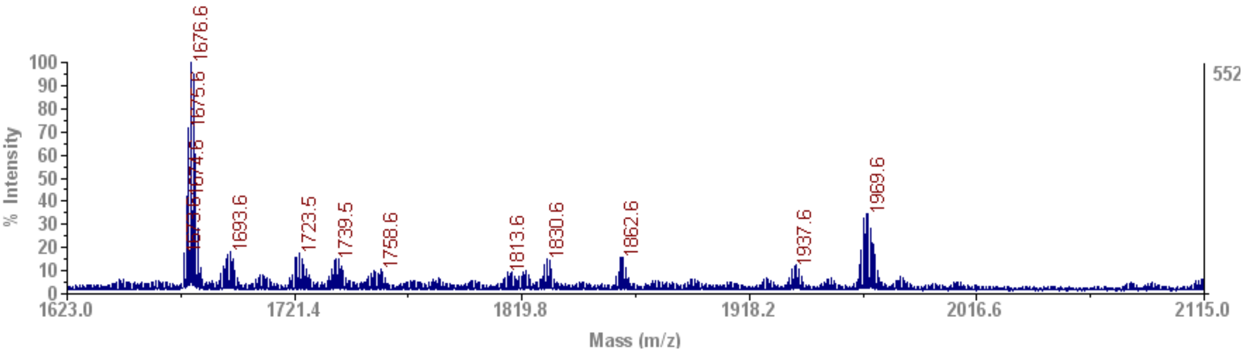

Figure **S37**. MALDI MS spectrum of **1b** [Ir(mesppy)$_2$(qpy)]PF$_6$: ZnTPP 1:2 ratio.

Iridium(III)bis[2-(2,4-difluoro)-phenyl-4-(2,4,6-trimethylphenyl)pyridinato]-4,4':2',2'':4'',4'''-quaterpyridine hexafluorophosphate, [Ir(dFmesppy)$_2$(qpy)](PF$_6$) : zinc tetraphenylphorphyrin(ZnTPP) 1:1 (2a)

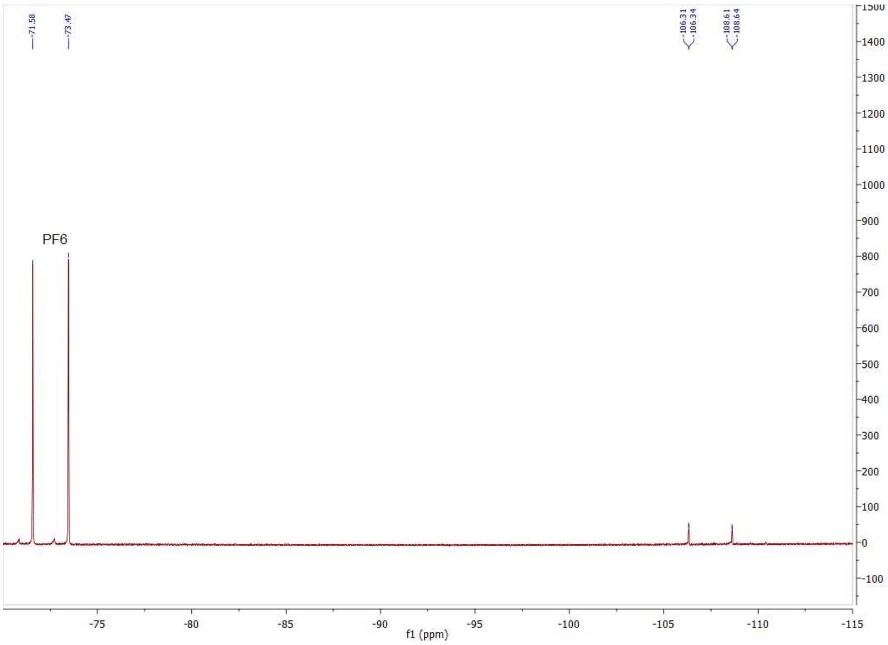

Figure **S38.** ^{19}F NMR spectrum of **[Ir(dFmesppy)$_2$(qpy)]PF$_6$ – ZnTPP : 1:1 (2a)** in CD$_2$Cl$_2$.

Iridium(III)bis[2-(2,4-difluoro)-phenyl-4-(2,4,6-trimethylphenyl)pyridinato]-4,4':2',2'':4'',4'''-quaterpyridine hexafluorophosphate, [Ir(dFmesppy)$_2$(qpy)](PF$_6$) : zinc tetraphenylphorphyrin(ZnTPP) 1:2 (2b)

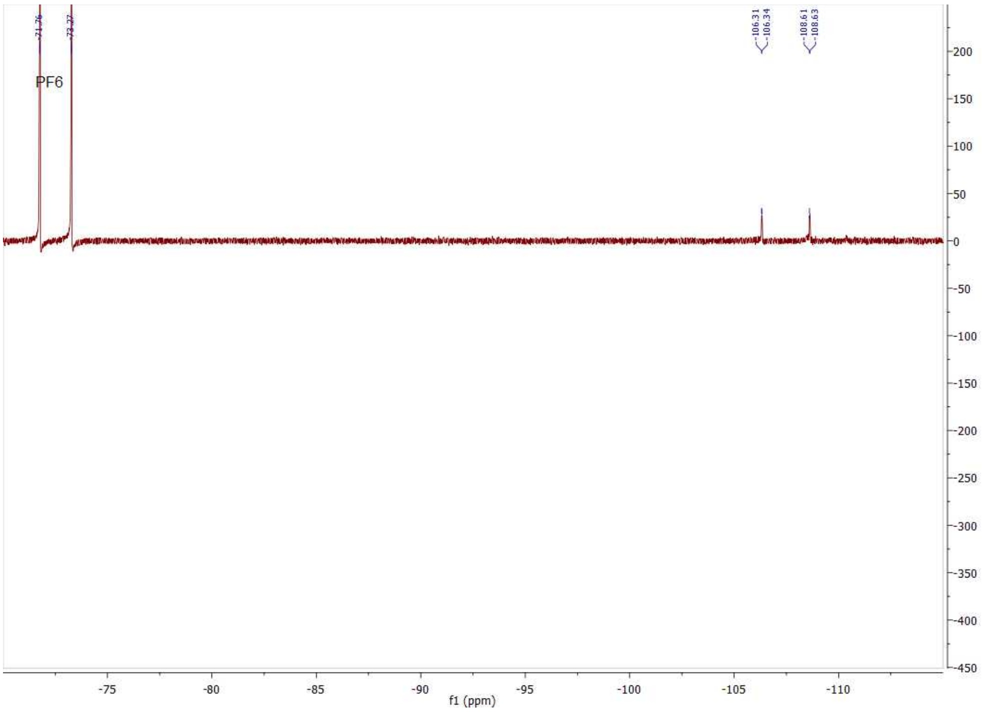

Figure **S39.** ^{19}F NMR spectrum of **[Ir(dFmesppy)$_2$(qpy)]PF$_6$ – ZnTPP : 1:2 (2b)** in CD$_2$Cl$_2$.

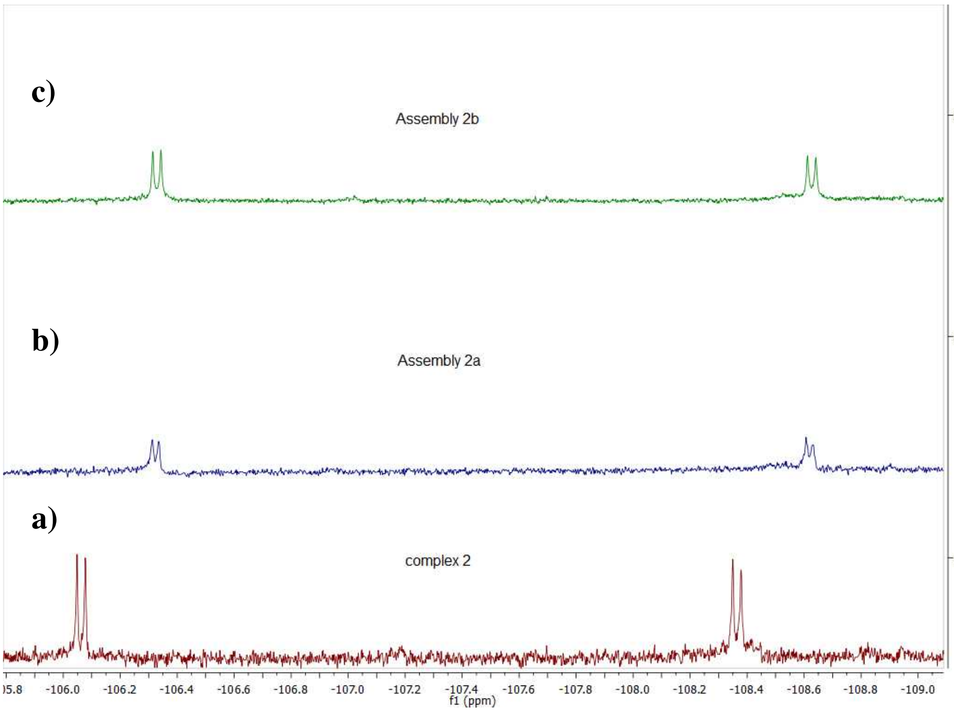

Figure **S40.** ^{19}F NMR spectra of**a) [Ir(dFmesppy)$_2$(qpy)]PF$_6$, b) [Ir(dFmesppy)$_2$(qpy)]PF$_6$– ZnTPP : 1:1 (2a)** and **c) [Ir(dFmesppy)$_2$(qpy)]PF$_6$– ZnTPP : 1:2 (2b)** in CD$_2$Cl$_2$.

^{1}H NMR with proton assignments of 1, ZnTPP, 1a and 1b.

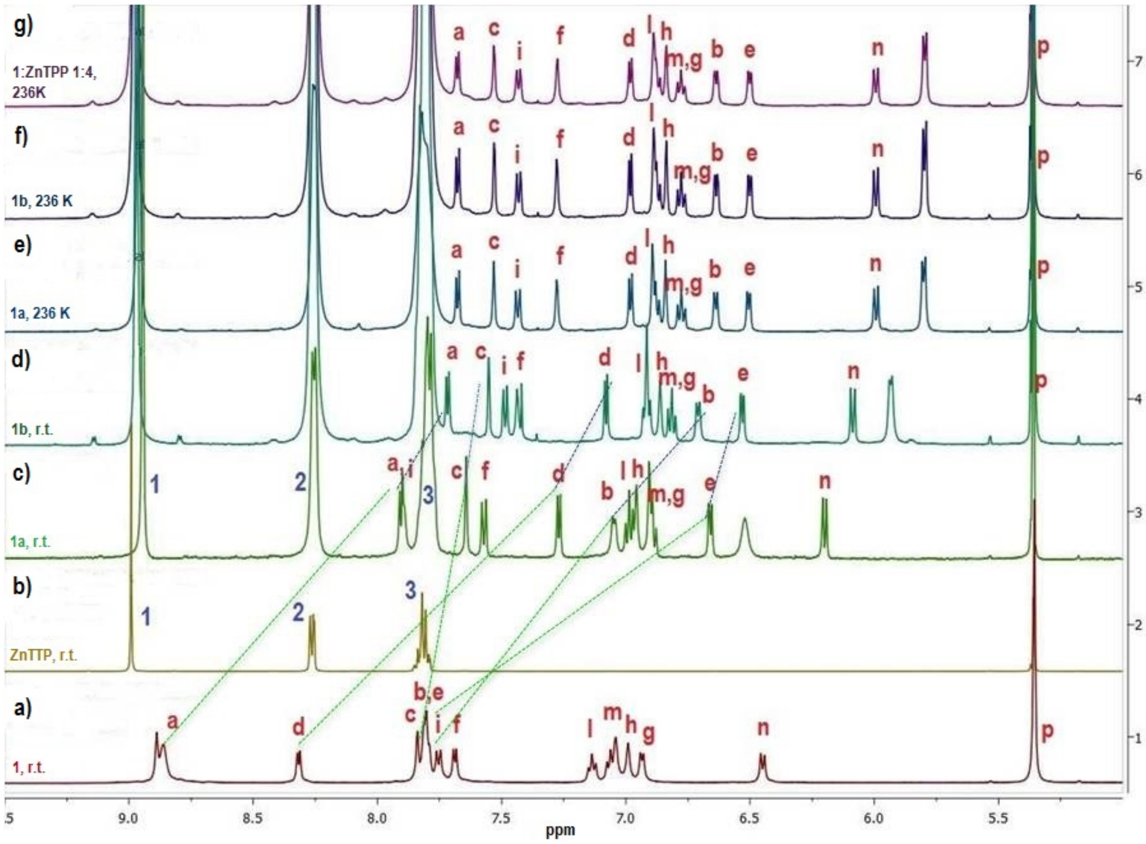

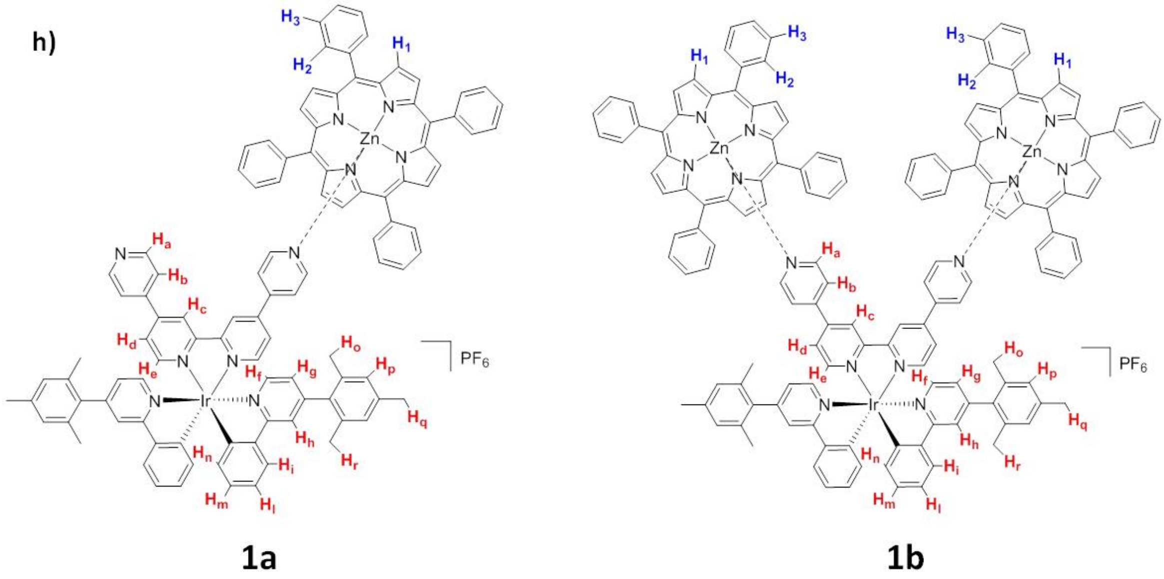

Figure **S41**. ^{1}H NMR spectra in CD_2Cl_2, 500 MHz.**a**) ^{1}H NMR spectrum of complex **1** (298 K); **b**) ^{1}HNMR spectrum of ZnTPP (298 K); **c**) ^{1}HNMR spectrum of the assembly **1a** (298 K); **d**) ^{1}HNMR spectrum of the assembly **1b** (298 K); **e**) ^{1}HNMR spectrum of the assembly **1a** (236 K); **f**) ^{1}HNMR spectrum of the assembly **1b** (236 K); **g**) ^{1}HNMR spectrum of complex **1** mixed with 4 equivalents of ZnTPP (236 K); **h**) chemical structures of the assemblies **1a** and **1b**. The assignments correspond to the labelling shown in **h**).

Determination of equilibrium constants for the formation of 1a and 1b.

Association constants for the 1:1 complex **1a** and the 1:2 complex **1b** were determined by standard NMR spectroscopic titration methods (see Figure **S42**). Small aliquots of ZnTPP were added to a 3.09 mM solution of **1** in CD_2Cl_2 such that the concentration of ZnTPP in the sample carried from 0 mM to 8.95 mM. A ^{1}H NMR spectrum was recorded on the solution after each addition and the variation of the chemical shift of H^a in **1** with respect to ZnTPP concentration determined from this data. This data was then fitted to the sequential binding model shown below using an iterative fitting procedure implemented within the Gepasi[10] program (see Figure **S43**).

$$\mathbf{1} + \text{ZnTPP} \xrightleftharpoons{K_1} \mathbf{1a}$$

$$\mathbf{1a} + \text{ZnTPP} \xrightleftharpoons{K_2} \mathbf{1b}$$

The fitting procedure is complicated by the fact that **1a** has a contribution to δ_{obs} from both an H^a proton on a pyridine ring bound to ZnTPP and an H^a proton that is unbound. Thus, δ_{obs} is obtained from the following expression:

$$\delta_{obs} = f_1\delta_1 + 0.5f_{1a}\delta_{1a}(bound) + 0.5f_{1a}\delta_{1a}(unbound) + f_{1b}\delta_{1b}$$

The best fit of the binding model to the ^{1}H NMR data afforded a value for K_1 of 8000 ± 370 M^{-1} and a value for K_2 of 2000 ± 190 M^{-1}.

Speciation data, using two scenarios – [**1**]/[ZnTPP] = 1 and [**1**]/[ZnTPP] = 0.5, were obtained using the parameter scan mode implemented in Gepasi (see main text, Figure **5**).

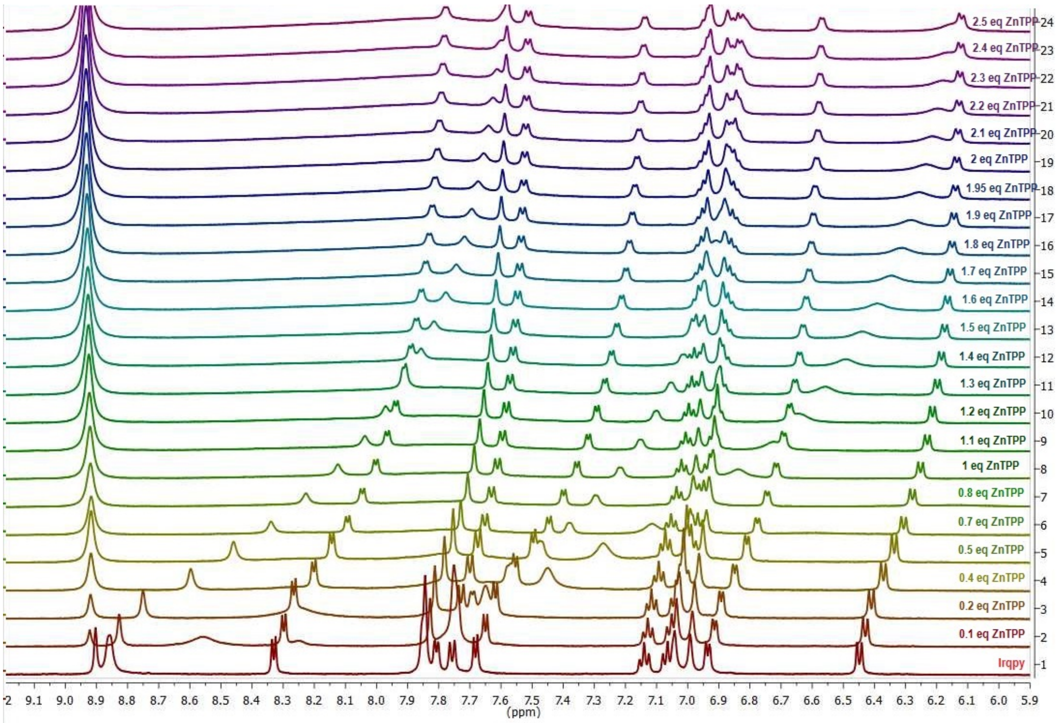

Figure **S42**. ^{1}H NMR titration experiments, with spectra collected after gradual addition of ZnTPP (from 0.1 equiv. to 2.5 equiv.) to a solution of **1**.

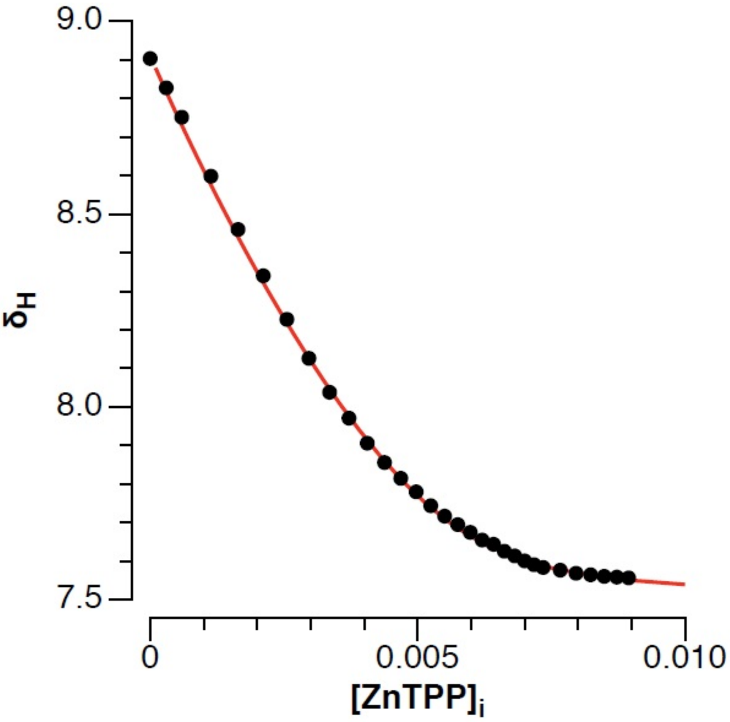

Figure **S43**. Binding isotherm obtained by titration experiments of complex **1** (host) after gradual addition of ZnTPP (guest) in CD_2Cl_2 at 298 K, while monitoring the chemical shift of H^a of **1** (Figure **4h**) by ^1H NMR spectroscopy.

Displacement assay for 1a and 1b after addition of DMAP monitored by ^{1}HNMR spectroscopy.

Figure **S44** illustrates a competitive displacement assay using the more basic 4-dimethylaminopyridine (DMAP).[11] Following the addition of DMAP to the solution of **1a** or **1b**, coordination between ZnTPP with DMAP with concomitant release of **1** was observed. In addition, the crystal structure of ZnTPP-DMAP adduct has been obtained and its structure matches with that previously reported.[11]

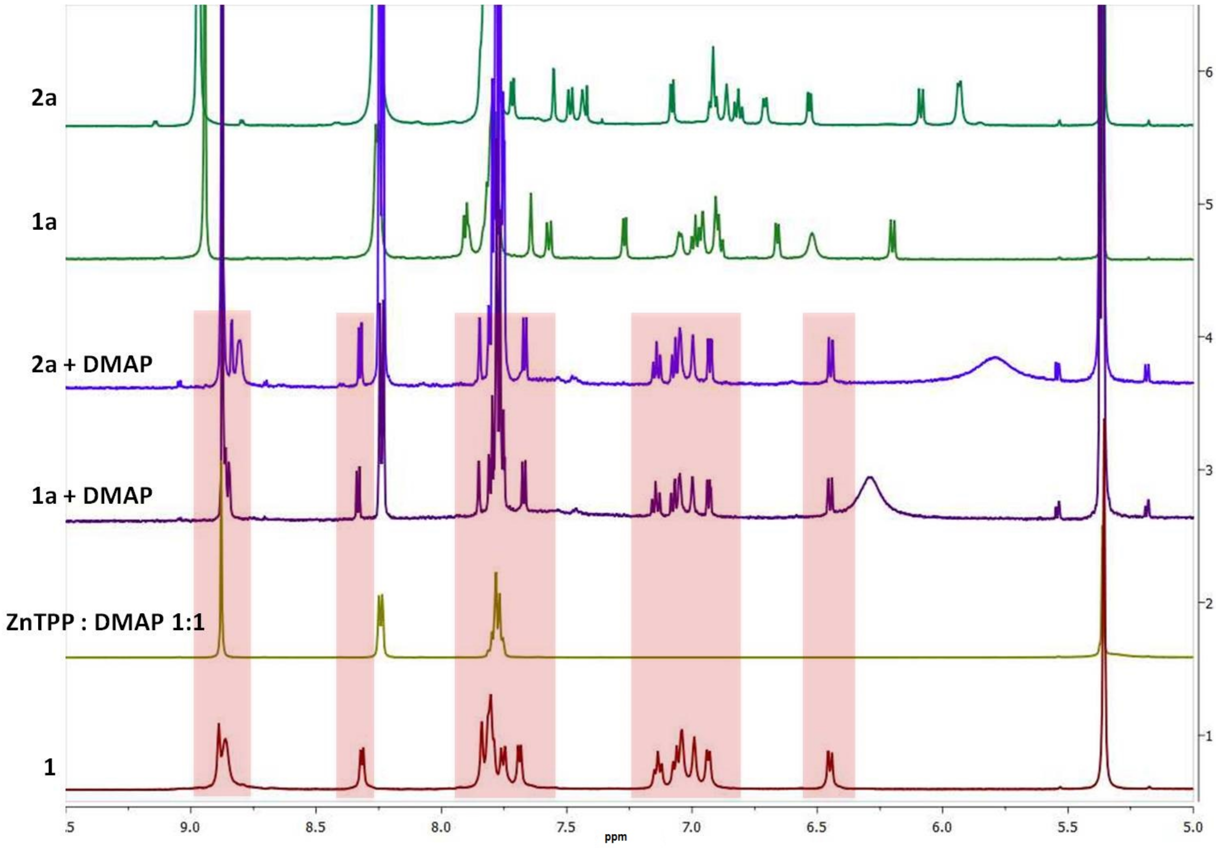

Figure **S44**. ^{1}HNMR spectra ($CD_2Cl_2$500 MHz, 298K) of **a) 1**, **b)** ZnTPP-DMAP 1:1, **c) 1a** + 2 equiv. DMAP, **d) 1b** + 2 equiv. DMAP, **e) 1a** and **f) 1b**. Pink boxes indicate the presence in solution of free **1** after addition of DMAP.

Control ^{1}H-NMR spectrum of the “non-assembly” 3a.

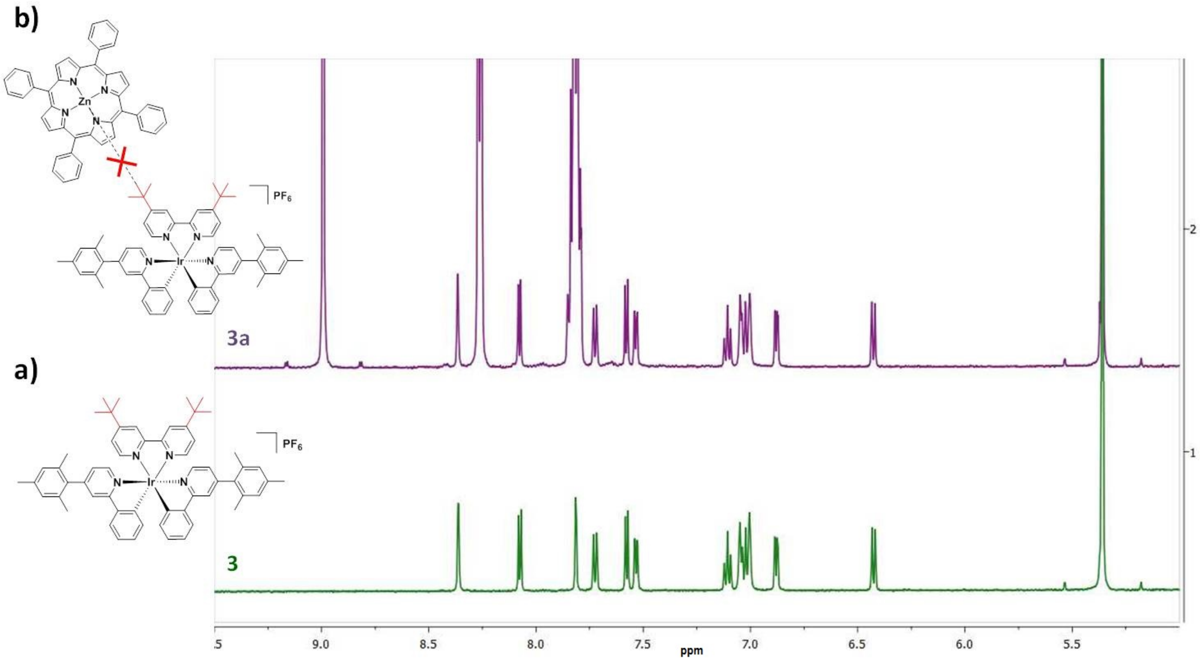

Figure **S45**. Control ^{1}H NMR spectra (CD_2Cl_2, 500 MHz, 298 K) of **a**) **3** and **b**) a mixture of **3** and ZnTPP (1:2 ratio).

X-Ray Crystallography.

Suitable crystals of **1**, **3** and **ZnTPP-ether** were obtained by diffusion of Et_2O into a dichloromethane solution of the complex. Suitable crystals of **1a** were obtained by diffusion of a mixture of hexane and pentane into a dichloromethane solution of the complex, while crystals of **1b** were obtained by diffusion of hexane into a chloroform solution of the complex. X-ray diffraction data for compounds **1**, **1a**, **1b**, **3** and **ZnTPP-ether** were collected at 173 K by using either a Rigaku MM-007HF High brilliance RA generator/confocal optics and Rigaku XtaLAB P100 system, with Cu Kα radiation (λ = 1.54187 Å) for compounds **1**, **1a**, **1b** and **ZnTPP-ether**, or a Rigaku FR-X Ultrahigh brilliance Microfocus RA generator/confocal optics and Rigaku XtaLAB P200 system, with Mo Kα radiation (λ = 0.71075 Å) for compound **3**. Intensity data were collected using either ω or both ω and φ steps accumulating area detector images spanning at least a hemisphere of reciprocal space. All data were corrected for Lorentz polarization effects. A multiscan absorption correction was applied by using CrystalClear.[12] Structures were solved by Patterson (PATTY),[13] direct (SIR2004)[14] or charge-flipping methods (Superflip),[15] and refined by full-matrix least-squares against F^2 (SHELXL-2013).[16] Non-hydrogen atoms were refined anisotropically, and hydrogen atoms were refined using a riding model. All calculations were performed using the CrystalStructure[17] interface, and figures were drawn using either Mercury[18] or Olex2.[19] The diffraction for both complexes **1a** and **1b** was very weak, particularly for **1a**, likely arising from void-space within the structures. This has led to high values of wR_2, low fractions of date with intensity above the $2\sigma(I)$ threshold, and unoccupied void spaces in the structures. Despite this, the atomic connectivity of both of these structures could be unambiguously determined, without recourse to large numbers of restraints. In an attempt to improve data-quality the use of the SQUEEZE[20] routine in PLATON[21] was investigated. This showed the void space in **1a** to comprise two small void-spaces per unit cell (of 351 and 407 Å^3) along with several other voids too small to contain solvent (< 40 Å^3 per void), containing electron density amounting to 91 electrons per unit cell. Refinement was tried with the SQUEEZEd data, but it did not show any significant improvement in R_1, wR_2 or thermal parameters in the ordered part of the structure. In **1b**, the void space was localized in two large void areas per unit cell (of 1497 and 1499 Å^3), containing 512 electrons per unit cell. On trying refinement with this SQUEEZEd data, the refinement showed slight improvement in R_1 and wR_2 In both structures, the improvements in data-quality from use of SQUEEZE are minor, with no change to the complexes. As such, we chose not to include the SQUEEZEd data.

CCDC-1472895-1472899 contain the supplementary crystallographic data for this paper. These data can be obtained free of charge from The Cambridge Crystallographic Data Centre via http://www.ccdc.cam.ac.uk/data_request/cif.

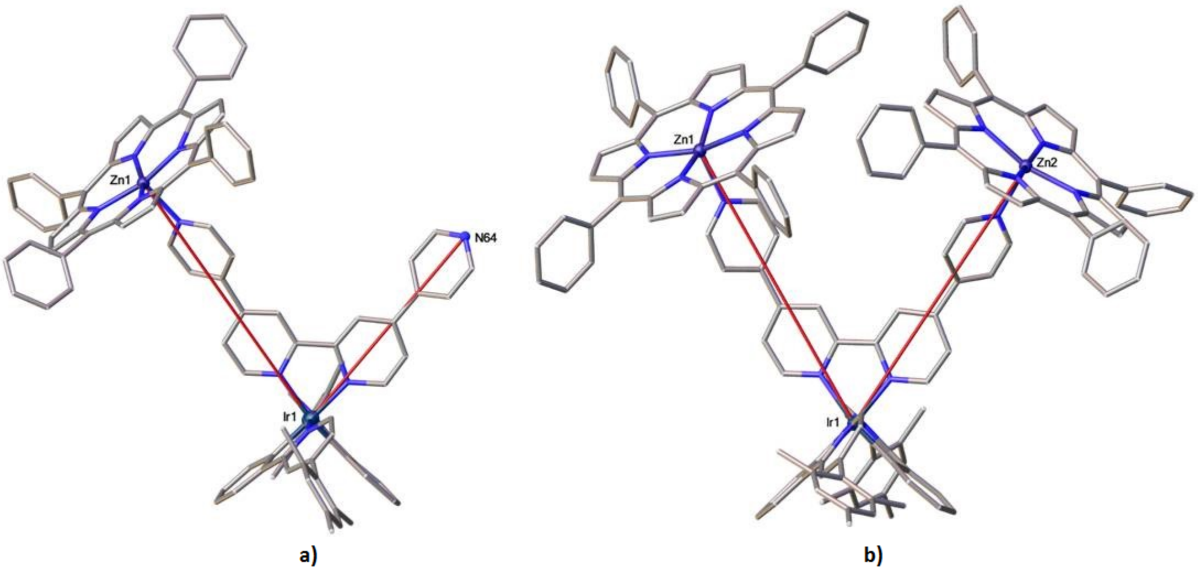

Figure **S46.** Views showing the relative orientation and positions of the ZnTPP and [Ir(C^N)$_2$] centres in **1a** (a) and **1b** (b), with Ir···N or Ir···Zn vectors highlighted in red. Selected distances (Å) and angles (°): **1a** Ir1···Zn1 11.33; Zn1-Ir1-N64 74.16. **1b** Ir1···Zn1 11.22, Ir1···Zn1 11.24; Zn1-Ir1-Zn2 64.68.

The structures of **3** and **ZnTPP-ether** are shown in Figure **S47**, and crystallographic data are presented in Table **S1**.

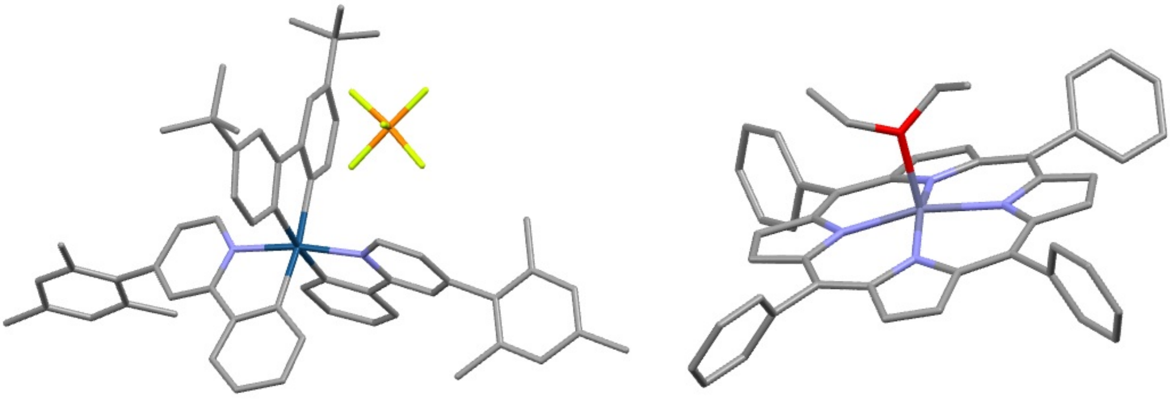

Figure **S47**. Crystal structures of **a)** [Ir(mesppy)$_2$(dtbubpy)]PF$_6$ (**3**) and **b)** ZnTPP coordinated to diethylether. In both cases solvent molecules and hydrogen atoms have been omitted for clarity.

Table S1. Crystallographic parameters for 1, 1a, 1b, 3 and ZnTPP-ether

	1	**1a**	**1b**	**3**	**ZnTPP-ether**
empirical formula	$C_{60}H_{50}F_6IrN_6P$	$C_{107}H_{85}F_6IrN_{10}PZn$	$C_{149}H_{107}Cl_3F_6IrN_{14}PZn_2$	$C_{58}H_{60}F_6IrN_4P$	$C_{48}H_{38}N_4OZn$
fw	1192.28	1913.48	2667.88	1150.32	752.23
crystal description	Orange prism	Red needle	Red platelet	Yellow platelet	Red platelet
crystal size [mm^3]	0.06×0.03×0.01	0.24×0.01×0.01	0.15×0.07×0.01	0.16×0.12×0.02	0.10×0.04×0.01
space group	$P2_1/n$	$P\bar{1}$	$P2_1/c$	$I2/a$	$C2/c$
a [Å]	11.8073(11)	10.986(6)	11.4270(12)	11.8361(13)	14.8095(16)
b [Å]	24.288(2)	20.260(12)	33.261(4)	19.8984(18)	17.054(2)
c [Å]	19.7882(19)	22.532(12)	37.861(4)	22.685(3)	14.9092(16)
α [°]		90.852(18)			
β [°]	103.905(2)	95.520(18)	91.978(2)	103.078(6)	90.0813(16)
γ [°]		90.267(12)			
vol [Å]^3	5508.5(9)	4991(5)	14381(3)	5204.2(10)	3765.5(7)
Z	4	2	4	4	4
ρ (calc) [g/cm^3]	1.438	1.273	1.232	1.468	1.327
μ [mm^{-1}]	5.395	3.427	3.199	2.667	1.235
F(000)	2392	1946	5424	2328	1568
reflns collected	68683	49726	181084	31541	19272
independent reflns (R_{int})	9979 (0.0681)	17349 (0.2207)	25911 (0.1545)	4744 (0.0228)	3425 (0.0294)
data/restraints/params	9979/0/673	17349/1191/1069	25911/195/1597	4744/0/324	3425/0/246
GOF on F^2	1.026	1.199	1.070	1.045	1.064
R_1 [$I > 2\sigma(I)$]	0.0600	0.1904	0.1051	0.0151	0.0279
wR_2 (all data)	0.1837	0.5484	0.3451	0.0376	0.0808
largest diff. peak/hole [e/Å^3]	3.15/-1.47	2.73/-2.92	2.01/-1.31	0.48/-0.33	0.30/-0.24

Selected geometric parameters from the crystal structures of 1, 1a and 1b. Selected bond lengths (Å) for **1**: Ir$_1$-N$_1$: 2.053(6); Ir$_1$-N$_{22}$: 2.030(5); Ir$_1$-C$_8$: 1.998(7); Ir$_1$-C$_{29}$: 2.010(6); Ir$_1$-N$_{55}$ (qpy): 2.118(5); Ir$_1$-N$_{43}$ (Irqpy): 2.139(5); C$_{46}$-C$_{49}$: 1.470(9); C$_{58}$-C$_{61}$: 1.481(9). Selected bond lengths (Å) for **1a**: Ir$_1$-N$_1$: 1.949(14); Ir$_1$-N$_{22}$: 1.948(14); Ir$_1$-C$_8$: 2.008(15); Ir$_1$-C$_{29}$*: 2.039(16); Ir$_1$-N$_{55}$ (qpy): 2.019(14); Ir$_1$-N$_{43}$ (qpy)*: 2.121(15); C$_{46}$-C$_{49}$*: 1.56(4); C$_{58}$-C$_{61}$: 1.45(4); N$_{52}$-Zn$_1$*: 2.14(2); Zn$_1$-N$_{80}$: 1.96(3); Zn$_1$-N$_{86}$: 2.08(3); Ir$_1$-Zn$_1$: 11.330(7). Selected bond lengths (Å) for **1b**: Ir$_1$-N$_1$: 2.040(11); Ir$_1$-N$_{22}$: 2.010(10); Ir$_1$-C$_8$: 2.008(10); Ir$_1$-C$_{29}$: 1.960(13); Ir$_1$-N$_{55}$ (qpy): 2.077(9); Ir$_1$-N$_{43}$ (qpy): 2.122(9); C$_{46}$-C$_{49}$: 1.495(16); C$_{58}$-C$_{61}$: 1.478(16); N$_{52}$-Zn$_1$: 2.149(10); N$_{64}$-Zn$_2$: 2.127(10); Zn$_1$-N$_{80}$: 2.050(10); Zn$_1$-N$_{86}$: 2.054(11); Zn$_2$-N$_{134}$: 2.047 (10); Zn$_2$-N$_{64}$: 2.128 (11); Ir$_1$-Zn$_1$: 11.2237(18); Ir$_1$-Zn$_2$: 11.2476(18). Selected bond angle (°) for **1**: N$_{43}$-Ir$_1$-N$_{55}$ (qpy): 76.29(19); N$_{22}$-Ir$_1$-C$_{29}$: 80.4(2); N$_1$-Ir$_1$-C$_8$: 80.8(3). Selected bond angle (°) for **1a**: N$_{43}$-Ir$_1$-N$_{55}$ (qpy): 79.2(7); N$_{22}$-Ir$_1$-C$_{29}$: 80.5(10); N$_1$-Ir$_1$-C$_8$: 78.6(8); N$_{80}$-Zn$_1$-N$_{86}$: 90.3(11). Selected bond angle (°) for **1b**: N$_{43}$-Ir$_1$-N$_{55}$ (qpy): 77.1(3); N$_{22}$-Ir$_1$-C$_{29}$: 80.5(5); N$_1$-Ir$_1$-C$_8$: 80.9(4); N$_{80}$-Zn$_1$-N$_{86}$: 88.1(4). Selected torsion angles (°) for **1**:C$_{50}$-C$_{49}$-C$_{46}$-C$_{47}$: 136.6(8); C$_{62}$-C$_{61}$-C$_{58}$-C$_{57}$: 140.3(8). Selected torsion angles (°) for **1a**: C$_{50}$-C$_{49}$-C$_{46}$-C$_{47}$*: -43(4); C$_{62}$-C$_{61}$-C$_{58}$-C$_{57}$: -34(4). Selected torsion angles (°) for **1b**: C$_{50}$-C$_{49}$-C$_{46}$-C$_{47}$: -160.5(13); C$_{62}$-C$_{61}$-C$_{58}$-C$_{57}$: 147.9(18).* indicates the values following the vector of the Ir-Zn coordination.

Solid-state NMR spectroscopy.

Solid-state ^{1}H magic angle spinning (MAS) NMR spectra of ZnTPP, **1** and **1a** are shown in Figure **S48(a)**. The spectra are of low resolution, even with rapid (35 kHz) MAS, but the observed shift ranges are broadly consistent with the corresponding solution-phase NMR spectra. The ^{13}C cross-polarized MAS NMR spectra of ZnTPP, **1** and **1a** are shown in Figure **S48(b)**. For all three solids characterized, the ^{13}C chemical shifts are consistent between the solid-state and solution-state

NMR spectra, although several of the resonances are split in the solid state, likely owing to crystallographic inequivalences.

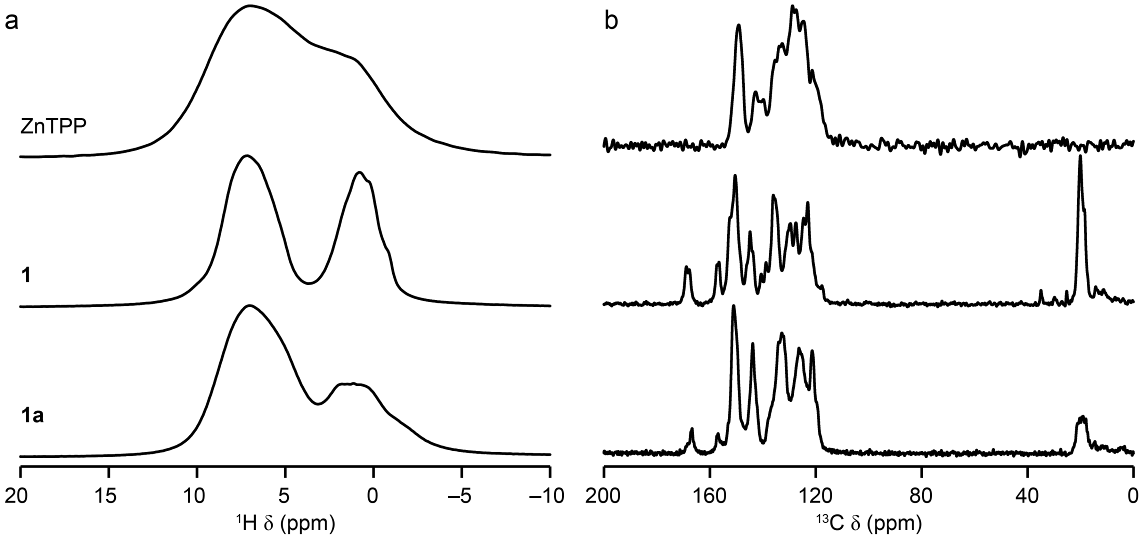

Figure **S48.** (a) ^{1}H (9.4 T, 35 kHz MAS) and (b) ^{13}C (9.4 T, 14 kHz CP MAS) NMR spectra of ZnTPP, **1** and **1a**.

Supplementary Optoelectronic Characterization.

UV-Vis spectroscopy.

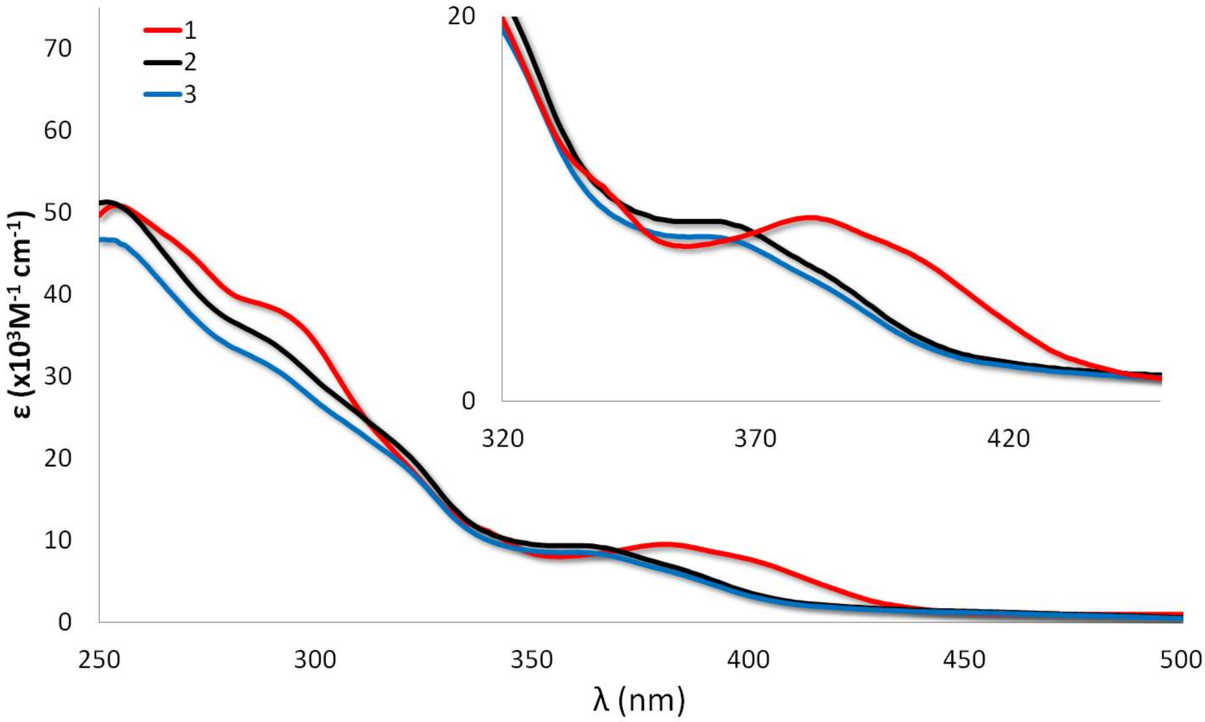

Figure **S49**. UV-Vis spectra of [Ir(mesppy)$_2$(qpy)]PF$_6$ (**1,** in red), [Ir(dFmesppy)$_2$(qpy)]PF$_6$ (**2,** in black)and [Ir(mesppy)$_2$(dtbubpy)]PF$_6$ (**3,** in blue)collected in CD$_2$Cl$_2$ at 298 K with a concentration on the order of 10^{-6}M.

Table **S2**. UV-Vis and NIR absorption data for ZnTPP, **1**, **1**:ZnTPP = 1:1 (**1a**), **1**:ZnTPP = 1:2 (**1b**), **2**, **2**:ZnTPP = 1:1 (**2a**), **2**:ZnTPP = 1:2 **(2b)**, **3** and **3**:ZnTPP = 1:1 (**3a**) and ZnTPP-py.

Compound	**λ_{max}(vis)**[a] [ε($\times 10^3$ M^{-1} cm^{-1})][c]	**λ_{max} (NIR)**[b] [ε($\times 10^3$ M^{-1} cm^{-1})][c]
ZnTPP	285 [43.0], 399 [48.5], 422 [598], 480 [1.9], 513 [3.4], 553 [23.0], 595 [5.7]	800 [0.24]
1	255 [50.4], 294 [37.3], 381 [9.4], 403 [7.7]	-
1:ZnTPP = 1:1	285 [51.1], 403 [55.5], 422 [623], 485 [2.3], 515 [7.0], 553 [22.3], 595 [5.6]	766 [1.10], 849 [1.11]
1:ZnTPP = 1:2	285 [51.5], 399 [56.2], 422 [585], 485 [5.0], 515 [7.1], 553 [22.8], 595 [5.9]	766 [1.15], 849 [1.16]
2	253 [51.0], 291 [33.7], 321 [18.9], 367 [8.2], 387 [5.2]	-

2:ZnTPP = 1:1	285 [49.0], 399 [40.9], 422 [599], 480 [6.9], 513 [7.6], 553 [23.4], 595 [6.2]	780 [1.21], 854 [1.34]
2:ZnTPP = 1:2	285 [49.4], 399 [43.0], 422 [610], 480 [7.0], 513 [7.8], 553 [23.7], 595 [6.4]	780 [1.45], 854 [1.62]
3	254 [46.8], 290 [31.3], 320 [19.4], 367 [8.3], 390 [5.0], 462 [1.0]	-
3:ZnTPP = 1:1	285 [51.1], 402 [55.5], 422 [624], 480 [7.8], 513 [7.3], 553 [28.1], 595 [6.5]	800 [0.20]
ZnTPP-py	285 [51.0], 399 [42.6], 422 [598], 480 [5.9], 515 [6.5], 553 [25.5], 595 [5.9]	800 [0.71]

---

[a] UV-Vis absorption in DCM with a concentration in the order of 10^{-6} M collected at 298 K. [b] NIR absorption in DCM with a concentration in the order of 5×10^{-6} M collected at 298 K. [c] concentration-independent extinction coefficients.

Emission studies at a concentration of 3×10^{-5} M.

In order to investigate the nature of the emission of the assemblies **1a** and **1b** and the presence of energy/electron transfer between the iridium moiety and ZnTPP we excited **1a** and **1b** into both ^{1}CT band (λ_{exc}= 360 nm) centered on the iridium complex, and Soret and Qbands centered on ZnTPP and we studied their steady-state spectroscopy. Unfortunately, the emission of **1** and ZnTPP coincidentally overlap and consequently the study of this system proved challenging.

However, some spectral features can be clearly extracted:(1) upon excitation at 360 nm, the emission of **1a** and **1b** are modestly quenched compared to **1** (**1a**: Φ_{PL} = 5.9% **1b**: Φ_{PL} = 2.2% *vs*. **1**: Φ_{PL} = 14%; values reported in Table **S3**); (2) the emission profiles of **1a** and **1b** are more structured compared to **1**, even though it is not initially clear if this is simply due to the superposition of the emission of **1** and ZnTPP or due to the presence of new transitions; (3) upon excitation at 420 nm or 550 nm, the emission spectra of **1a** (λ_{em} = 656 nm) and **1b** (λ_{em} = 662 nm) are slightly red-shifted relative to ZnTPP (λ_{em} = 653 nm), although similar emission profiles are observed between the three systems (Figure **S50**) and; (4) bi-exponential luminescence decay kinetics are observed for **1a** and **1b**. With respect to the last observation, the observed lifetimes (τ_e) attributed to emission from iridium in **1a** (294 ns) and **1b** (343 ns) are not significantly different compared to the emission lifetime of **1** (300 ns) and this result would argue against any energy transfer in these systems at this concentration.

Table **S3**. Relevant photophysical data of ZnTPP, **1**, **1**:ZnTPP = 1:1 (**1a**), **1**:ZnTPP = 1:2 (**1b**), **2**, **2**:ZnTPP = 1:1 (**2a**), **2**:ZnTPP = 1:2 (**2b**), **3** and **3**:ZnTPP = 1:1 (**3a**).

	λ_{em} / nm ^{a,b}		Φ_{PL} / % ^{a}		τ_e / ns ^{e}	
	λexc = 360 nm	λexc = 420 nm	λexc = 360 nm ^{c}	λexc = 420 nm ^{d}	3×10^{-5} M	5×10^{-4} M
ZnTPP	605 [0.6], 651 [1], 716 [0.04]	605 [0.6], 651 [1], 716 [0.04]	0.9	3.7	1.7	1.7
1	638 [1]	-	14	-	300	306
1:ZnTPP = 1:1	607 [0.74], 651 [1], 713 [0.48]	606 [0.72], 658 [1], 723 [0.07]	5.9	3.6	2.3 (0.32), 294 (0.68)	1.9 (0.45), 193 (0.55)
1:ZnTPP = 1:2	611 [0.70], 653 [1], 710 [0.56]	610 [0.72], 661 [1], 730 [0.06]	2.2	5.1	9.3 (0.52), 343 (0.48)	1.9 (0.55), 161 (0.45)
2	565 [1]	-	34	-	993	1000

2:ZnTPP = 1:1	541 [0.64], 583 [1], 612 [1], 647 [0.68], 715 [0.17]	537 [0.02], 610 [0.66], 661 [1], 717 [0.07]	10	5.0	1.88 (0.38), 906 (0.62)	1.9 (0.60), 384 (0.40)
2:ZnTPP = 1:2	537 [0.60], 580 [0.87], 605 [1], 650 [0.86], 716 [0.13]	602 [0.62], 654 [1], 713 [0.06]	6.2	5.1	1.89 (0.40), 866 (0.60)	1.9 (0.80), 192 (0.20)
3	576 [1]	-	40	-	757	800
3:ZnTPP = 1:1	576 [0.97], 604 [1], 651 [0.63]	601 [0.72], 651 [1], 720 [0.07]	38	3.6	1.90 (0.32), 759 (0.68)	1.9 (0.70), 194 (0.30)

[a] Measurements in deaerated DCM at 298 K at *ca.* 10^{-5} M. [b] Relative intensity of principal emission peaks listed in [ ]. [c] Using quinine sulfate as the standard (Φ_{PL} = 54.6% in 0.5 M H_2SO_4 at 298 K).[6] [d] Using $[Ru(bpy)_3]Cl_2$ as the standard (Φ_{PL} = 4% in aerated H_2O at 298 K).[7] [e] λ_{exc} = 378 nm. The values in parentheses are relative pre-exponential weighting factors of the emission decay kinetics for samples where a biexponential fit to the decay was required.

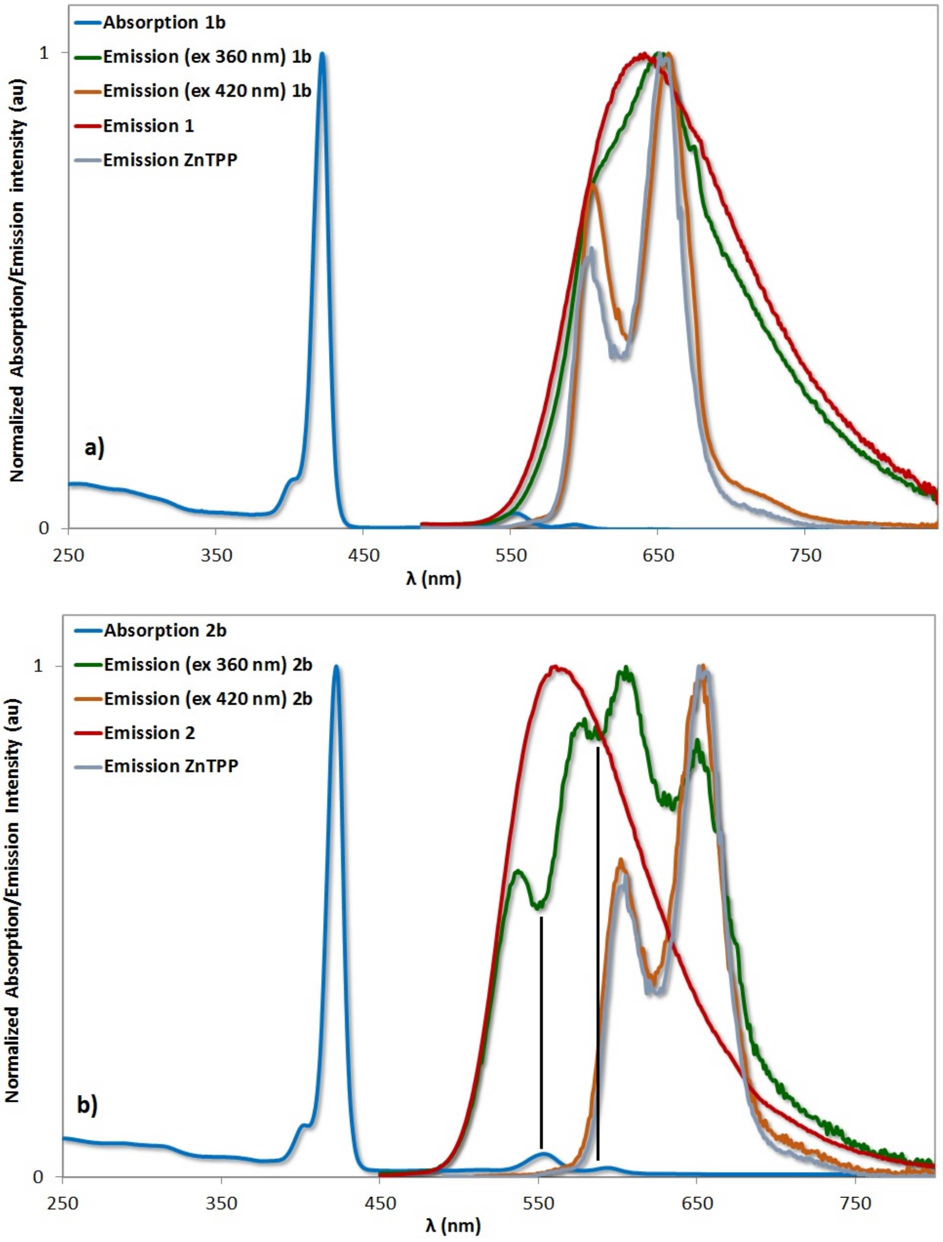

Figure **S50**. **a**) Normalized UV-Vis spectrum of **1b** and normalized luminescence spectra of**1b**, **1** and ZnTPP recorded in degassed DCM at 298 K with a concentration in the order of 10^{-6} M. **b**) Normalized absorption spectrum of **2b** and normalized luminescence spectra of **2b**, **2** and ZnTPP recorded in degassed DCM at 298K with a concentration of 3×10^{-5} M. Dark green and red lines indicate the emissions recorded with λ_{exc}= 360 nm and light blue and orange lines indicate the emissions recorded with λ_{exc} = 420 nm.

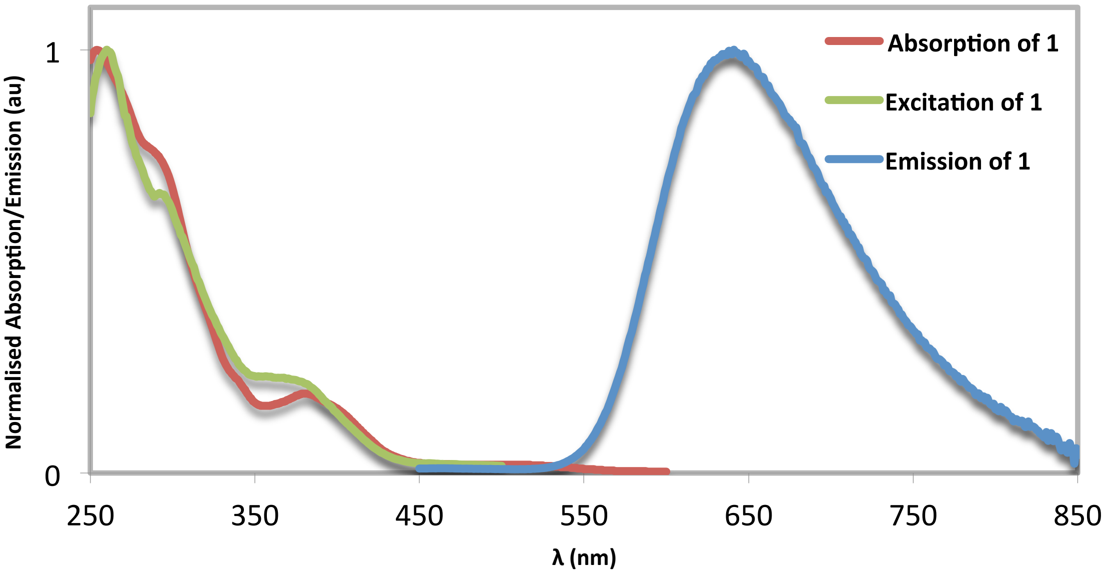

Figure **S51**. UV-Vis (red, in DCM at 298 K with a concentration on the order of 10^{-6}M), excitation (green) and emission (blue, λ_{exc} = 360 nm, in degassed DCM at 298 Kat a concentration of 3×10^{-5} M)spectra for [Ir(mesppy)$_2$(qpy)]PF$_6$ **(1).**

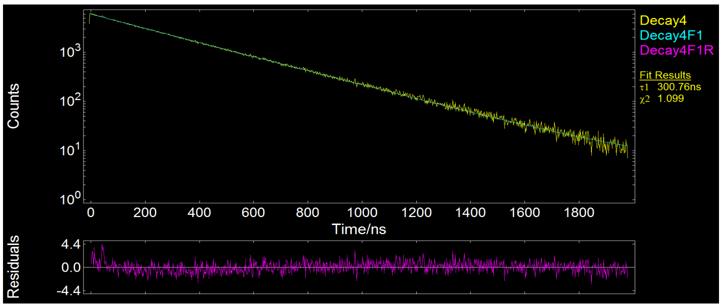

Figure **S52**. Lifetime decay of [Ir(mesppy)$_2$(qpy)](PF$_6$) **(1)** after excitation at 379 nm in degassed DCM at 298 K at a concentration of 3×10^{-5} M.

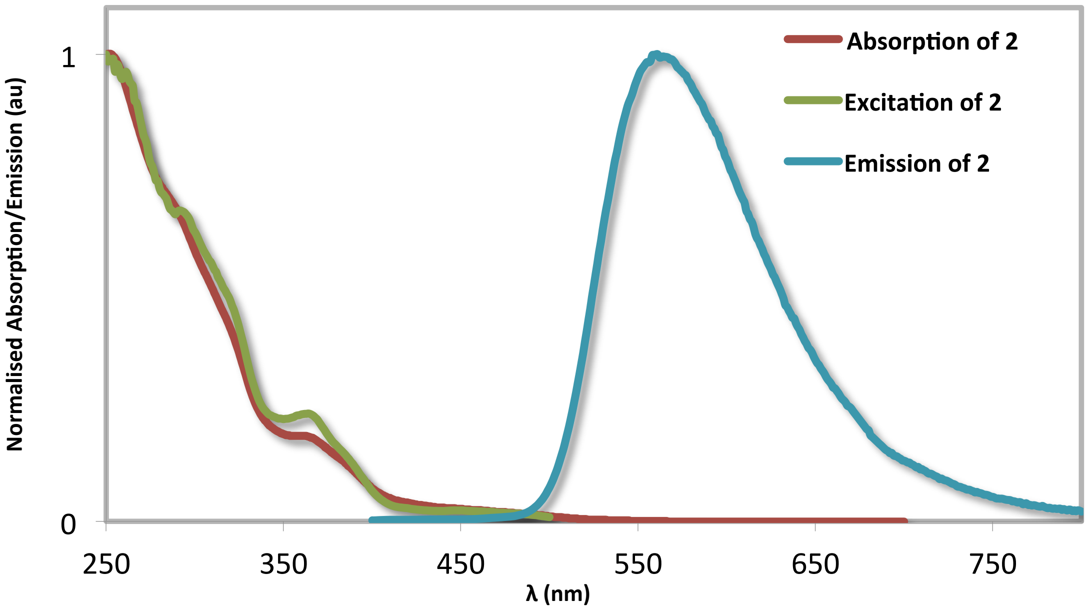

Figure **S53**. UV-Vis (red, in DCM at 298 K with a concentration on the order of 10^{-6}M), excitation (green) and emission (blue, λ_{exc} = 360 nm, in degassed DCM at 298 K at a concentration of 3 × 10^{-5} M) spectra of [Ir(dFmesppy)$_2$(qpy)]PF$_6$ **(2).**

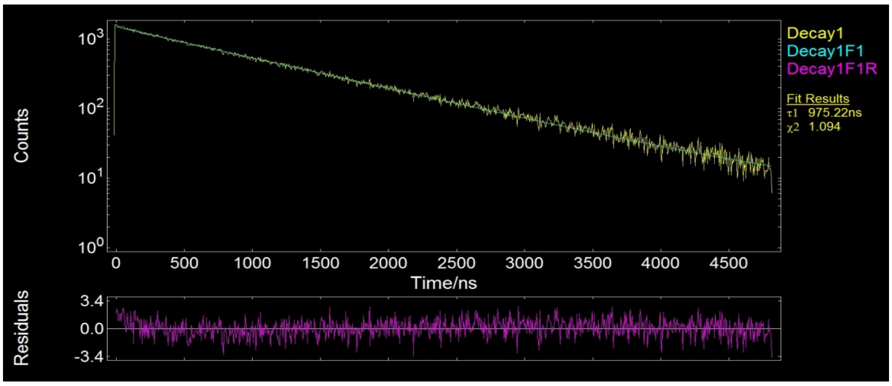

Figure **S54**. Lifetime decay of **[Ir(dFmesppy)$_2$(qpy)](PF$_6$) (2)** after excitation at 379 nm in degassed DCM at 298 K at a concentration of 3×10^{-5} M.

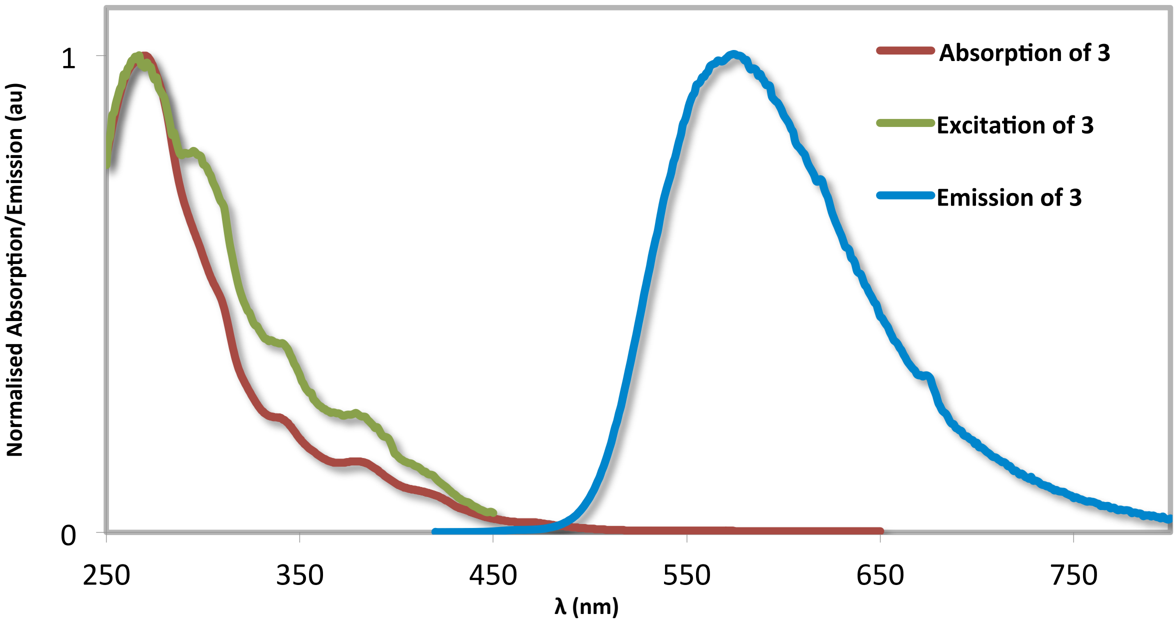

Figure **S55**. UV-Vis (red, in DCM at 298 K with a concentration on the order of 10^{-6} M), excitation (green) and emission (blue, λ_{exc} = 360 nm, in degassed DCM at 298 K at a concentration of 3×10^{-5} M) spectra of $[Ir(mesppy)_2(dtbubpy)]PF_6$ **(3).**

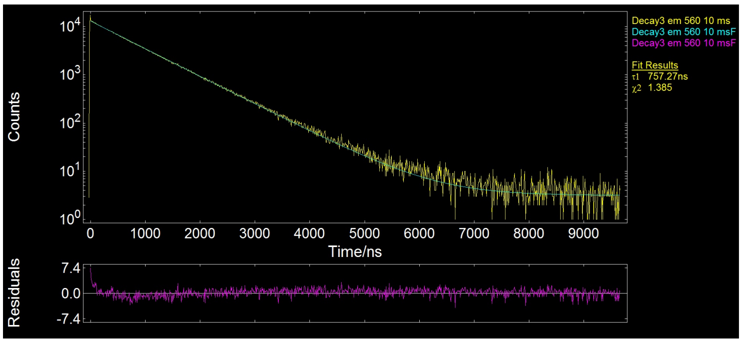

Figure **S56**. Lifetime decay of $[Ir(mesppy)_2(dtbubpy)](PF_6)$ **(3)** after excitation at 379 nm in degassed DCM at 298 K at a concentration of $3{\times}10^{-5}$ M.

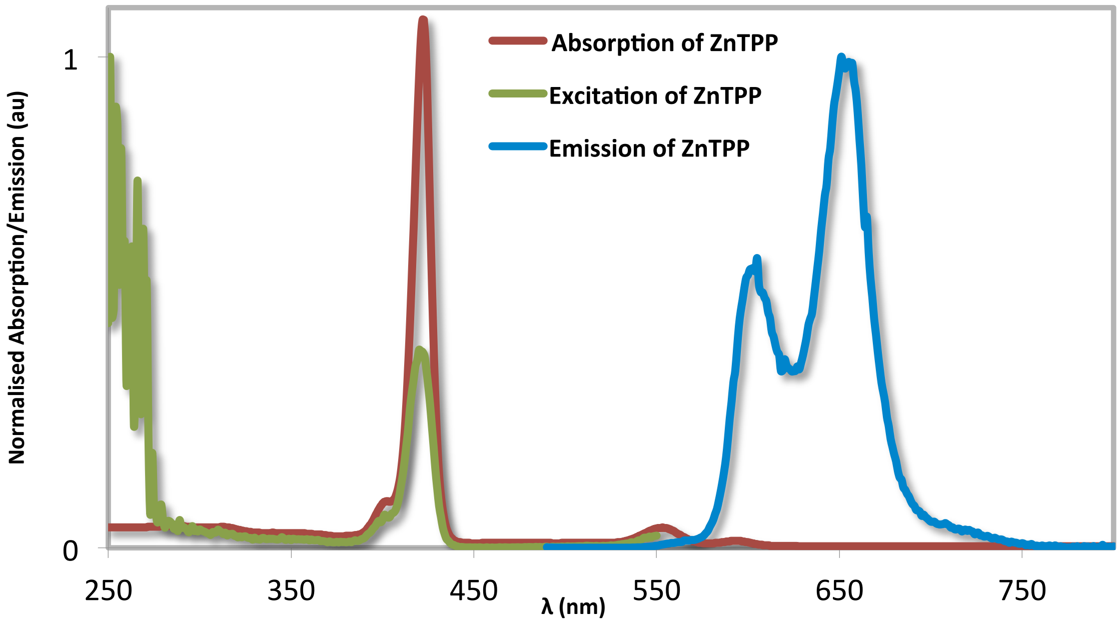

Figure **S57**. UV-Vis (red, in DCM at 298 K with a concentration on the order of 10^{-6} M), excitation (green) and emission (blue, λ_{exc} = 360 nm, in degassed DCM at 298 Kat a concentration of 3 × 10^{-5} M) spectra of ZnTPP.

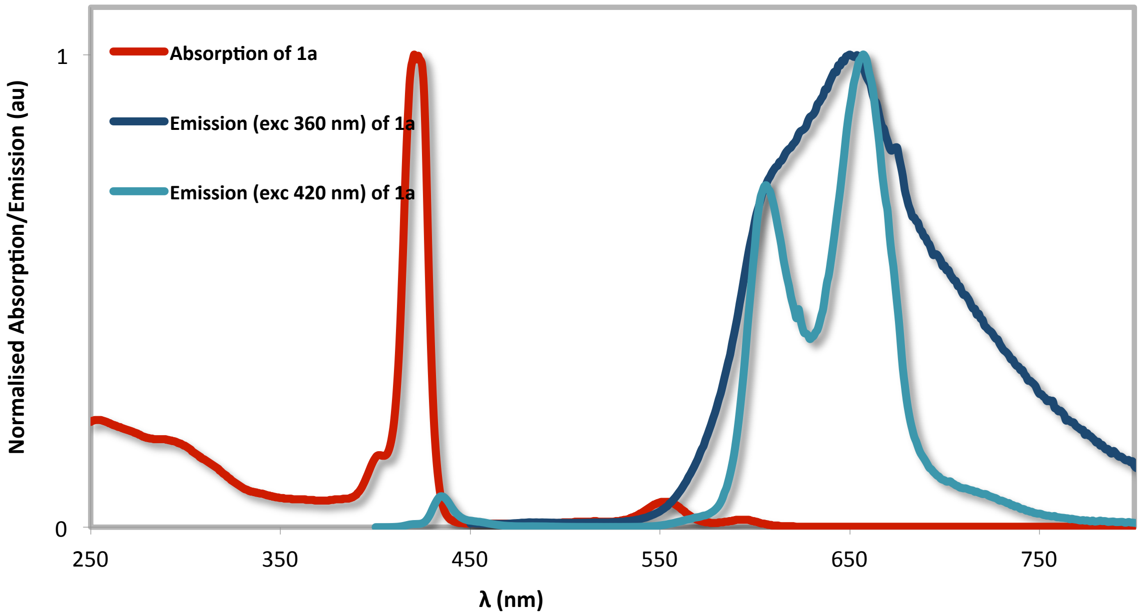

Figure **S58**. UV-Vis (red, in DCM at 298 K with a concentration on the order of 10^{-6} M) and emission spectra (dark blue (λ_{exc} = 360 nm) and light blue (λ_{exc} = 420 nm)) of **1a** in degassed DCM at 298 K at a concentration of 3×10^{-5} M.

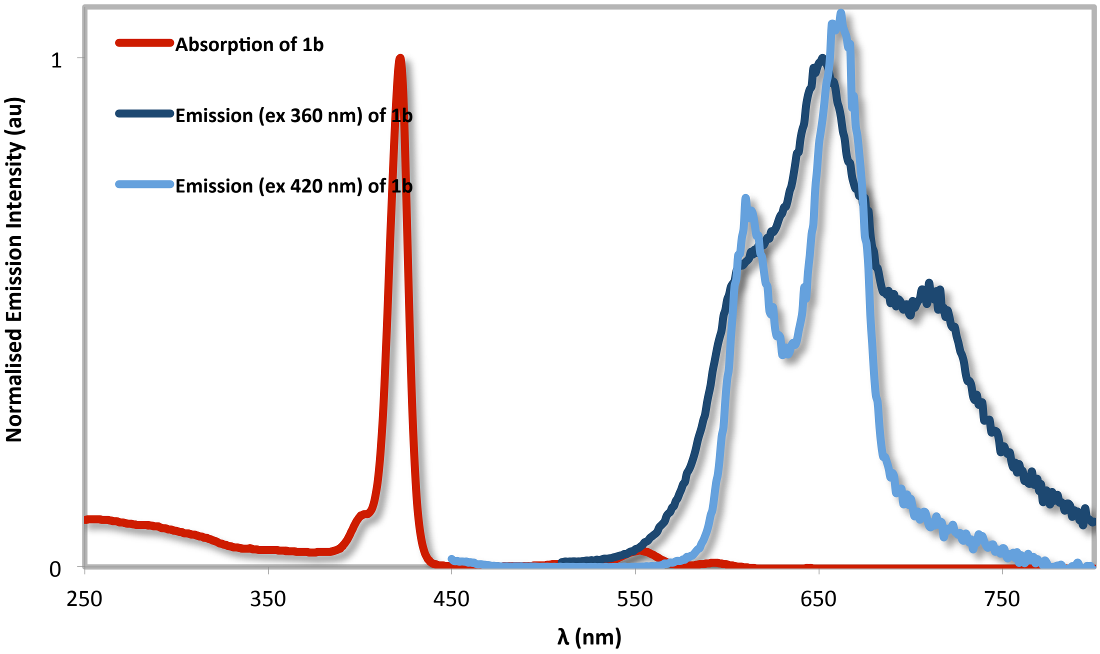

Figure **S59**. UV-Vis (red, in DCM at 298 K with a concentration on the order of 10^{-6} M) and emission spectra (dark blue (λ_{exc} = 360 nm) and light blue (λ_{exc} = 420 nm)) of **1b** in degassed DCM at 298 K at a concentration of 3×10^{-5} M.

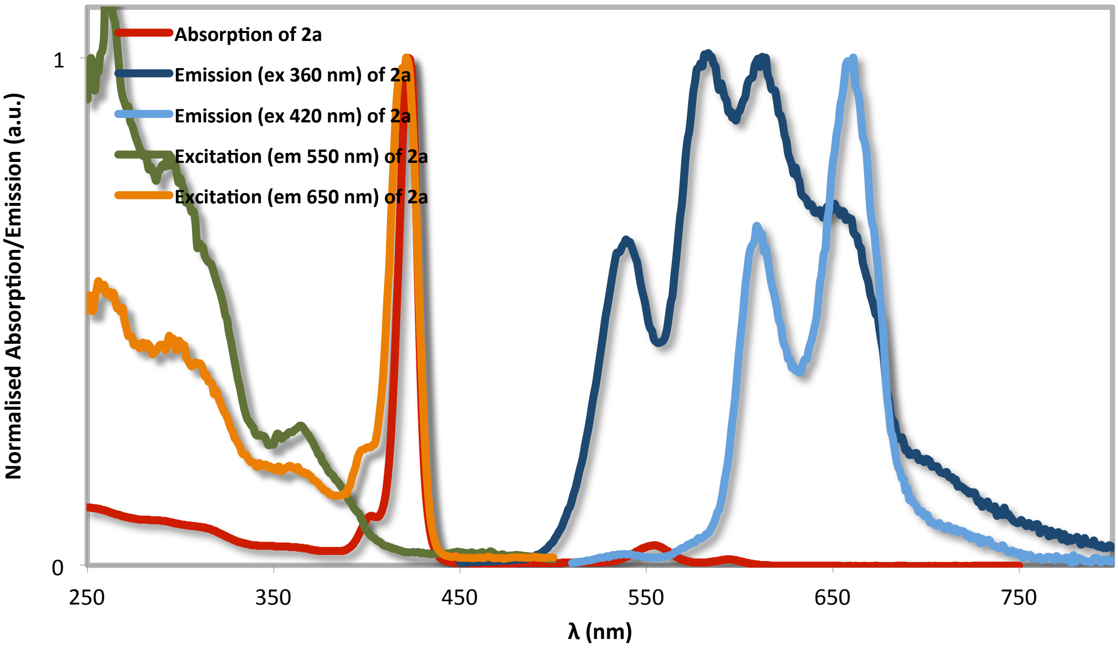

Figure **S60**. UV-Vis (red, in DCM at 298 K with a concentration on the order of 10^{-6} M), excitation (green (λ_{em} = 570 nm) and orange (λ_{em} = 650 nm)) and emission spectra (dark blue (λ_{exc} = 360 nm) and light blue (λ_{exc} = 420 nm)) of **2a** in degassed DCM at 298 K at a concentration of 3×10^{-5} M.

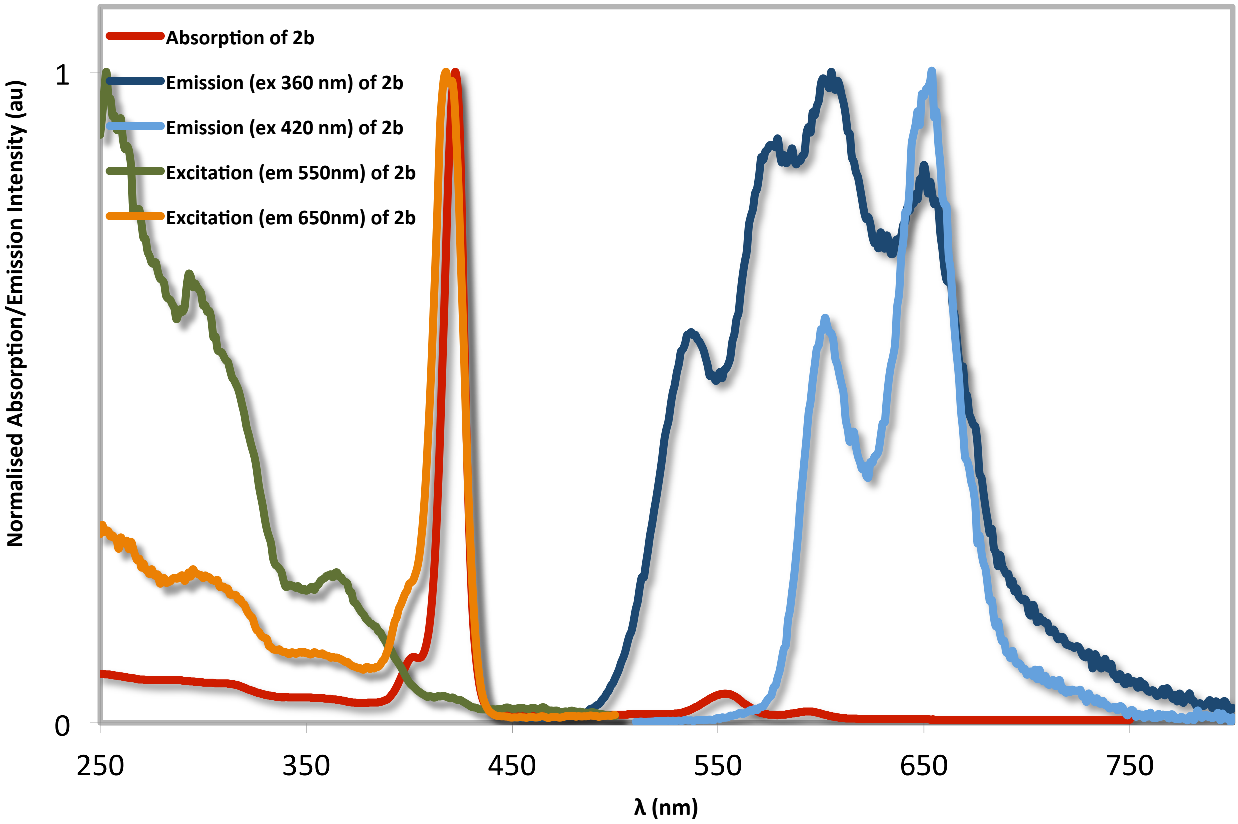

Figure **S61**. UV-Vis (red, in DCM at 298 K with a concentration on the order of 10^{-6} M), excitation (green (λ_{em} = 570 nm) and orange (λ_{em} = 650 nm)) and emission spectra (dark blue (λ_{exc} = 360 nm) and light blue (λ_{exc} = 420 nm)) of **2b** in degassed DCM at 298 K at a concentration of 3×10^{-5} M.

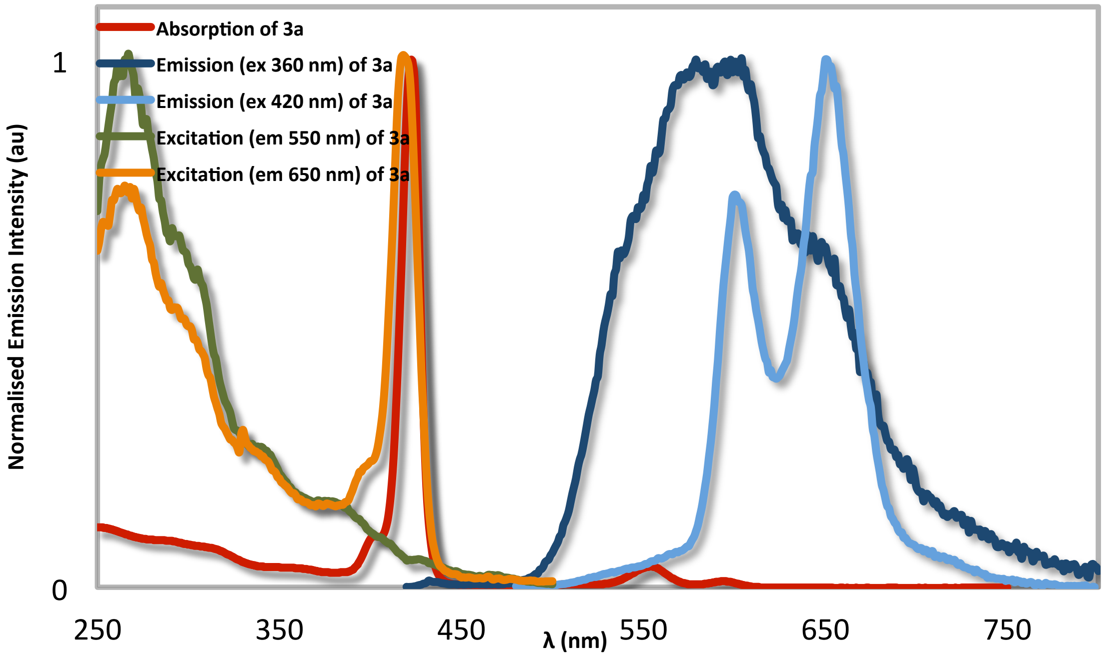

Figure **S62**. UV-Vis (red, in DCM at 298 K with a concentration on the order of 10^{-6} M), excitation (green (λ_{em} = 570 nm) and orange (λ_{em} = 650 nm)) and emission spectra (dark blue (λ_{exc} = 360 nm) and light blue (λ_{exc} = 420 nm)) of **3a** in degassed DCM at 298 K at a concentration of 3 × 10^{-5} M.

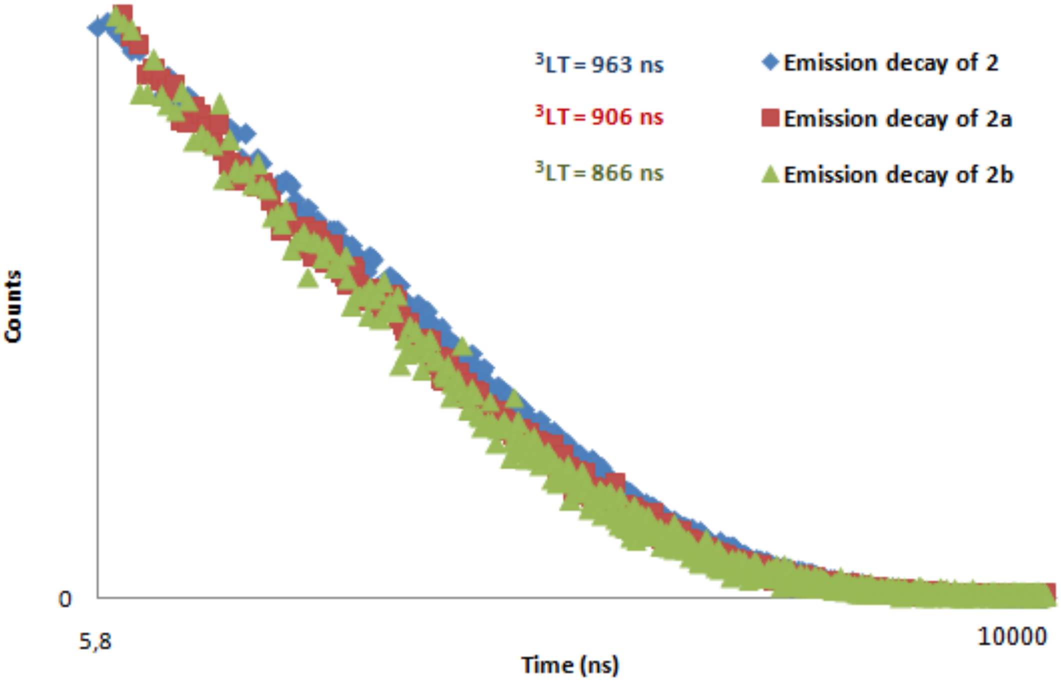

Figure **S63**. Lifetime decays of **2** (blue)**, 2a** (red) and **2b** (green) after excitation at 379 nm in deareated DCM at 298 K at a concentration of 3 × 10^{-5} M.

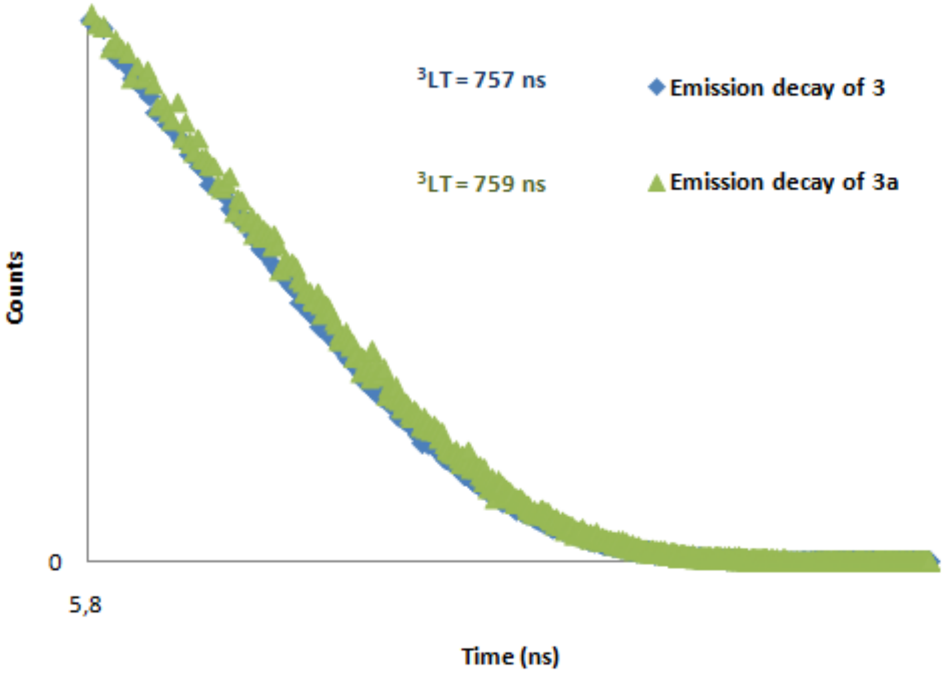

Figure **S64**. Lifetime decays of **3** (blue) and **3a** (green) after excitation at 379 nm in deareated DCM at 298 K at a concentration of 3×10^{-5} M.

Emission titration experiments at a concentration of 5×10^{-4} M.

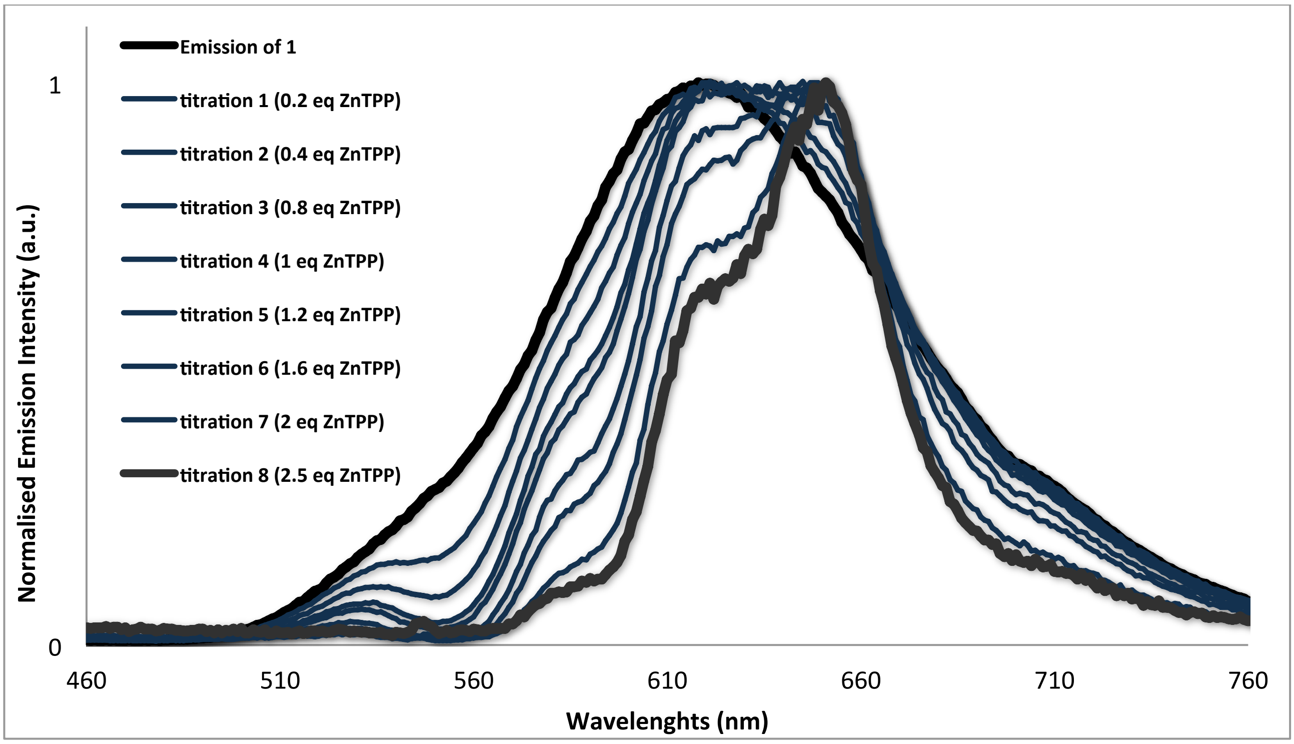

Figure **S65**. Room-temperature emission spectra of **1**(black line) and emission spectra of **1** upon addition of ZnTPP (from 0 to 2.5 equiv.) collected in DCM (λ_{exc} = 360 nm). The concentration of **1** was maintained constant at 5×10^{-4} M whereas the concentration of ZnTPP varied from 5×10^{-5} to 1.25×10^{-3} M.

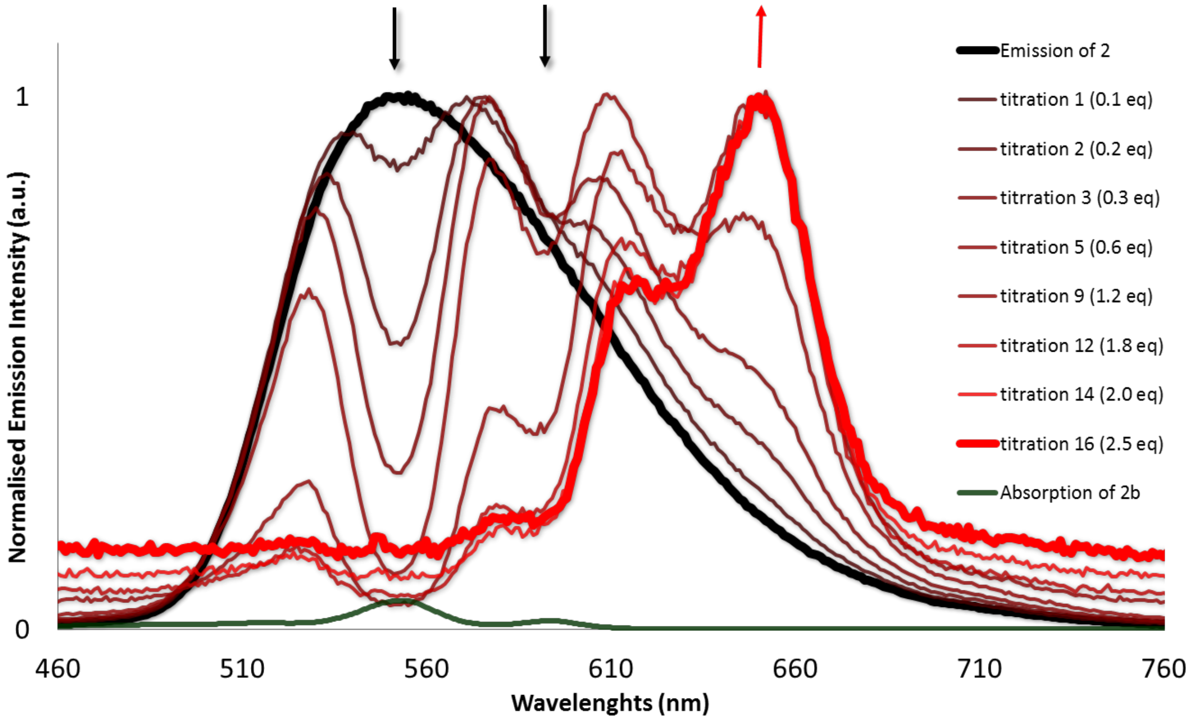

Figure **66**. Room-temperature emission spectra of **2** (black line) and **2** upon addition of ZnTPP (from 0 to 2.5 equivalents, from dark red to red) collected in deaerated DCM (λ_{exc} = 360 nm). The Q absorption band of ZnTPP is shown in green. The concentration of **2** was maintained constant at 5×10^{-4} M while the concentration of ZnTPP varied from 5×10^{-5} M to 1.25×10^{-3} M. Only subset of the emission spectra are shown for clarity.

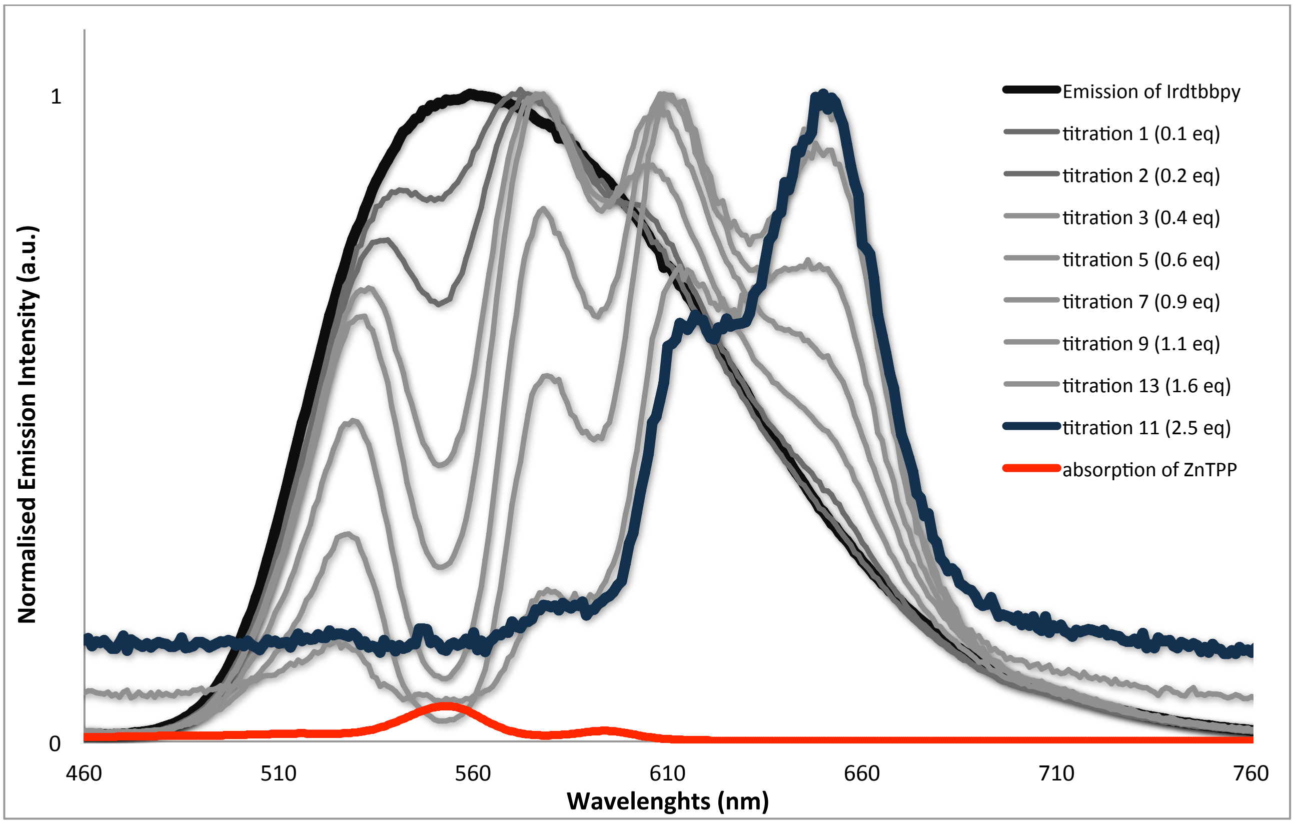

Figure **S67**. Room-temperature emission spectra of **3** (black line) and emission spectra of **3** upon addition of ZnTPP (from 0 to 2.5 equiv.) collected in DCM (λ_{exc} = 360 nm). The Q absorption band of ZnTPP is shown in red. The concentration of **3** was maintained constant at 5 × 10^{-4} M whereas the concentration of ZnTPP varied from 5 × 10^{-5} to 1.25 × 10^{-3} M.

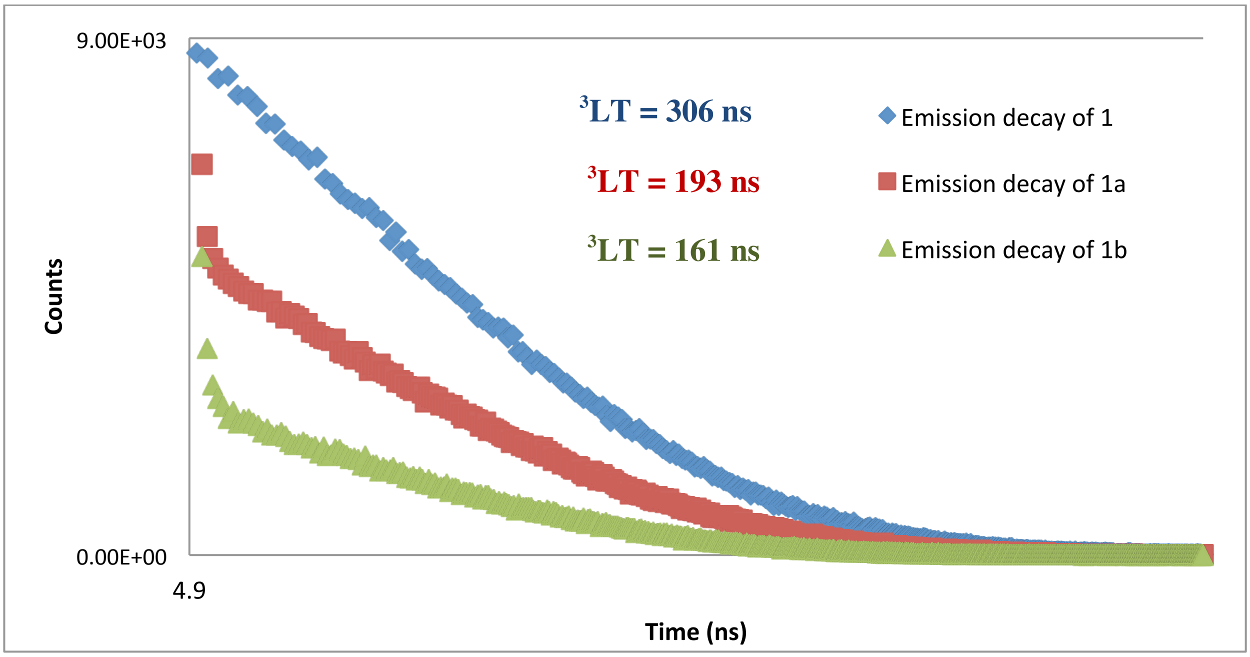

Figure **S68**. Lifetime decays of **1** (blue), **1a** (red) and **1b** (green) after excitation at 379 nm in deareated DCM at 298 K at a concentration of 5×10^{-4} M.

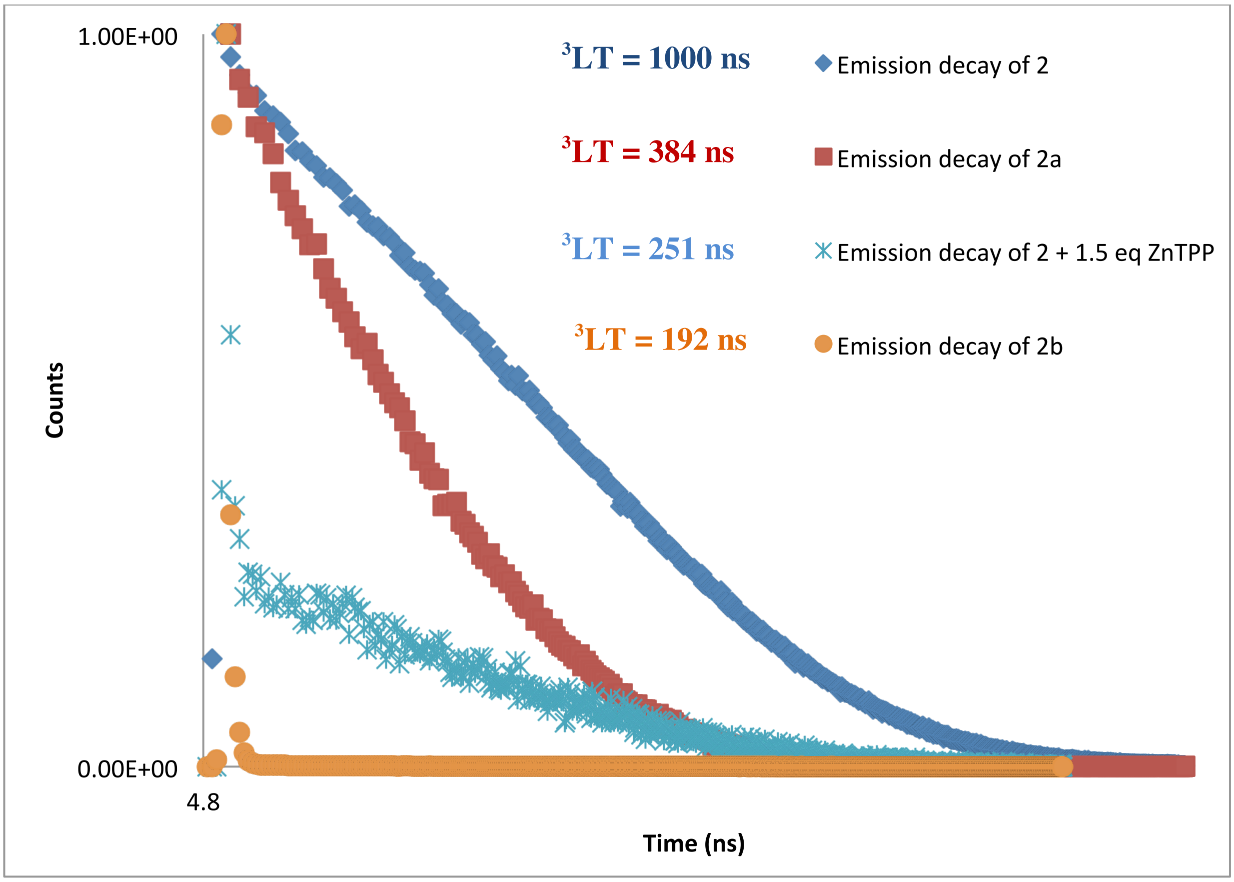

Figure **S69**. Lifetime decays of **2** (blue)**, 2a** (red) and **2 +** 1.5 equivalents of ZnTPP (light blue) and **2b** (orange) after excitation at 379 nm in deareated DCM at 298 K at a concentration of 5×10^{-4} M.

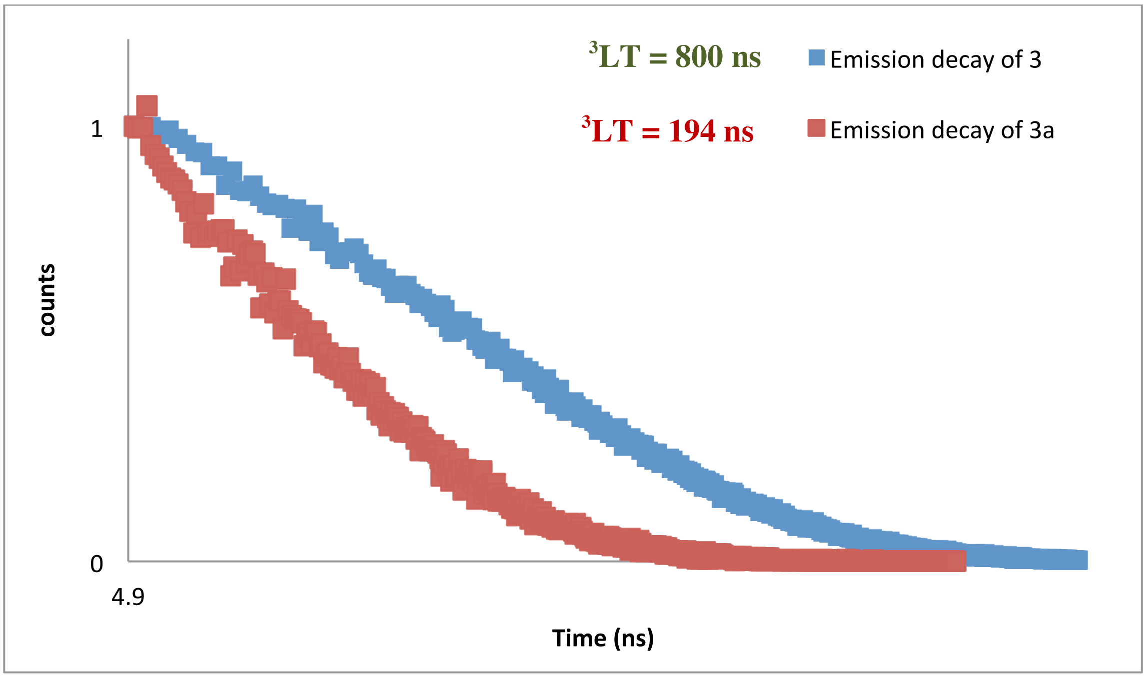

Figure **S70**. Lifetime decays of **3** (green) and **3a** (red) after excitation at 379 nm in deareated DCM at 298 K at a concentration of 5×10^{-4} M.

Emission studies at a concentration of 1×10^{-3} M.

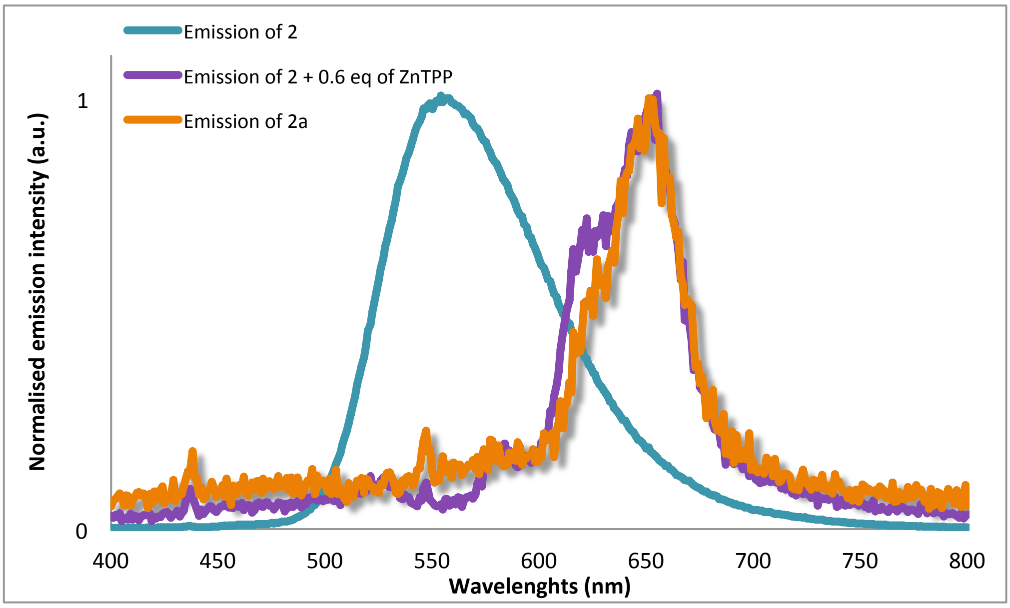

Figure **S71**. Room-temperature emission spectra of **2** (blue) and emission spectra of **2** + 0.6 equivalents of ZnTPP (violet) and **2a** (orange) collected in DCM (λ_{exc} = 360 nm) at a concentration of 1×10^{-3} M.

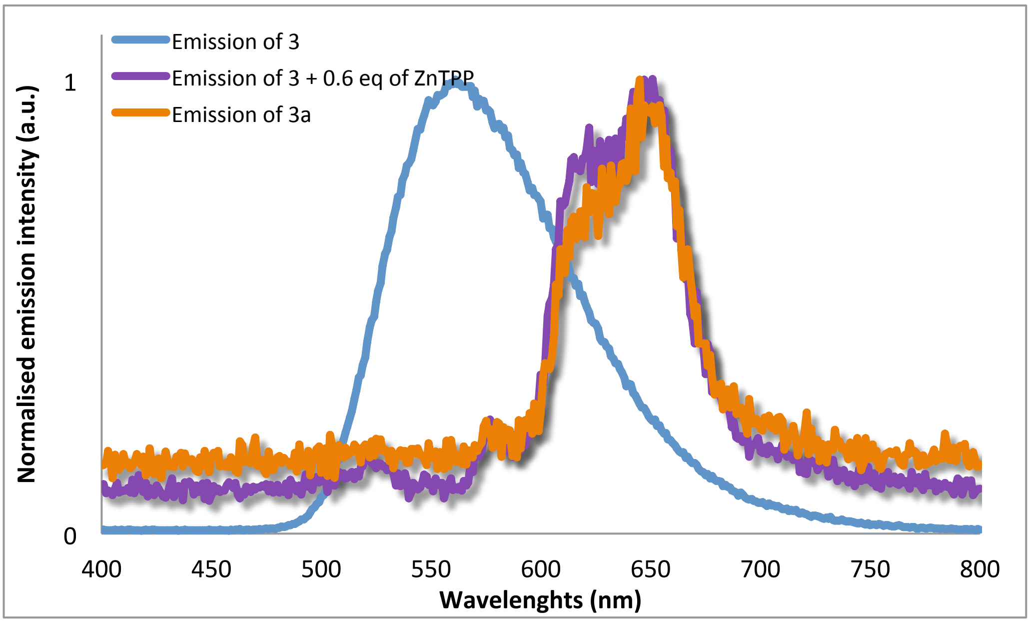

Figure **S72**. Room-temperature emission spectra of **3** (blue) and emission spectra of **3** + 0.6 equivalents of ZnTPP (violet) and **2a** (orange) collected in DCM (λ_{exc} = 360 nm) at a concentration of 1×10^{-3} M.

Electrochemical properties.

Table **S4**. Electrochemical data and optical data ($E_{0,0}$) for ZnTPP, complexes **1-3**, assemblies **1**:ZnTPP = 1:1 (**1a**), **1**:ZnTPP = 1:2 (**1b**), **2**:ZnTPP = 1:1 (**2a**), **2**:ZnTPP = 1:2 (**2b**) and **3**:ZnTPP = 1:1 (**3a**)and ZnTPP-py.

Complex	E_{ox} [a] / V	E_{ox} [a] / V	E_{ox} [a] / V	E_{red} [a] / V	E_{red} [a] / V	E_{red} [a] / V	$E_{0,0}$ [d] / eV
ZnTPP	0.73[b]	1.05[b]	-	-	–1.29[c]	–1.52[c]	2.19
1	-	-	1.35[c]	–1.21[b]	-	-	2.21[e]
2	-	-	1.46[c]	–1.26[c]	–1.44[c]	-	2.55
3	-	-	1.17[b]	–1.15[c]	-	-	2.55
1:ZnTPP =	0.52[c]	1.08[c]	1.34[c]	–1.13[c]	–1.39[c]	–1.80[c]	-

1:1							
1:ZnTPP = 1:2	0.55[c]	0.96[c]	1.33[c]	−1.13[c]	−1.40[c]	−1.78[c]	-
2:ZnTPP = 1:1	0.68[c]	-	1.41[c]	−1.25[c]	−1.44[c]	-	-
2:ZnTPP = 1:2	0.67[c]	-	1.40[c]	−1.19[c]	−1.35[c]	-	-
3:ZnTPP = 1:1	0.65[b]	1.01[b]	1.15[b]	−1.27[c]	−1.52[c]	-	-
ZnTPP-py	0.37[b]	0.69[b]	-	-	−1.31[b]	−1.73	-

[a] CV traces recorded in DCM solution with 0.1 M (n-Bu_4N)PF_6 at 298 K at 50 mV·s^{-1}. Values are in V *vs.* SCE (Fc/Fc$^+$ *vs.* SCE = 0.46 V). [b] $E_{1/2} = (E_{pa} + E_{pc})/2$ and result from one-electron processes. [c] Irreversible oxidation and reduction peak potentials. [d] $E_{0,0}$ estimated from the intersection point of the absorption and emission spectra at 298 K in DCM. [e] $E_{0,0}$ estimated from 10% of the onset of the absorption spectra at 298 K in DCM.

Cyclic Voltammetry.

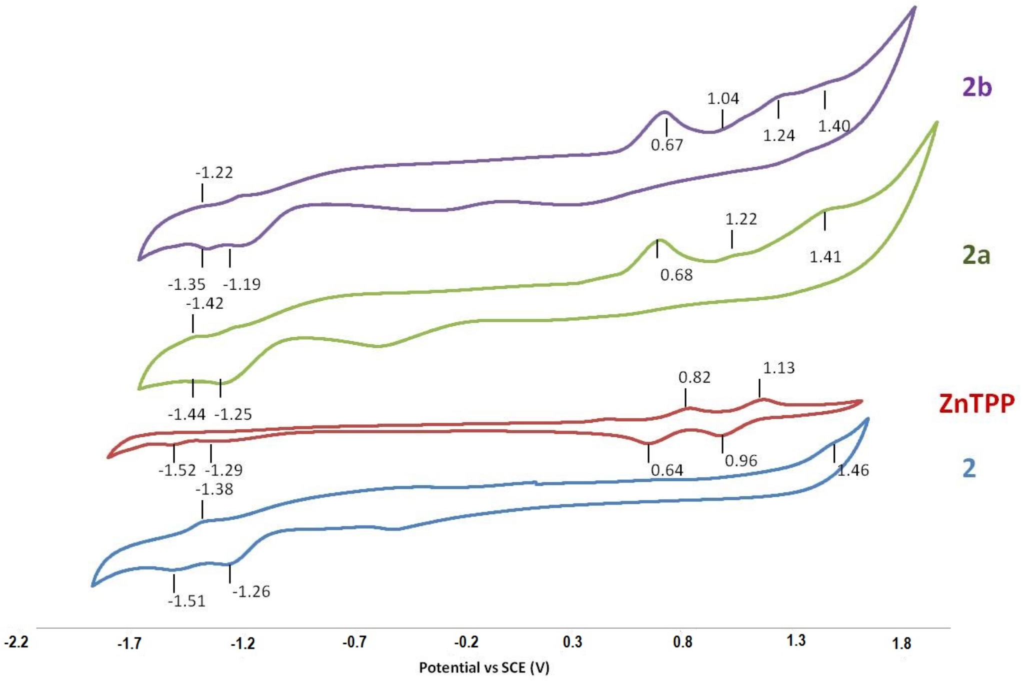

Figure **S73**. **a**) Cyclic Voltammograms for complex **2**, ZnTPP and assemblies **2a** and **2b** recorded at 298 K in deareated DCM solution containing *n*-NBu_4PF_6 as the supporting electrolyte and using Fc/Fc^+ as an internal standard (Fc/Fc^+ = 0.46 V in DCM with respect to SCE).[9]

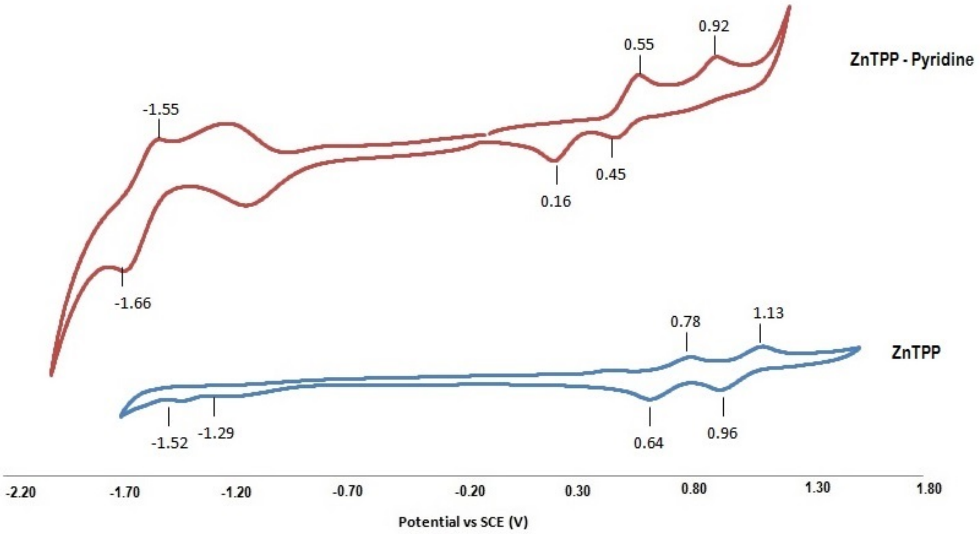

Figure **S74**. **a**) Cyclic Voltagramms for ZnTPP and ZnTPP after coordination with pyridine (ZnTPP-py) recorded at 298 K in deareated DCM solution containing *n*-NBu_4PF_6 as the supporting electrolyte and using Fc/Fc^+ as an internal standard (Fc/Fc^+ = 0.46 V in DCM with respect to SCE).[9]

Streak camera studies.

High-time-resolution streak camera measurements of **2b** and **3a** at a concentration of 5×10^{-4} M have been carried out to investigate ultrafast energy transfer processes between the iridium center and ZnTPP (Figure **S75** and **S76**).[22] However, at these elevated concentrations only self-absorption (followed by re-emission) was observed (from 0 to 140 ps in Figure **S74b**) and there is no evidence of rapid ET processes in these systems.

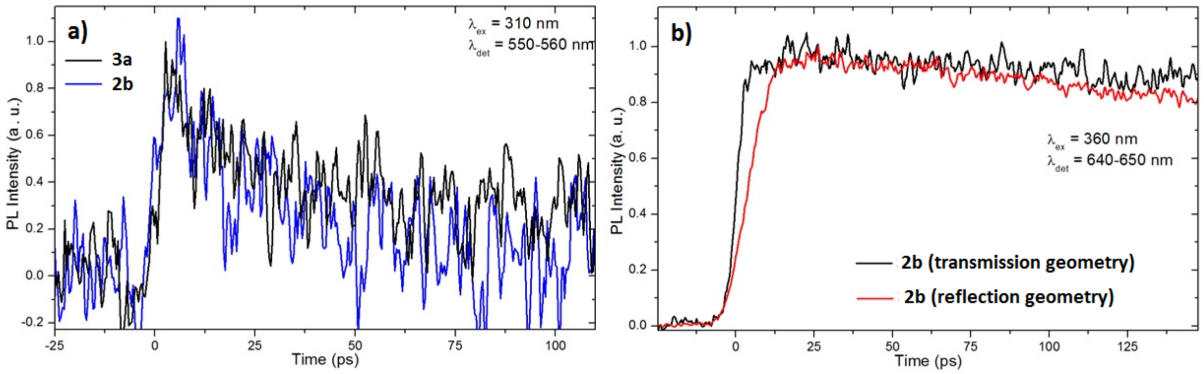

Figure **S75**. **a)** Streak camera decays at the iridium emission (λ_{em}: 550–560 nm) upon excitation at 310 nm of **2b** (blue line) and **3a** (black line). **b)** Streak camera decays at the ZnTPP emission (λ_{em}: 640–650 nm) upon excitation at 360 nm of **2b** at a concentration of 3×10^{-5} M (black line) and at a concentration of 5×10^{-4} M (red line).

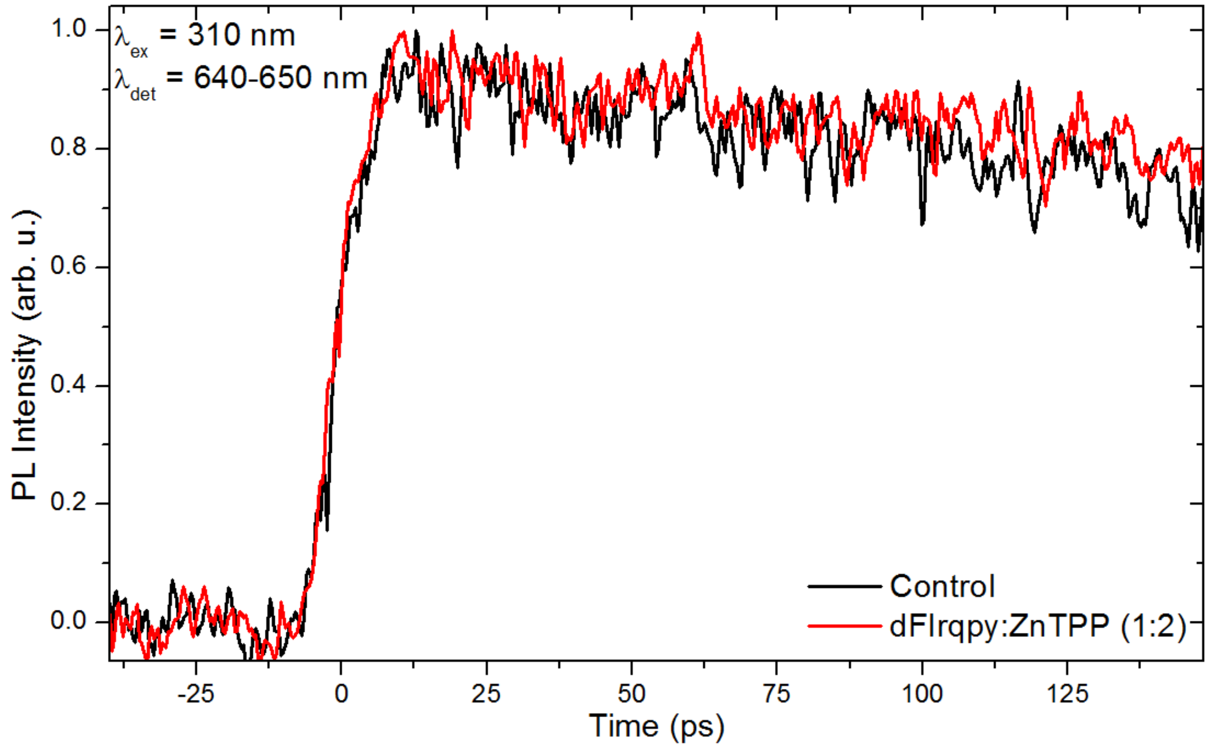

Figure **S76**. Streak camera ZnTPP emission decays in the assembly **2b** (blue line, λ_{em} : 640 - 650 nm) and of the "non assembly" **3a** (black line, λ_{em} : 640 - 650 nm) upon photoexcitation at 310 nm.

Computational details.

All calculations are based on density functional theory (DFT). The geometries of the singlet ground-state (S_0) and the lowest triplet excited-state were optimized for complexes **1** and **2**, ZnTPP and assemblies **1a-1b** and **2a-2b** using the hybrid exchange-correlation functional B3LYP[23] in combination with the def2-SVP atomic basis set under the resolution of the identity (RI) approximation. Scalar relativistic effects were included for the Ir atom by using the ECP-60-mwb Stuttgart/Dresden pseudopotential.[24] The nature of the stationary points was confirmed by computing the Hessian at the same level of theory. Gas-phase TD-B3LYP and TD-CAM-B3LYP vertical singlet energies were obtained at the S_0 geometry using the 6-31G(d) atomic basis set. Optimizations and TD-DFT calculations were carried out with the Turbomole 6.6[25] and Gaussian09[26] program packages, respectively.

a)

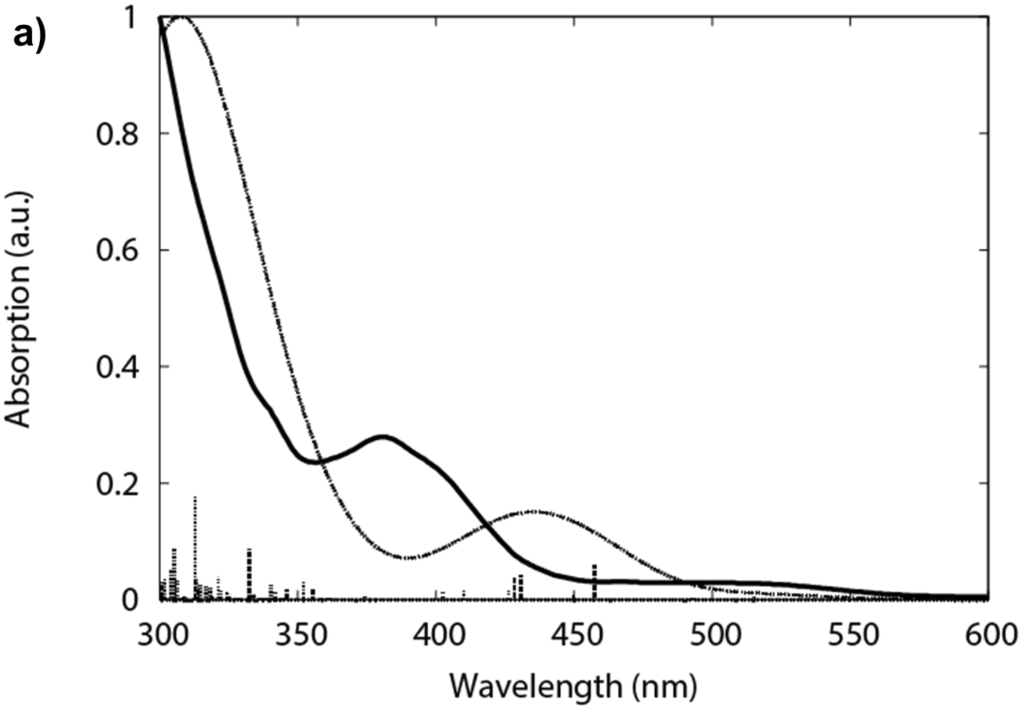

b)

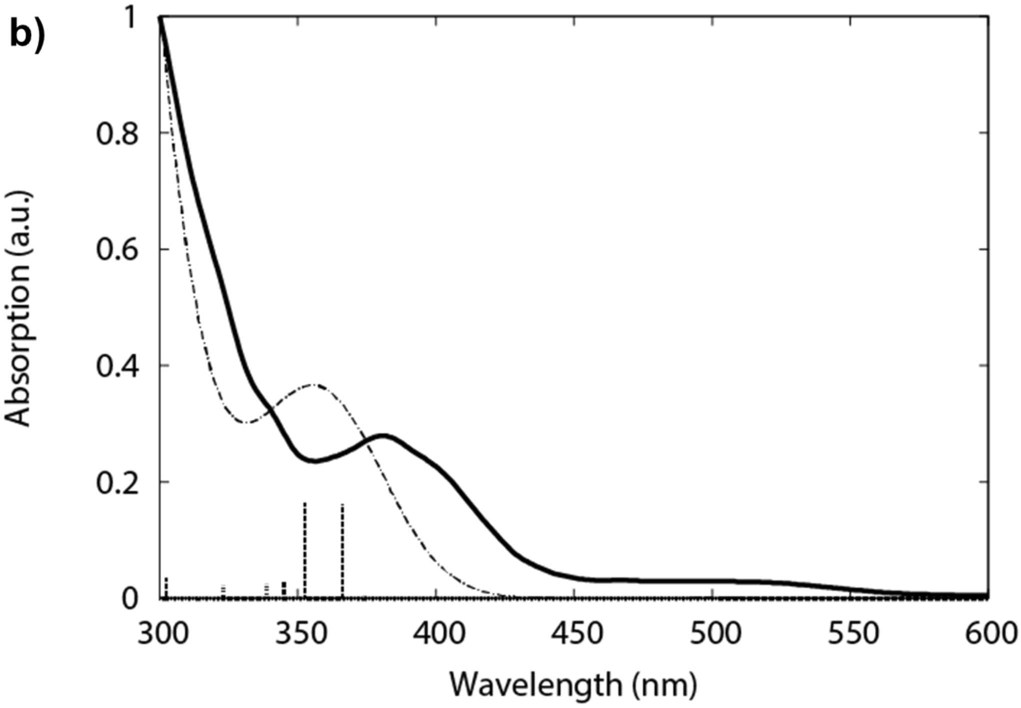

Figure **S77**. **a**) Normalized UV-Vis absorption of **1** (solid line) and TD-B3LYP/6-31G(d) (ECP-60-mwb for Ir) vertical excitations with the theoretically convoluted UV-Vis spectrum (dashed line). **b**) Normalized UV-Vis absorption of **1** (solid line) and TD-CAM-B3LYP/6-31G(d) (ECP-60-mwb for Ir) vertical excitations with the theoretically convoluted UV-Vis spectrum (dashed line)**.**

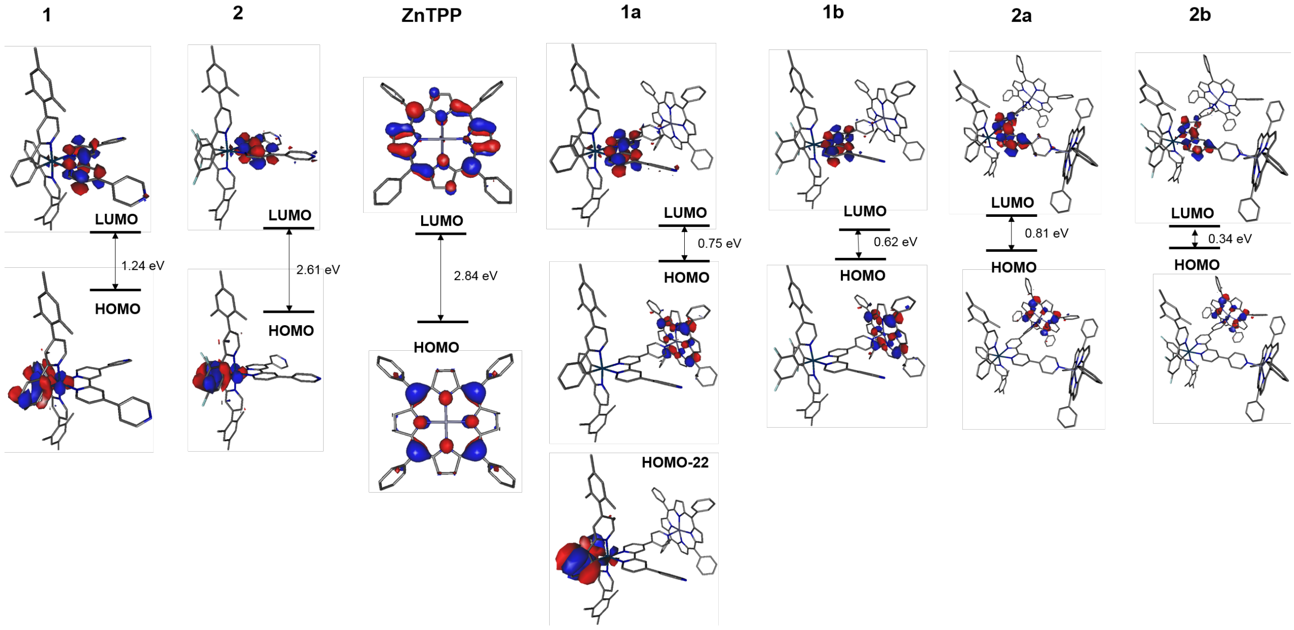

Figure **S78**. Energy levels of the Kohn-Sham orbitals (B3LYP/6-31G(d) - ECP-60-mwb for Ir) of **1-2**, **ZnTPP** and the assemblies 1**a-1b** and **2a-2b**.

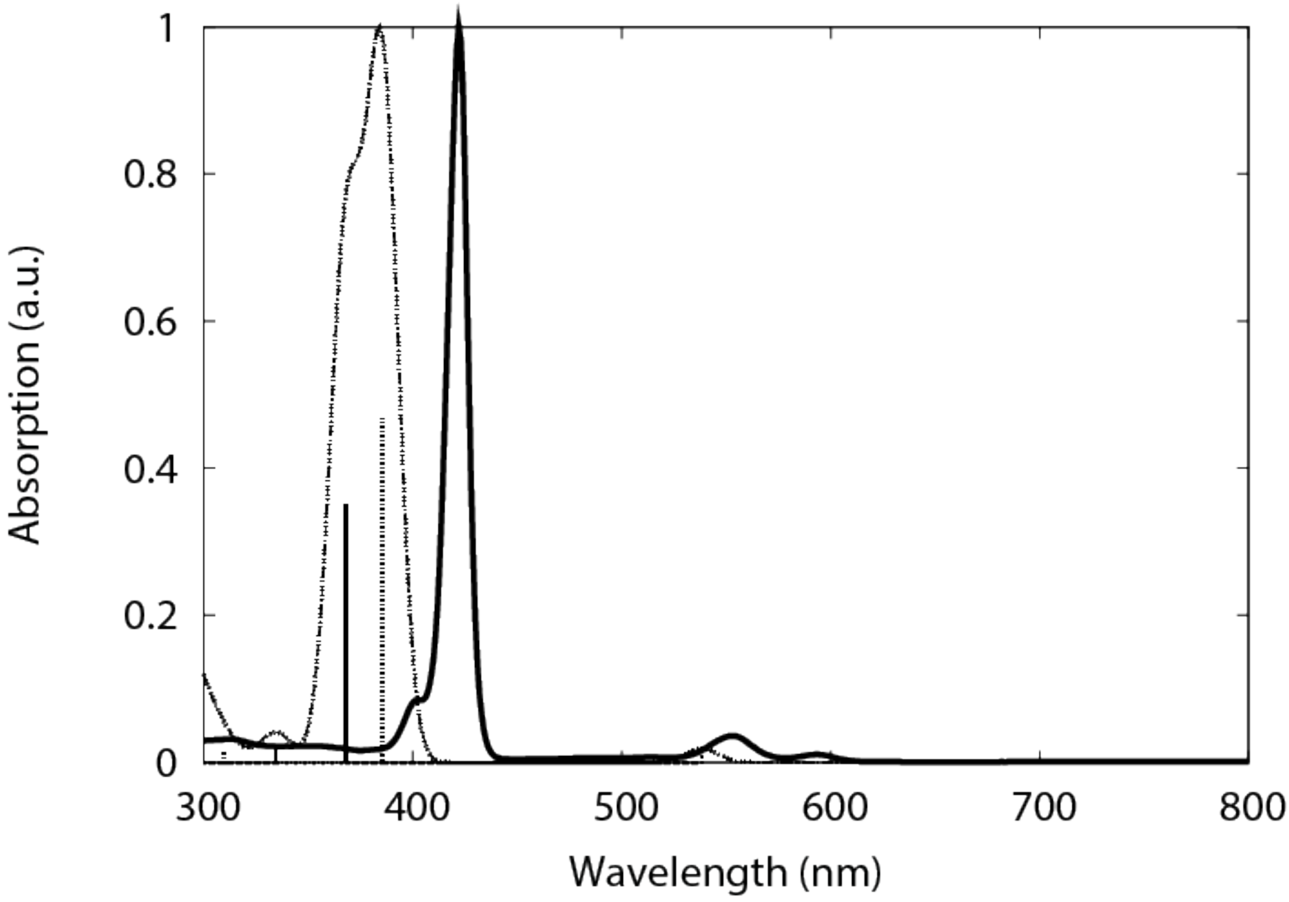

Figure **S79**. Normalized UV-Vis absorption of **ZnTPP** (solid line) and TD-B3LYP/6-31G(d) (ECP-60-mwb for Ir) vertical excitations with the theoretically convoluted UV-Vis spectrum (dashed line)**.**

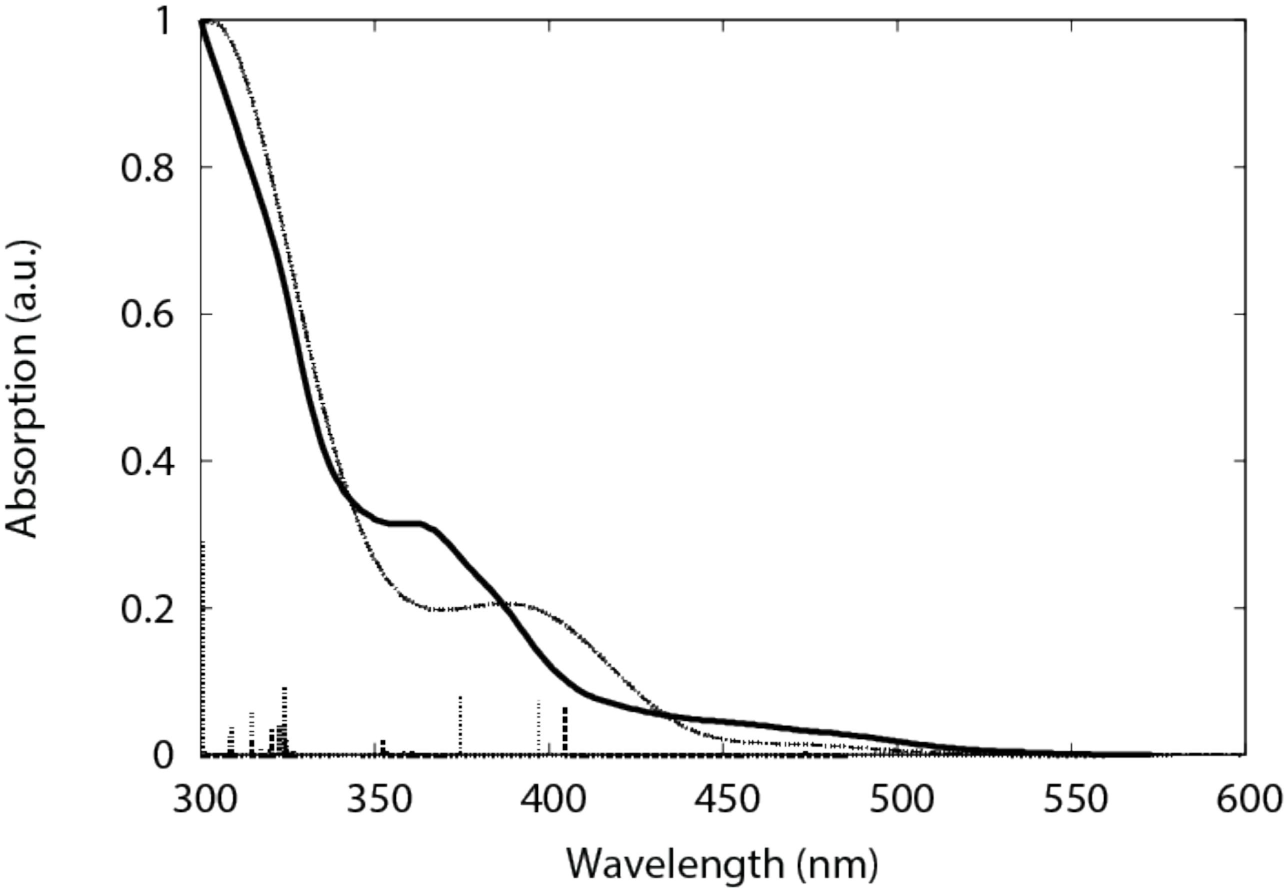

Figure **S80**. Normalized UV-Vis absorption of **2** (solid line) and TD-B3LYP/6-31G(d) (ECP-60-mwb for Ir) vertical excitations with the theoretically convoluted UV-Vis spectrum (dashed line).

Theoretical estimation of photoinduced electron transfer (PeT) processes.

Photoinduced Electron Transfer (PeT) in a typical Donor–Acceptor system (D-A, bimolecular process) is an electron exchange process between the two chromophoric units upon initial photoexcitation of the donor component, resulting in the formation of a non-emissive charge separated state ($D^{\cdot+}$—$A^{\cdot-}$).[27]

The first step in determining the feasibility of a PeT process in a bimolecular system involves the determination of the free energy (ΔG_{CS}) associated with the charge-separated state, which can be calculated following the Rehm-Weller equation.[27b, 27c, 28]

$$\Delta G_{CS} = e\left[E_{1/2}(D^{\cdot+}/D^{*}) - E_{1/2}(A^{*}/A^{\cdot-})\right] - E_{0,0} + Gs \qquad \textbf{(1)}$$

In eq (**1**) the first term on the right-hand-side, $e\left[E_{1/2}(D^{\cdot+}/D^{*}) - E_{1/2}(A^{*}/A^{\cdot-})\right]$ contains the redox potential for the excited states couples (Donor, D; Acceptor, A), which can be inferred given:[27a, 29]

$$E_{1/2}(D^{\cdot+}/D^{*}) = E_{1/2}(D^{+}/D) - E_{0,0} \qquad \textbf{(2)}$$

and

$$E_{1/2}(A^{*}/A^{\cdot-}) = E_{1/2}(A/A^{\cdot}) + E_{0,0} \qquad \textbf{(3)}$$

The *Gs* in eq (**1**) is the ion-pair stabilization energy and involves both the solvent-dependent columbic interactions and structural parameters of the system and it can be calculated from:[27b, 28]

$$G_S = \frac{e^2}{4\pi\varepsilon^0}\left[\left(\frac{1}{2R_D} + \frac{1}{2R_A} - \frac{1}{R_{DA}}\right)\frac{1}{\varepsilon_S} - \left(\frac{1}{2R_D} + \frac{1}{2R_A}\right)\frac{1}{\varepsilon_R}\right] \qquad \textbf{(4)}$$

where R_D and R_A are, respectively, the radius of the donor and acceptor, R_{DA} is the center-to-center distance between the donor and the acceptor and ε_S and ε_R are, respectively, the dielectric constants of the solvents used for the photophysical and electrochemical studies. The structural parameters of the assemblies elucidated by X-ray diffraction (Figure **S46**) were used to calculate *Gs*, with $R_D = 9.20$ Å, $R_A = 7.21$ Å and $R_{DA} = 11.33$ Å for **1a** and $R_{DA} = 11.24$ Å for **2a**.[30] For both optical and electrical studies, DCM was used as the solvent and, therefore, $\varepsilon_S = \varepsilon_R = 8.93$.

The redox potentials combined with the optical data were used to estimate the free energies associated with PeT processes in **1a**, **1b**, **2a** and **2b**. Only the assemblies **1a** and **2a** have been considered for determining the ΔG_{CS} associated to PeT process, but due to the very similar optoelectronic data obtained for **1b** and **2b**, the same results can be readily extended to the 1:2 assemblies.

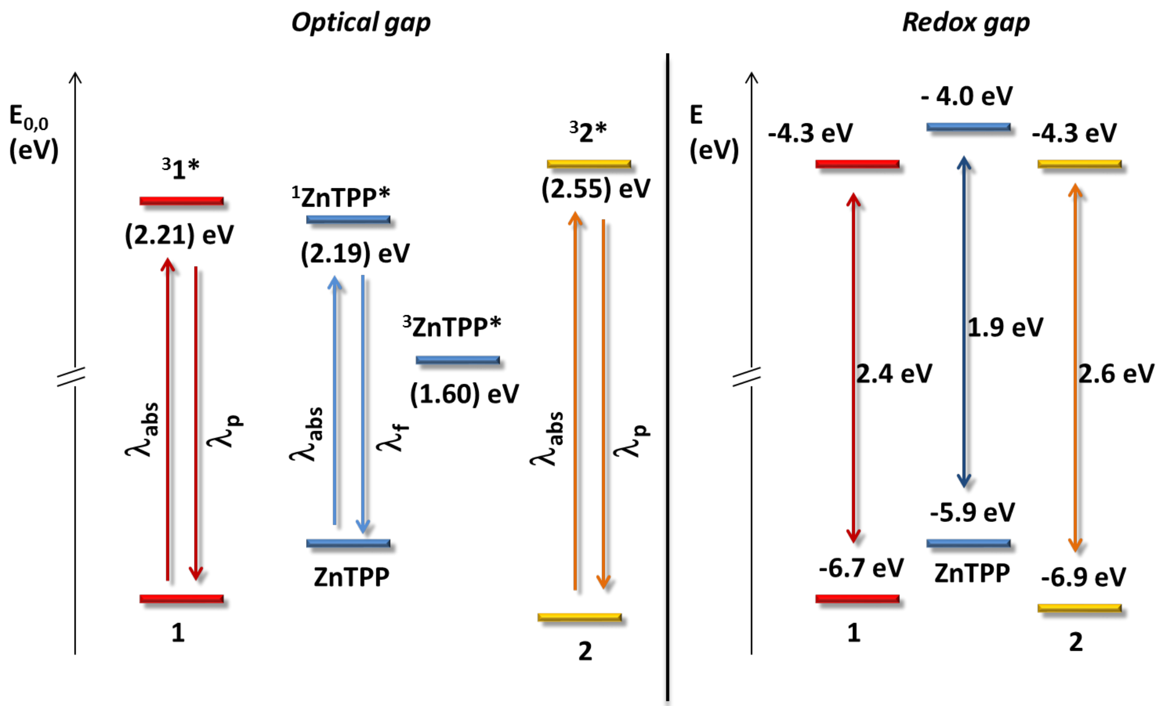

Figure **S81**. **a**) Representation of the energy of the zero-zero transition ($E_{0,0}$) to the lowest excited states of **1**, ZnTPP and **2** obtained by spectroscopic analysis. As the energy of the lowest triplet state of ZnTPP (^{3}ZnTPP*) we used the value previously reported.[31] **b**) Representation of the energies of the first oxidation and first reduction waves, the associated redox gap and inferred HOMO – LUMO levels of complex **1**, ZnTPP and **2** obtained by electrochemical analysis of **1a** and **2a**. $E_{\mathrm{HOMO}} = -(E^{\mathrm{ox}}_{\mathrm{pa\ vs\ Fc/Fc+}} + 5.39)$ eV, $E_{\mathrm{LUMO}} = -(E^{\mathrm{red}}_{\mathrm{pc\ vs\ Fc/Fc+}} + 5.39)$ eV.[32]

Figure **S81a** shows the lowest triplet excited-state energies of **1** and **2** and the lowest singlet excited-state energy of ZnTPP estimated from the intersection point between their respective absorption and luminescence spectra (Tables **S2** and **S3**). The $E_{0,0}$ values reported in Table **S4** and Figure **S81a** have been estimated from the room-temperature rather than the low-temperature (77 K) emissions required for a rigorous estimation of the zero-zero excited-state values.[27b] However, we are confident that this approximation does not significantly influence our qualitative approach for evaluating possible PeT pathways in our systems. The lowest transition energy ($E_{0,0}$) is located at 2.55 eV for **2**, and at 2.21 eV for **1**, both of which are higher than $E_{0,0}$ calculated for ZnTPP (2.19 eV). As the energy of the lowest triplet excited-state of ZnTPP (^{3}ZnTPP*) we used the previously reported value of 1.60 eV.[31]

Figure **S81b** represents the inferred energies of HOMO and LUMO levels of **1** and **2** and ZnTPP obtained by CV analysis of **1a** and **2a** (*cf.* Table **S4**). The HOMO and LUMO levels of ZnTPP are located at –5.9 and –4.0 eV, respectively, whereas for both **1** and **2** the HOMO and LUMO are stabilized (–6.7 and –4.3 eV for **1** and –6.9 and –4.3 eV for **2**, respectively). Thus, the ground-state electrochemical data suggest that, from an electron transfer point of view, ZnTPP is a better donor than the iridium complexes due to its higher ionization potential, whereas both **1** and **2** are better electron acceptors due to their higher electron affinity. This is consistent with the DFT calculations (Figure **9**). Following this assumption, we calculated ΔG_{CS} for a PeT process in **1a** and **2a**, where ZnTPP is the donor and the iridium complex acts as the acceptor. For **1a**, the ground-state oxidation potential of ZnTPP is –5.9 eV and the ground-state reduction potentials of both **1** and **2** are –4.3 eV. Thus, the excited-state redox gap $e\left[E_{1/2}(D^{+}/D^{*}) - E_{1/2}(A^{*}/A^{-})\right]$ for **1a** and **2a**, is 1.65 eV. The ion-pair stabilization energy, *Gs* for both **1a** and **2a** is –0.14 eV. Thus, for **1a** and **2a**, ΔG_{CS} is found to be exergonic in DCM ($\Delta G_{CS} = -0.68$ eV), suggesting that upon photoexcitation of ZnTPP, electron transfer to the iridium centers is thermodynamically favorable. By contrast, due to the higher energy required to extract an electron from the iridium complexes, ΔG_{CS} for PeT processes, in which **1** and **2** act as donors and ZnTPP acts as the acceptor, are found to be +0.38 eV for **1a** and +0.08 eV for **1b**. Thus, in this direction the processes are slightly endergonic and not thermodynamically favorable. From the steady-state and time-resolved photophysical studies presented, we only observed emission quenching of the iridium complexes by self-absorption due to the presence of ZnTPP. Consequently, we have no evidence of emission quenching due to charge recombination following PeT, despite the favorable thermodynamics.

References.

(1). D. Rota Martir, A. K. Bansal, V. Di Mascio, D. B. Cordes, A. F. Henwood, A. Slawin, P. Kamer, L. Martinez-Sarti, A. Pertegas, H. J. Bolink, I. Samuel and E. Zysman-Colman, *Inorganic Chemistry Frontiers*, 2015, **ASAP**, DOI: 10.1039/C1035QI00177C.

(2). S. Bossmann, A. Shi and M. Pokhrel, *Synthesis*, 2007, **2007**, 505-514.

(3). M. Nonoyama, *Bull. Chem. Soc. Jpn.*, 1974, **47**, 767-768.

(4). J. C. Manton, C. Long, J. G. Vos and M. T. Pryce, *Dalton Trans*, 2014, **43**, 3576-3583.

(5). G. A. Crosby and J. N. Demas, *J. Phys. Chem.*, 1971, **75**, 991-1024.

(6). W. H. Melhuish, *J. Phys. Chem.*, 1961, **65**, 229-235.

(7). K. Suzuki, A. Kobayashi, S. Kaneko, K. Takehira, T. Yoshihara, H. Ishida, Y. Shiina, S. Oishi and S. Tobita, *Phys Chem Chem Phys*, 2009, **11**, 9850-9860.

(8). A. M. Brouwer, *Pure Appl. Chem.*, 2011, **83**, 2213-2228.

(9). N. G. Connelly and W. E. Geiger, *Chem. Rev.*, 1996, **96**, 877-910.

(10). (a) P. Mendes, *Computer applications in the biosciences : CABIOS*, 1993, **9**, 563-571; (b) P. Mendes and D. Kell, *Bioinformatics*, 1998, **14**, 869-883.

(11). P. S. Sobolev, V. P. Andreev and T. A. Ekimova, *Russ. J. Gen. Chem.*, 2014, **84**, 1399-1403.

(12). *CrystalClear-SM Expert v. 2.1;* , Rigaku Americas, Rigaku Americas, The Woodlands, Texas, USA and Rigaku Corporation, Tokyo, Japan, 2010-2014.

(13). P. T. Beurskens, G. Beurskens, R. de Gelder, S. Garcia-Granda, R. O. Gould, R. Israel and J. M. M. Smits, Crystallography Laboratory, University of Nijmegen, The Netherlands, , 1999.

(14). M. C. Burla, R. Caliandro, M. Camalli, B. Carrozzini, G. L. Cascarano, L. De Caro, C. Giacovazzo, G. Polidori and R. Spagna, *J. Appl. Crystallogr.*, 2005, **38**, 381-388.

(15). L. Palatinus and G. Chapuis, *J. Appl. Crystallogr.*, 2007, **40**, 786-790.

(16). G. Sheldrick, *Acta Crystallogr., Sect. C: Cryst. Struct. Commun.*, 2015, **71**, 3-8.

(17). *CrystalStructure v4.1.*, The Woodlands, Texas, USA and Rigaku Corporation, Tokyo, Japan, 2014.

(18). C. F. Macrae, I. J. Bruno, J. A. Chisholm, P. R. Edgington, P. McCabe, E. Pidcock, L. Rodriguez-Monge, R. Taylor, J. van de Streek and P. A. Wood, *J. Appl. Crystallogr.*, 2008, **41**, 466-470.

(19). O. V. Dolomanov, L. J. Bourhis, R. J. Gildea, J. A. K. Howard and H. Puschmann, *J. Appl. Crystallogr.*, 2009, **42**, 339-341.

(20). A. Spek, *Acta Crystallogr., Sect. C: Cryst. Struct. Commun.*, 2015, **71**, 9-18.

(21). A. Spek, *J. Appl. Crystallogr.*, 2003, **36**, 7-13.

(22). For **2b**: [2] = 5 × 10^{-4} M, [ZnTPP] = 1 × 10^{-3} M; For **3a**: [3] = 5 × 10^{-4} M, [ZnTPP] = 1 × 10^{-3} M.

(23). (a) A. D. Becke, *J. Chem. Phys.*, 1993, **98**, 5648-5652; (b) C. Lee, W. Yang and R. G. Parr, *Phys. Rev. B*, 1988, **37**, 785-789.

(24). D. Andrae, U. Häußermann, M. Dolg, H. Stoll and H. Preuß, *Theoretica chimica acta*, **77**, 123-141.

(25). *TURBOMOLE V6.6; a development of University of Karlsruhe and Forschungszentrum Karlsruhe GmbH, 1989–2007; TURBOMOLEGmbH, since2007. Available from* http://www.turbomole.com., 2014.

(26). M. J. Frisch, G. W. Trucks, H. B. Schlegel, G. E. Scuseria, M. A. Robb, J. R. Cheeseman, G. Scalmani, V. Barone, B. Mennucci, G. A. Petersson, H. Nakatsuji, M. Caricato, X. Li, H. P. Hratchian, A. F. Izmaylov, J. Bloino, G. Zheng, J. L. Sonnenberg, M. Hada, M. Ehara, K. Toyota, R. Fukuda, J. Hasegawa, M. Ishida, T. Nakajima, Y. Honda, O. Kitao, H. Nakai, T. Vreven, J. A.

Montgomery Jr., J. E. Peralta, F. Ogliaro, M. Bearpark, J. J. Heyd, E. Brothers, K. N. Kudin, V. N. Staroverov, R. Kobayashi, J. Normand, K. Raghavachari, A. Rendell, J. C. Burant, S. S. Iyengar, J. Tomasi, M. Cossi, N. Rega, J. M. Millam, M. Klene, J. E. Knox, J. B. Cross, V. Bakken, C. Adamo, J. Jaramillo, R. Gomperts, R. E. Stratmann, O. Yazyev, A. J. Austin, R. Cammi, C. Pomelli, J. W. Ochterski, R. L. Martin, K. Morokuma, V. G. Zakrzewski, G. A. Voth, P. Salvador, J. J. Dannenberg, S. Dapprich, A. D. Daniels, Ö. Farkas, J. B. Foresman, J. V. Ortiz, J. Cioslowski and D. J. Fox, Gaussian Inc., Wallingford, CT, 2009.

(27). (a) F. Scandola, C. Chiorboli, A. Prodi, E. Iengo and E. Alessio, *Coord. Chem. Rev.*, 2006, **250**, 1471-1496; (b) G. J. Kavarnos and N. J. Turro, *Chem. Rev.*, 1986, **86**, 401-449; (c) S. Doose, H. Neuweiler and M. Sauer, *Chemphyschem*, 2009, **10**, 1389-1398.

(28). P. K. Poddutoori, L. P. Bregles, G. N. Lim, P. Boland, R. G. Kerr and F. D'Souza, *Inorg Chem*, 2015, **54**, 8482-8494.

(29). (a) J.-L. Bredas, *Materials Horizons*, 2014, **1**, 17; (b) V. Balzani, F. Bolletta, F. Scandola and R. Ballardini, *Pure Appl. Chem.*, 1979, **51**, 299-311.

(30). R_D is defined as the Ir-Nqpy distance, where Nqpy is the distal nitrogen on the quaterpyridine; R_A is defined as the distance from the Zn to the C_4 of the one of the phenyl groups on the TPP ligand; and R_{DA} is defined as the Ir-Zn distance. All distances determined from the crystal structure of **2a**.

(31). V. A. Walters, J. C. de Paula, B. Jackson, C. Nutaitis, K. Hall, J. Lind, K. Cardozo, K. Chandran, D. Raible and C. M. Phillips, *J. Phys. Chem.*, 1995, **99**, 1166-1171.

(32). C. M. Cardona, W. Li, A. E. Kaifer, D. Stockdale and G. C. Bazan, *Adv. Mater.*, 2011, **23**, 2367-2371.